INVESTIGATION OF WETTING STATES ON MICROSTRUCTURES AFTER LIQUID DROPS CONTACT GROOVE BASE

by

MINGMING XIANG

Presented to the Faculty of the Graduate School of

The University of Texas at Arlington in Partial Fulfillment

of the Requirements

for the Degree of

DOCTOR OF PHILOSOPHY

THE UNIVERSITY OF TEXAS AT ARLINGTON

AUGUST 2014

Acknowledgements

I would never have been able to finish my dissertation without the help from my advisor, committee members, my friends and my family.

Foremost, I would like to express my sincere gratitude to my research advisor, Prof. Cheng Luo, for the guidance and support of my Ph.D study during these past five years. Without his constant help this dissertation would not have been possible.

Besides my advisor, I would like to thank my thesis committee members, Prof. Moon, Prof. Tong, Prof. Meng, Prof. Yang and Prof. Wang, for their helpful suggestions and comments.

I thank my group members, Xinchuan Liu, Anirban Chakraborty, Hui Wang, Lei Qiao, Xin Heng, Zhihui Lu, Anderson Wilhelm, Varun Gary, and Prasha Sarwate for their co-operation and continuous support.

Last but not least, I would like to thank my dear parents, Shihai Xiang and Cui Wang, for giving birth to me and supporting me spiritually throughout my life. I would like to thank my beloved wife, Fen Chen, for all the sacrifices that you have made on my behalf. You are always there cheering me up and standing by me through the good times and bad times. Without you all, I wouldn't be where I am today. I always love you.

July 01, 2014

Abstract

INVESTIGATION OF WETTING STATES ON MICROSTRUCTURES AFTER LIQUID DROPS CONTACT GROOVE BASE

Mingming Xiang, PhD

The University of Texas at Arlington, 2014

Supervising Professor: Cheng Luo

Wetting properties of roughness surfaces have attracted a considerable attention because of both the scientific insight and the practical applications. One of the most intriguing topics of wetting is the so-called Cassie-Baxter and Wenzel transition. Recently, theoretical and experimental works have been done to explore this transition on microstructure-formed surfaces. One of the criteria that most commonly used to judge such transition is whether a liquid drop contacts the base of a roughness groove. It is expected that, after the contact, liquid immediately fills the roughness groove, and subsequently the wetting state is changed from Cassie-Baxter state to that of Wenzel.

However, this transition criterion does not always hold true in the case of microchannels. Through theoretical and experimental investigations, we show that, when an angle criterion is satisfied, there may exist an intermediate wetting state inside a microchannel after a water drop contacts the bottom of the microchannel. In this wetting state, water does not completely fill the microchannel, and air pockets still exist in its bottom corners. Also, the wetting state is stable in the sense that its energy state is lower than that of the Wenzel model. In addition to microchannels, the aforementioned intermediate state may also exist on a single corner, when the angle criterion is met.

Moreover, we demonstrate that the angle criterion also applies to the case of micropillars with circular or polygonal cross-sections. Finally, based on the results achieved in the cases of microchannels and micropillars, we further investigate the applicability of the angle criterion to the cases of microballs and lotus leaf surfaces.

Table of Contents

List of Illustrations

Chapter 1

Introduction and Dissertation Overview

1.1 Introduction

Wetting properties of roughness surfaces have attracted a considerable attention due to both the scientific insight and the practical applications, such as self-cleaning, [1,2] hydrodynamic friction reduction, [3-5] anti-icing, [6-8] anticorrosion, [9-11] biotechnology, [12-14] thermal systems, [15-19] and micro- and nano-devices. [20-22] It is well-known that the surface roughness plays an important role on the wetting properties, and micropillars and microchannels are often applied as structures to enhance surface hydrophobicity. [23, 24, 26, 29, 30, 37, 38, 45-50, 62, 65] When a water drop is placed on a rough surface, there are two possible wetting states: Wenzel [23] (Figure 1.1(a)) or Cassie-Baxter [24] (Figure 1.1(b)). In the Wenzel state, the drop completely fills grooves between microstructures (e.g., pillars and channels), while in the Cassie-Baxter state air is trapped between these microstructures and the drop stays on top of the microstructures and trapped air. The Wenzel state favors the creation of a super-wetting surface. [27, 28] In contrast, in a Cassie-Baxter state, a liquid drop is easy to roll off from a hydrophobic surface, [27] and drag friction of a liquid flow is also reduced on the corresponding surface. [28]

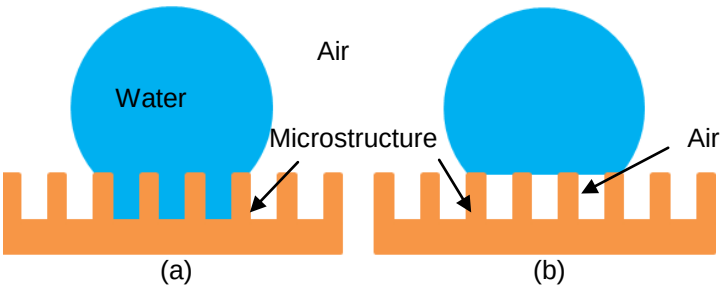

Figure 1.1: Wenzel state (a) and Cassie-Baxter state (b).

The states of wetting are mainly judged indirectly according to the penetration of light through a water droplet [45, 46], the trace of dusts left by the evaporation of a water droplet [45], the shape change of a water droplet [47], or the change in apparent contact angles with the variation of the distance between neighboring pillars [48].

One of the most intriguing topics of wetting is the transition from Cassie-Baxter to Wenzel state. [29-31]. When a liquid/air interface hangs between pillars, for example, in the Cassie-Baxter state, the interface is curved due to the pressure difference across it. [36-38]. If the hanging interface cannot remain pinned at the top corner of pillars, then it will precede downward into the roughness grooves. Even when a liquid-air interface can remain pinned at the corner of pillars, the sag of the curved liquid-air interface may make this interface touch the bottom of the roughness groove [36, 37]. The depinning or sagging may be caused by external stimuli, such as pressure,[29] vibration,[32] electric voltage,[33] or evaporation,[34]. It is expected that, once a liquid-air interface has contact with the groove base due to depinning or sagging, liquid immediately fills the roughness groove, [27, 28, 45, 49, 50] and subsequently the wetting state is changed to that of Wenzel. Accordingly, whether the contact has occurred is employed as a criterion to judge the transition between the two wetting states [27, 28, 45, 50]. For simplicity, the aforementioned transition criterion is called “contact criterion.”

However, in our recent pressing tests on (i) ZnO nanowires-covered microchannels, (ii) ZnO nanowires-covered micropillars, (iii) hydrophobic microballs and (iv) leaf surfaces of three different varieties of lotuses (which are *Carolina Queen*, *Chawan Basu*, and *The President*), [53] we found that the transition did not occur when the contact happened. Therefore, the objective of this dissertation is to exam the applicability of the “contact criterion” on different microstructured surfaces, and to develop a new transition criterion when the contact criterion can’t be of value.

First, although direct observation of wetting states has been conducted using an environmental scanning electron microscope (ESEM) [45, 51] or a goniometer [30], the evolution of air/water interfaces suspended between microstructures has not been reported in the literature during the transition from Cassie-Baxter to Wenzel states. However, this evolution gives the whole picture about the transition process. The corresponding information can be used to validate existing transition criteria, and can also be applied to aid in the establishment of new criteria. As such, with the aid of an optical microscope, we have directly observed the evolution of air/water interfaces suspended between microline-formed PDMS surfaces when the water droplets reduced their sizes during their evaporation and pressing.

Second, as a water drop is placed on microchannels, air/water interfaces suspended on the microchannels have approximately cylindrical shapes. This makes it simple to mathematically model these air/water interfaces. The interfaces between neighboring micropillars have more complicated shapes. For easily characterizing the air/water interfaces, we first explored the case of microchannels, and derived an angle criterion to judge the applicability of the contact criterion, which was subsequently validated by experimental tests.

Third, we further considered the application range of the contact criterion in the case of micropillars. Since the approach used in the case of microchannels did not apply here, a different method was adopted for the corresponding consideration. Employing this method, we also derived an angle inequality, which, to our surprise, is identical to the one derived for the case of microchannels. On the other hand, this angle inequality is both sufficient and necessary conditions in the case of microchannels, while it is only the necessary condition in the case of the micropillars.

Fourth, due to lack of analytical expression of the related air/liquid interfaces in the case of micropillars, we consider the case of circular pillars with vertical sidewalls using a new approach. This approach does not rely on the explicit expression of the interface profile, making it feasible to explore the applicability of the contact criterion. Subsequently, we apply the derived theoretical results to interpret some experimental results shown in both of our previous work and Verho et al. [52].

Fifth and finally, in our recent pressing tests on three different lotus varieties: *Carolina Queen*, *Chawan Basu* and *The President*, we found that the transition did not occur when the contact happened, [53] and thus in this work would like to explore the reason behind. The lotus surface may be structured by micropillars, which are covered with nanopillars. [27] The lotus micropillars were measured [27] and modeled [54] approximately as paraboloids of revolution, which means that these micropillars can be considered as circular pillars whose sidewalls have convex shapes in the vertical planes. In addition, microparticles are also employed to modify surface wetting.[55-58] It is also interesting to know whether the contact criterion applies to the case of microparticles. The microparticles may have spherical shapes, which can also be considered as circular pillars with convex sidewalls. Thus, we would like to explore the applicability of the contact criterion to circular pillars with convex sidewalls.

1.2 Dissertation Outline

Chapter 1 introduced current researches, motivations and objective of this dissertation. Chapter 2 investigated the changes of the air/water interfaces on microline-formed surfaces when the water droplets reduced their sizes during their evaporation and pressing. Chapter 3 explored the application ranges of the contact criterion in the cases of microchannels. Chapter 4 further considered the application range of the contact

criterion in the case of micropillars. Chapter 5 discussed the contact criterion in the case of circular pillars with vertical sidewalls using a new approach. Chapter 6 demonstrated the applicability of the contact criterion to circular pillars with convex sidewalls. Finally, Chapter 7 summarized and concluded this work.

Chapters 2-6 have been published in [77, 79, 82, 63, 88], respectively. Since some other papers [53, 72, 78, 80, 89] are not directly related to this dissertation subject, they are not presented here.

Chapter 2

Transition from Cassie-Baxter to Wenzel States on Microline-formed PDMS Surfaces Induced by Evaporation or Pressing of Water Droplets

In this chapter, we directly observed the evolution of air/water interfaces suspended between polydimethylsiloxane (PDMS) microlines when water droplets reduced their sizes due to evaporation. The inclined angles of the microline sidewalls were slightly larger than 90^0. Two important phenomena were observed regarding the transition from Cassie-Baxter to Wenzel States. Based on these two phenomena, the equilibrium of a triple line and the uniformity of pressure inside a small water droplet, critical values of droplet sizes and Laplace pressure were derived to predict when the transition would occur on microlines. In addition, we also directly observed the evolution of air/water interfaces on PDMS microlines when a water droplet was slowly pressed using a glass slide. The critical values of the droplet sizes derived in the case of evaporation applied to this pressing case as well, and had a good match with experimental results on the three arrays of PDMS microlines. In addition to the cases of evaporation and pressing, the theoretical relationships derived in this work may also apply to other cases, in which Laplace pressure is gradually increased inside a liquid droplet and half sizes of the droplet are less than the capillary length of the liquid. Finally, based on developed transition criteria, a set of criteria were also proposed to design microlines for reducing the critical droplet size that triggers the transitions from Cassie-Baxter to Wenzel States.

2.1 Experimental Design

2.1.1. Experimental Setup

Figure 2.1(a) gives experimental setup used to observe the transition from Cassie-Baxter state to that of Wenzel when a water droplet gradually evaporated. An optical microscope (model: mm0013000m of Metallurgical Microscopes Company) was employed to observe the water droplet. The microscope was rotated by 90º with its sample stage oriented vertically. A glass slide was glued on the sample stage, and had a horizontal orientation. A microline-formed PDMS film was placed on the glass slide. This microscope was applied to observe the evolution of the air/water interfaces suspended between PDMS microlines when the water droplet evaporated on the PDMS film. The viewing direction of the optical microscope was along that of the PDMS microlines.

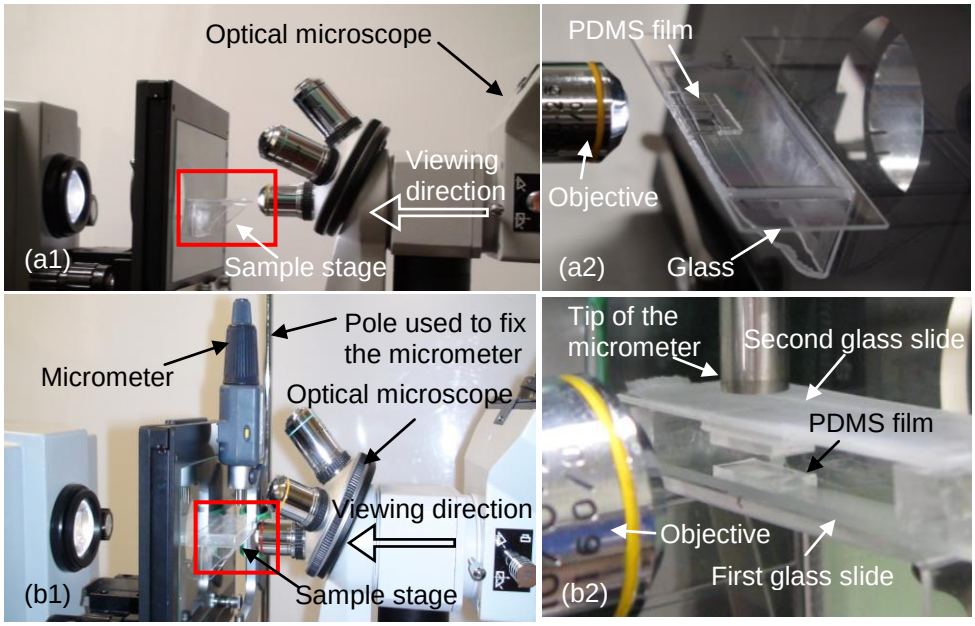

Figure 2.1: (a1) Experimental setup for observing cross-sectional profiles of a water droplet on a microline-formed PDMS surface during the evaporation of the droplet. (a2) Close-up view of the sample stage. (b1) Setup for observing cross-sectional profiles of a water droplet on a microline-formed PDMS surface in the case of pressing. (b2) Close-up view of the sample stage.

Figure 2.1(b) shows experimental setup applied to observe the transition from Cassie-Baxter state to that of Wenzel when a water droplet was slowly pressed. The optical microscope was also employed in this case to directly observe the evolution of the air/water interfaces. A first glass slide was glued on the sample stage of the microscope, and had a horizontal orientation. A microline-formed PDMS film was placed on this glass slide. After a water droplet was loaded on the PDMS film using a syringe. A second glass slide was placed on the droplet. The shapes of the water droplet changed with the distance between the two glass slides. To control this distance, a micrometer (model: SPI IP54 of Swiss Precision Instruments Incorporate) was further put above the second glass slide with its tip against this slide. As such, the distance between the two glass slides could be well controlled as the tip of the micrometer moved down with a precision of 1 μm.

Microlines and micropillars are often applied as structures to enhance surface hydrophobicity. The air/water interfaces suspended between neighboring microlines have approximately cylindrical shapes, whose cross-sectional profiles are easy to observe through side views of the water droplet. The interfaces between neighboring micropillars have more complicated shapes. For easily characterizing the interfaces, microlines were chosen in this work as the surface structures.

The pictures of the air/water interfaces observed through the optical microscope were taken using Minisee software of ScopeTek Company. The dimensions of these interfaces (such as radii of curvature and maximum deflections), as well as their contact angles with PDMS microlines, were determined using MB-Ruler software.

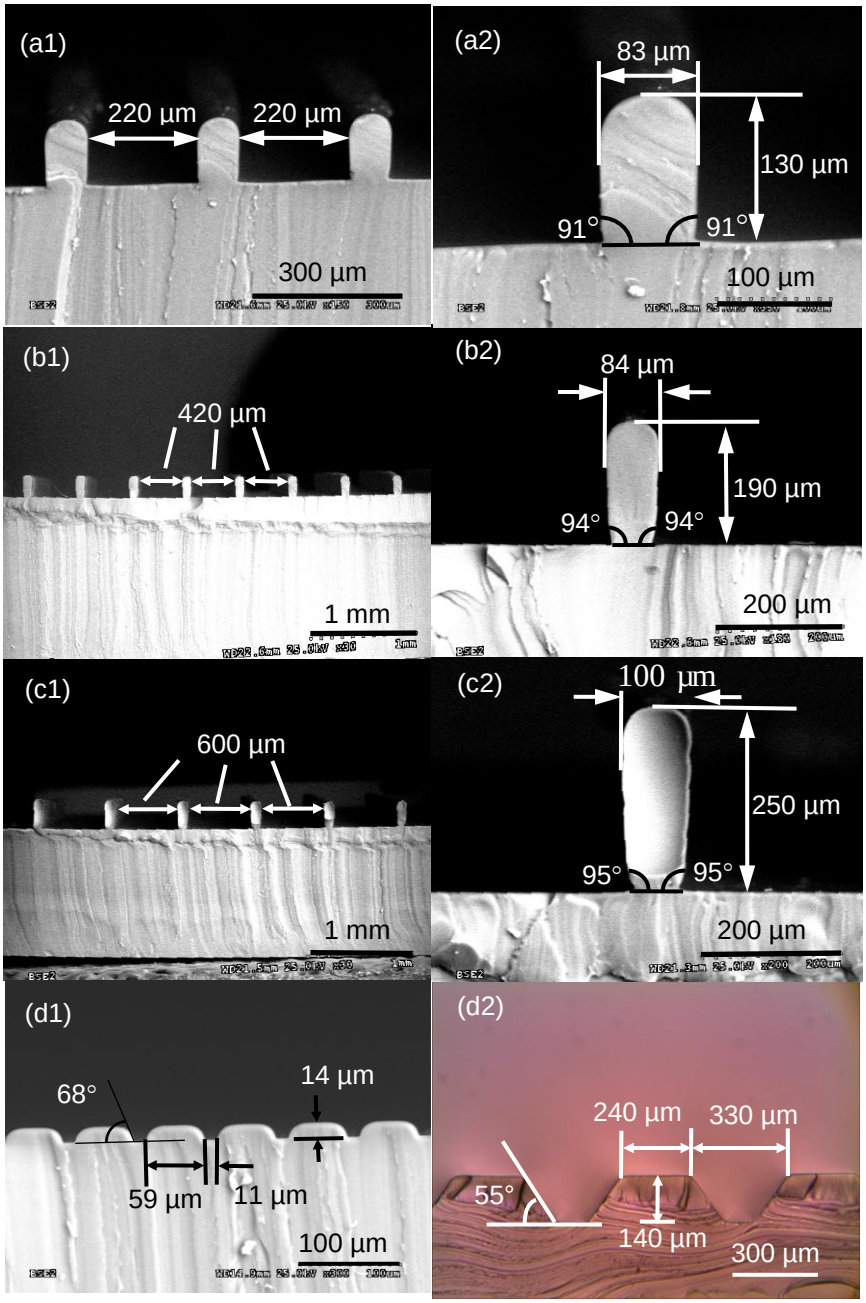

Figure 2.2: Cross-sectional views of five arrays of PDMS microlines. (a-c) First set of three arrays of PDMS microlines, and (d) second set of two arrays of PDMS microlines. (a1)-(d1) are SEM images, while (d2) is an optical picture. The angles marked in this figure were measured on the originally taken pictures, and had measurement error of 2º. The same also applies to Figures 2.3-2.6.

2.1.2 Fabrication Process of Microstructure-formed PDMS Films

Two sets of PDMS microlines were investigated. Their SEM images and dimensions are given in Fig. 2.2. The first set includes three types of microlines, respectively (Figs. 2.2a-2.2c). They differed much in the distances between two neighboring microlines, which are 220 μm, 420 μm and 600 μm, separately. For the sake of simplicity, these three arrays of PDMS microlines are called 220-, 420- and 600-μm lines, respectively. The sidewalls of all these microlines form angles slightly larger than 90^0 with their corresponding substrates (Figs. 2.2(a2), 2.2(b2) and 2.2(c2)). The second set includes two arrays of microlines (Fig. 2.2d). The sidewalls of the two arrays of microlines have angles of 68º and 55º, respectively, with their corresponding substrates. The first set of microlines has relatively large sizes, and was employed to directly observe the transition of the two wetting states. The second set of microlines was used to validate some theoretical predictions, as will be further addressed in section 2.2.3. The two sets of PDMS microlines were generated using a molding approach with either SU-8 or Si structures as molds [48, 59].

All the PDMS microlines considered in this work have flat, smooth sidewalls. The inclined angle of a sidewall refers to the angle formed by the sidewall and the bottom edge of the microline. The top corners of these microlines are round, whose radii are much smaller than both the heights and neighboring distances of the microlines.

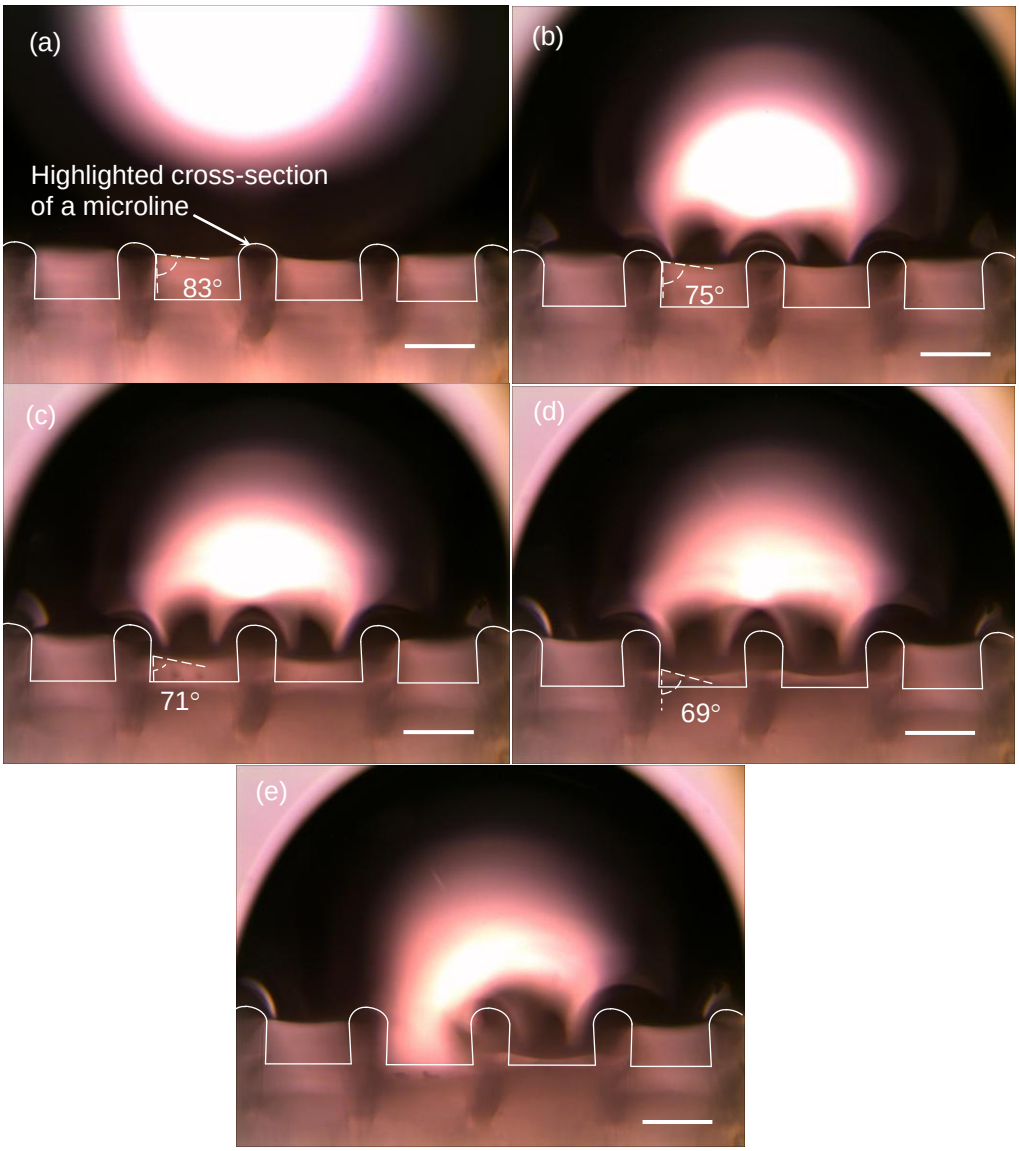

Figure 2.3: Change of an air/water interface on 220-μm lines when a water droplet of volume 5 μl gradually evaporated (see the interface marked with an angle for example): (a) stayed at the top corners of two PDMS microlines at the initial state of evaporation, (b) crossed the low edges of the top corners, (c) moved down along the gap sidewalls, (d) continued to move down along the gap sidewalls, and (e) had contact with the bottom of the gap and collapsed. The clear images of air/water interfaces and microlines may appear at different focus points of the microscope. The above images were obtained by highlighting the profiles of microlines on the clear images of the air/water interfaces. The same techniques were also used to generate the images given in Fig. 2.9. The same transition phenomena were observed as well on 420- and 600-μm lines. For simplicity, the corresponding images are not given here (optical pictures and cross-sectional views).

2.2. Evaporation of Water Droplets

2.2.1. In-situ Observation of Air/Water Interfaces

Four phenomena were observed on the first set of PDMS microlines regarding the evolution of an air/water interface between two neighboring microlines during the evaporation of water droplets (see, for example, Fig. 2.3). First, when a water droplet gradually shrank, the air/water interface between two neighboring microlines increased its deflection but decreased its angles with the sidewalls of these two microlines (see the first two images in Fig. 2.3). In the meanwhile, the two edges of this interface were still at the top corners of the two microlines. Second, once water passed the top corners of these two microlines, it kept moving down and filled the gap between the two microlines (see the last three images in Fig. 2.3). Third, as a water droplet shrank, the number of microlines on which the droplet sat also decreased. Fourth, the gaps between microlines might not be filled simultaneously by water when transition occurred, as seen from Fig. 2.3. Instead, they were filled one by one. In reality, the pressure may be not ideally uniform inside the droplet or the microlines may not be exactly identical. Either cause might lead to the occurrence of this filling phenomenon. The first two phenomena are specifically addressed in the following sub-sections through theoretical models.

2.2.2. Shape change of air/water interfaces on the top corners of microlines

As illustrated in Fig. 2.4, let *abc* denote the cross-sectional profile of the air/water interface between two neighboring microlines. Without loss of generalization, the following analysis focuses on the three-phase (air/liquid/solid) contact line *a* located at one end of *abc*. Due to geometric symmetry, the same analysis also applies to the other three-phase line *c* located at the other end of *abc*. Set θ_0 to be the intrinsic contact angle of *abc* with a microline. This angle is defined to be apparent contact angle of a water

droplet on a smooth film which has the same surface energy as the microline. Accordingly, the surface tensions at *a* are related by well-known Young-Dupré equation [60], which is

$$\gamma_{SA} = \gamma_{SL} + \gamma \cos\theta_0 , \tag{2.1}$$

where γ_{SL} and γ_{SA} denote surface tensions of solid/water and solid/air interfaces, respectively. This equation implies that, if the contact angle of *abc* with a microline is larger than, equal to, or smaller than θ_0, then *a* moves downwards, is stationary or moves upwards on the microline.

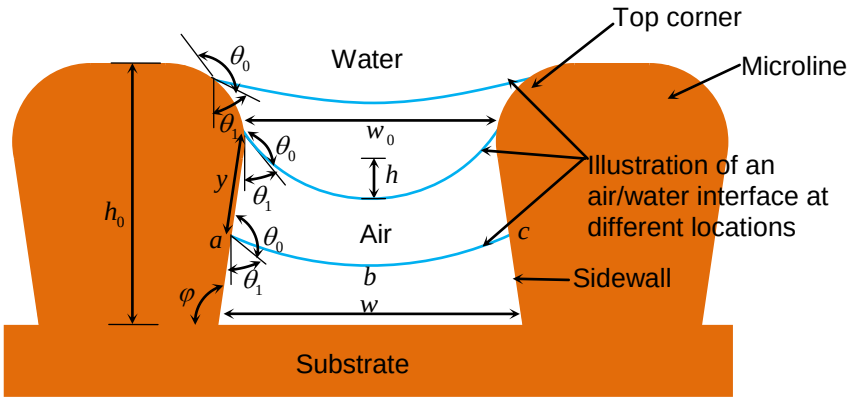

Figure 2.4: Schematic of the cross-sectional profile *abc* of the air/water interface between two neighboring microlines when this interface changed its location during the evaporation of a water droplet.

Let p_a and p_w denote atmospheric pressure and pressure inside a water droplet, respectively. p_a is assumed to be constant during the evaporation. According to Young-Laplace equation [60], the pressure difference across the surface of the water droplet is:

$$p_w - p_a = \gamma(\frac{1}{R_1} + \frac{1}{R_2}) , \tag{2.2}$$

where γ represents surface tension of water, R_1 and R_2 are, respectively, radii of the maximal and minimal curvatures at a point of the water surface, $(p_w - p_a)$ is so-called

Laplace pressure, and the mean curvature at this point is one half of $(\frac{1}{R_1}+\frac{1}{R_2})$. R_1 and R_2 are considered positive if their associated curves on the water surface bend towards air. Eq (2.2) gives the relationship between Laplace pressure and the size of the water droplet. Assume that half sizes of water droplets are less than the capillary length of water (i.e., 2.7 mm). This assumption holds in our case. Small water droplets were used in this work, and their volumes ranged from 1 μl to 6 μl. Consequently, the gravity effect on the droplets can be neglected [29, 40]. Hence, p_w is uniform inside the water droplet. Accordingly, by eq (2.2), $(\frac{1}{R_1}+\frac{1}{R_2})$ is constant on the surface of the water droplet. At the apex of a water droplet, R_1 is the curvature associated with the curve, which passes through the apex along the direction perpendicular to the microlines, while R_2 is the curvature associated with another curve, that passes through the apex along the direction of the microlines. As observed in our tests, before the occurrence of transition, both curves gradually increase their bending degrees during the evaporation, implying that both $(\frac{1}{R_1}+\frac{1}{R_2})$ and $(p_w - p_a)$ increase with the size reduction of the water droplet.

Since the span of the water droplet along the microline direction is much larger than the distance between two neighboring microlines, the air/water interface between two neighboring microlines is considered to have a cylindrical shape, whose cross-sectional profile (e.g., *abc*) is what was observed through the optical microscope. The two principal curvatures at a point of *abc* are, respectively, 0 and $\frac{1}{R}$, where R denotes the radius of curvature. Therefore, at this point,

$$\frac{1}{R_1}+\frac{1}{R_2}=\frac{1}{R}. \qquad (2.3)$$

Since $(\frac{1}{R_1}+\frac{1}{R_2})$ is constant on the surface of the water droplet, R should be constant along *abc*. Thus, *abc* is a circular arc of radius R. Set θ_1 to be the angle subtended by the tangent to *abc* at *a* and the vertical direction. Let *h* denote the deflection of *abc* at its middle point. It is also the maximum deflection of *abc*. Set w_0 to be the distance between the two top corners of the gap. Based on eq (2.3) and simple geometric analysis, on the top corner of a microline, it is readily derived:

$$\cos\theta_1 = \frac{w_0}{2}(\frac{1}{R_1}+\frac{1}{R_2}),\ h = (\frac{1}{R_1}+\frac{1}{R_2})^{-1} - \sqrt{(\frac{1}{R_1}+\frac{1}{R_2})^{-2} - \frac{{w_0}^2}{4}}\ . \qquad (2.4)$$

It can be observed from these two relationships that, on the top corner of a microline, θ_1 and *h* decrease and increase, respectively, with the size reduction of the water droplet during the evaporation, which interprets the first phenomenon described in section 2.2.1.

On the first set of PDMS microlines, θ_1, *h* and $\frac{1}{R}$ can be determined according to the observed profiles of *abc*. Therefore, experimentally measured relationships of θ_1 and *h* with $(\frac{1}{R_1}+\frac{1}{R_2})$, which equals $\frac{1}{R}$ at *abc*, are compared with the corresponding relationships predicted by eq (2.4). As shown in Figs. 2.5 and 2.6, the experimental relationships match well with the theoretical relationships, indicating that eq (2.4) may give good prediction of θ_1 and *h* based on the value of $(\frac{1}{R_1}+\frac{1}{R_2})$ during the evaporation.

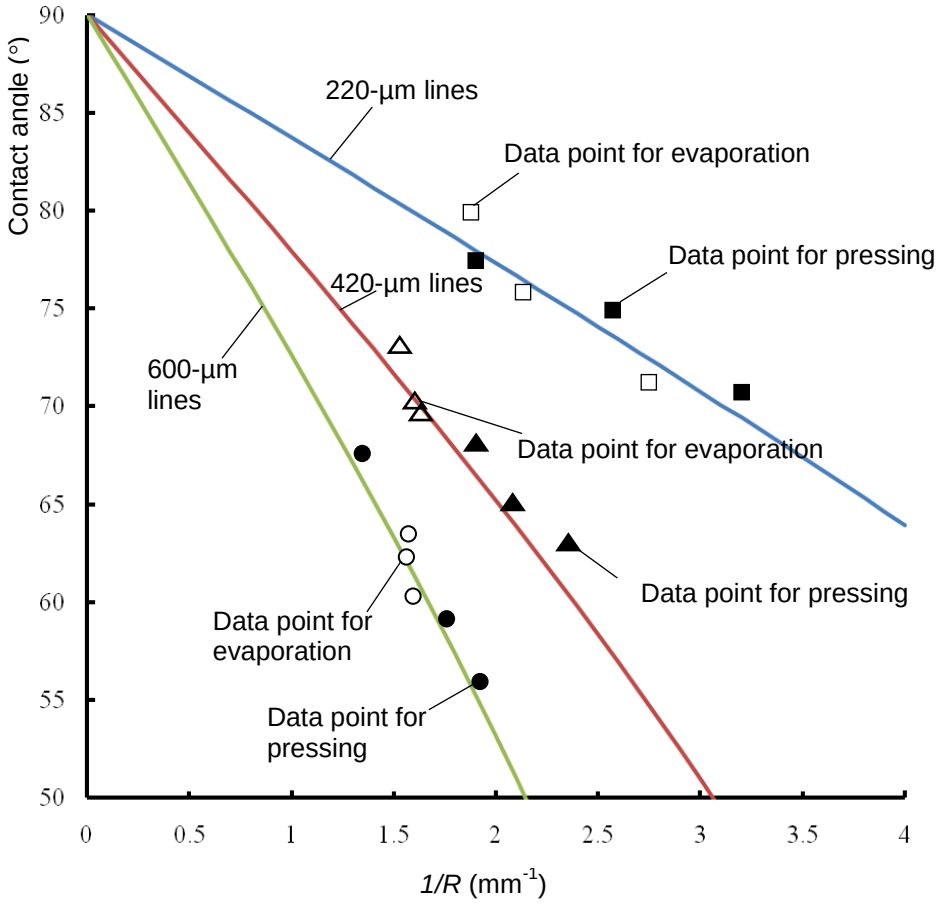

Figure 2.5: Comparison of eq $(2.4)_1$ with experimental results in the cases of evaporation and pressing.

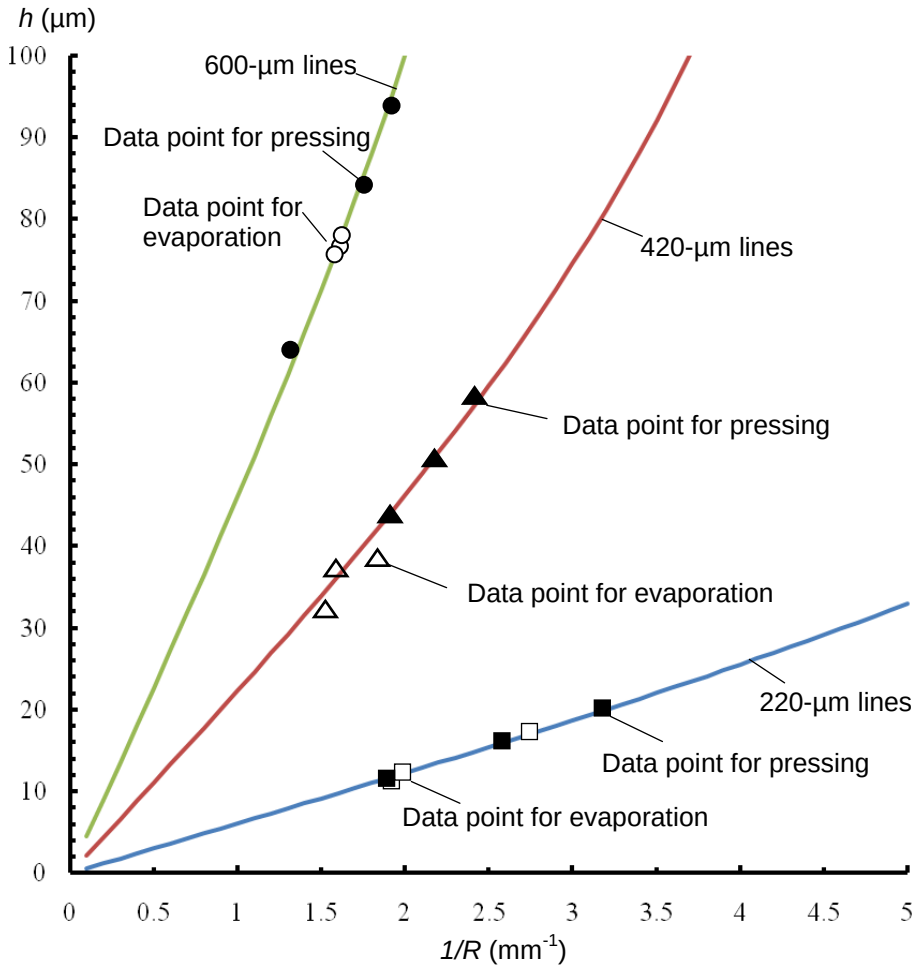

Figure 2.6: Comparison of eq $(2.4)_2$ with experimental results in the cases of evaporation and pressing.

2.2.3 Critical Values of Heights, Drop Sizes and Laplace Pressure

2.2.3.1. Critical heights of microlines.

As illustrated in Fig. 2.4, as θ_1 gradually decreases, *a* should change its location on the top corner of a microline to ensure that it is in the state of equilibrium. Set φ to be the angle between the sidewall and bottom of the microline. This angle ranges between 0 and 180^0. Let's consider a special case: put a water droplet only on the top surface of a single line and gradually increase the volume of this droplet by adding extra water at its center. Then, when the water droplet spreads over the top corner of the line, *a* is stationary on the top corner if θ_1 falls in the range

$$270^0 - \varphi - \theta_0 \le \theta_1 \le 270^0 - \theta_0, \tag{2.5}$$

which is actually so-called Gibbs inequality condition expressed in terms of θ_1 [62]. In this case, the inequality has the following geometric meaning [62]: when *a* is in the state of equilibrium while changes its location around the top corner of the line from the top edge to the low edge of this corner, θ_1 decreases from $270^0 - \theta_0$ to $270^0 - \varphi - \theta_0$. However, in our case, a water droplet sat on at least two microlines, and its volume was gradually decreased due to evaporation. Therefore, condition (2.5) does not entirely apply to our case. During the evaporation, a water droplet normally curves up at its apex before the occurrence of evaporation, such as in our tests, indicating that $(\frac{1}{R_1} + \frac{1}{R_2})$ is positive. By eq (2.3), $\frac{1}{R}$ is also positive. Consequently, the interface *abc* should curve down. According to the geometry (Fig. 2.4), θ_1 should be less than 90^0. Thus, with the aid of eq (2.5), when *a* is stationary at the top corner, the range of θ_1 is

$$270^0 - \varphi - \theta_0 \le \theta_1 < 90^0, \tag{2.6}$$

which gives the limits of θ_1 in eq $(2.4)_1$.

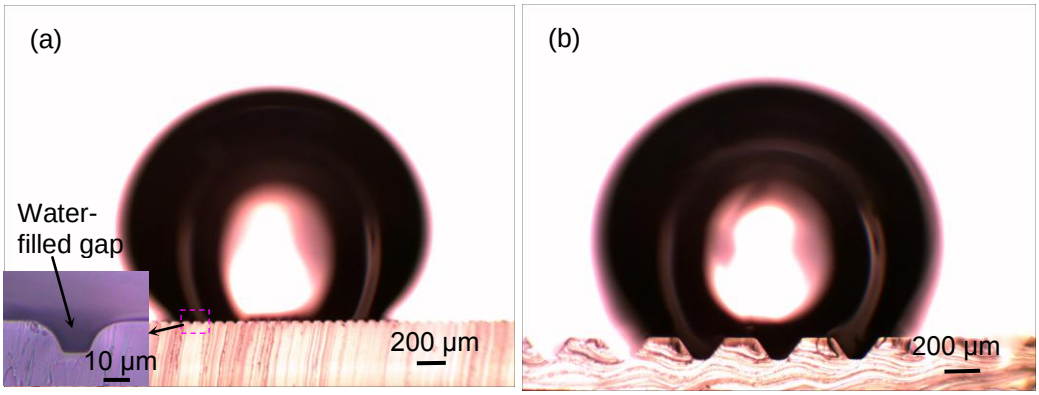

Figure 2.7: After water droplets of volumes 5 μl had been placed on the second set of PDMS microlines, water immediately filled the gaps between the PDMS microclines, whose values of φ were (a) 68º and (b) 55º, respectively. The close-up views of the corresponding microlines are given in Figs. 2.2(d1) and 2.2(d2), respectively (optical pictures and cross-sectional views).

In view of eq (2.6) and the geometric meaning of φ, we have

$$180^0 - \theta_0 < \varphi < 180^0. \tag{2.7}$$

Following the same reasoning, conditions (2.6) and (2.7) also apply to the situation when *a* is stationary on the sidewall of a microline. In this work, the value of θ_0 was considered to be the apparent contact angle on a smooth PDMS film. It was measured to be 105^0. By eq (2.6), the minimum values of θ_1 on 220-, 420- and 600-μm lines are 74^0, 70^0 and 69^0, respectively. They are close to experimentally measured results (see, for instance, Fig. 2.3b), which are 75^0, 74^0 and 66^0 separately. In addition, in view of eq (2.7), we should have $75^0 < \varphi < 180^0$. This requirement implies that, if $\varphi < 75^0$, then *a* could not be stationary on the top corner and sidewall of the corresponding PDMS microline. This point was validated on the second set of PDMS microlines, whose values of φ are 68^0 and 55^0. Water droplets of volumes in the range of 1 μl to 6 μl were placed on this set of

two arrays of microlines. When any of these droplets was put on either array of PDMS microlines, water immediately filled the gap between two neighboring microlines (Fig. 2.7), indicating that *a* could be stationary neither on the top corners nor at the sidewalls of this set of microlines. In case $\theta_0 < 90^0$ (i.e., the material of a microline is hydrophilic), it follows from eq (2.7) that φ should be at least greater than 90^0. Otherwise, *a* could not be stationary at the top corner and sidewall of the microline. This point was also validated by putting droplets of an isopropyl alcohol solution (IPA) (91% IPA and 9% water by volume; CVS Pharmacy) on the second set of PDMS microlines. IPA immediately filled the gap between two neighboring microlines. The value of θ_0 between IPA and PDMS was measured to be 34^0.

With eq $(2.4)_1$, the particular value of $(\frac{1}{R_1}+\frac{1}{R_2})$ for θ_1 to equal $270^0-\varphi-\theta_0$, i.e., for *a* located at the low edge of the top corner, is:

$$(\frac{1}{R_1}+\frac{1}{R_2})_{pa}=\frac{2\cos(270^0-\varphi-\theta_0)}{w_0}. \tag{2.8}$$

In the above discussions, the gaps between neighboring microlines are considered deep. If the gaps are shallow, then it is possible that *abc* has direct contact with the bottom of a gap when *a* is still on the top corner of a microline, making the transition occur. If *a* is located at the low edge of the top corner, then it follows from eqs $(2.4)_2$ and (2.8) that the critical value of *h* is

$$h_{cr}=\frac{w_0[1-\sin(270^0-\varphi-\theta_0)]}{2\cos(270^0-\varphi-\theta_0)}, \tag{2.9}$$

which is also the maximum deflection of *abc* when *a* is at the top corner. To avoid the contact of *abc* with the bottom of the gap, the height of the microlines, h_0, should be above this critical value. By eq (2.9), the values of h_{cr} for 220-, 420- and 600-μm lines

are 14 μm, 18 μm, and 24 μm**,** respectively, less than the heights of the corresponding lines, which are 130 μm, 190 μm and 250 μm, separately. Hence, as observed from Fig. 2.3(a), *abc* did not have contact with the bottom of the gap when *a* was located at the top corner of any of these lines.

If $h_0 < h_{cr}$, then, according to simple geometric analysis and with the aid of eq (2.3), the critical value of θ_1 and $(\frac{1}{R_1}+\frac{1}{R_2})$ for the transition to occur are, respectively,

$$\theta_{1cr} = \arccos[\frac{2h_0 w_0}{({w_0}^4 + 4{h_0}^4)^{0.5}}], \qquad (\frac{1}{R_1}+\frac{1}{R_2})_{cr} = \frac{4h_0}{({w_0}^4 + 4{h_0}^4)^{0.5}}. \qquad (2.10)$$

These two equations are equivalent in the sense that one equation can be derived from the other. The procedure used to derive eq $(2.10)_2$ has been previously adopted in [47] and [62] to determine $(\frac{1}{R_1}+\frac{1}{R_2})_{cr}$ in terms of h_0 for the case that a water droplet evaporated on micropillars (when $h_0 < h_{cr}$). However, the situation that $h_0 > h_{cr}$ was not considered in these two references.

2.2.3.2 Critical values of droplet sizes and Laplace pressure in case $180^0 - \theta_0 < \varphi < 90^0$

In the following discussions, we assume that $h_0 > h_{cr}$. After the water droplet continues to evaporate, making the value of $(\frac{1}{R_1}+\frac{1}{R_2})$ larger than the particular value given in eq (2.8), by eqs $(2.4)_1$ and (2.8), θ_1 is smaller than $270^0 - \varphi - \theta_0$. Consequently, the contact angle between *abc* and the microline is larger than θ_0 . As implied by eq (2.1), the surface tensions at *a* yield a downward force, making *a* cross the low edge of the top corner.

Assume that *a* is in the state of equilibrium at a point on the sidewall. Let *y* denote the distance between this point and the low edge of the top corner measured along the sidewall. According to the geometry (Fig. 2.4), *y* ranged from 0 to $\frac{h_0}{\sin\varphi}$. Set *w* to be the width of the gap measured at the location of *a*. Then,

$$w = w_0 - 2y\cos\varphi . \tag{2.11}$$

With w_0 replaced by *w*, eq $(2.4)_1$ also applies to this state of equilibrium. In order for *a* to be stationary on the straight sidewall of the gap, in view of the geometry (Fig. 2.4) and eq (2.1), θ_1 should equal $270^0 - \varphi - \theta_0$. To make this condition satisfied, invoking eqs $(2.4)_1$ and (2.8), we have

$$w(\frac{1}{R_1} + \frac{1}{R_2}) = w_0(\frac{1}{R_1} + \frac{1}{R_2})_{pa} . \tag{2.12}$$

In case $180^0 - \theta_0 < \varphi < 90^0$, which holds only if $90^0 < \theta_0$ (i.e., the material of the microlines is hydrophobic), with the aid of eq (2.11), it follows from eq (2.12) that

$$(\frac{1}{R_1} + \frac{1}{R_2}) = \frac{w_0}{w_0 - 2y\cos\varphi}(\frac{1}{R_1} + \frac{1}{R_2})_{pa} . \tag{2.13}$$

This equation indicates that $(\frac{1}{R_1} + \frac{1}{R_2})$ increases with *y*. It is possible that, although the condition (2.12) is met, *abc* has direct contact with the bottom of a gap, making the transition occur. Based on geometric analysis, this contact happens when *y* equals a critical value

$$y_{cr} = h_0 \frac{\cos\theta_0 + \cos\varphi\sin(270^0 - \varphi - \theta_0)}{\cos\theta_0 \sin\varphi} + w_0 \frac{1 - \sin(270^0 - \varphi - \theta_0)}{2\cos\theta_0}. \tag{2.14}$$

This equations shows that y_{cr} increases with the increase in h_0 and the decrease in w_0. Two limits of y_{cr} can be found from this equation. As $\varphi \to 180^0 - \theta_0$,

$y_{cr} \to 0$. When $\varphi \to 90^0$, $y_{cr} \to h_0 + \frac{w_0(1-\sin\theta_0)}{2\cos\theta_0}$. y_{cr} is also the maximum value of *y* that allows *a* to be stationary on the sidewall. Accordingly, by eq (2.13), the critical value of $(\frac{1}{R_1}+\frac{1}{R_2})$ for *a* not to be stationary at any point on the sidewall is

$$(\frac{1}{R_1}+\frac{1}{R_2})_{cr} = \frac{w_0}{w_0 - 2y_{cr}\cos\varphi}(\frac{1}{R_1}+\frac{1}{R_2})_{pa}. \tag{2.15}$$

This relationship also gives the ratio between $(\frac{1}{R_1}+\frac{1}{R_2})_{cr}$ and $(\frac{1}{R_1}+\frac{1}{R_2})_{pa}$, which is $\frac{w_0}{w_0 - 2y_{cr}\cos\varphi}$. This ratio shows how much change is needed in $(\frac{1}{R_1}+\frac{1}{R_2})$ to make the transition occur after *a* crosses the low edge of a top corner. With the aid of eq (2.8), it follows from eq (2.15) that

$$(\frac{1}{R_1}+\frac{1}{R_2})_{cr} = \frac{2\cos(270^0 - \varphi - \theta_0)}{w_0 - 2y_{cr}\cos\varphi}. \tag{2.16}$$

This equation indicates that the critical droplet size for the transition to occur decreases with the increase in θ_0 and the decrease in w_0.

By eqs (2.2) and (2.16), the critical value of $(p_w - p_a)$ is:

$$(p_w - p_a)_{cr} = \frac{2\gamma\cos(270^0 - \varphi - \theta_0)}{w_0 - 2y_{cr}\cos\varphi}. \tag{2.17}$$

This relationship shows that the critical Laplace pressure for the transition to occur increases with the increase in θ_0 and the decrease in w_0. Eqs (2.16) and (2.17) are suited to predict $(\frac{1}{R_1}+\frac{1}{R_2})_{cr}$ and $(p_w - p_a)_{cr}$, respectively. They are equivalent in the sense that one equation can be derived from the other.

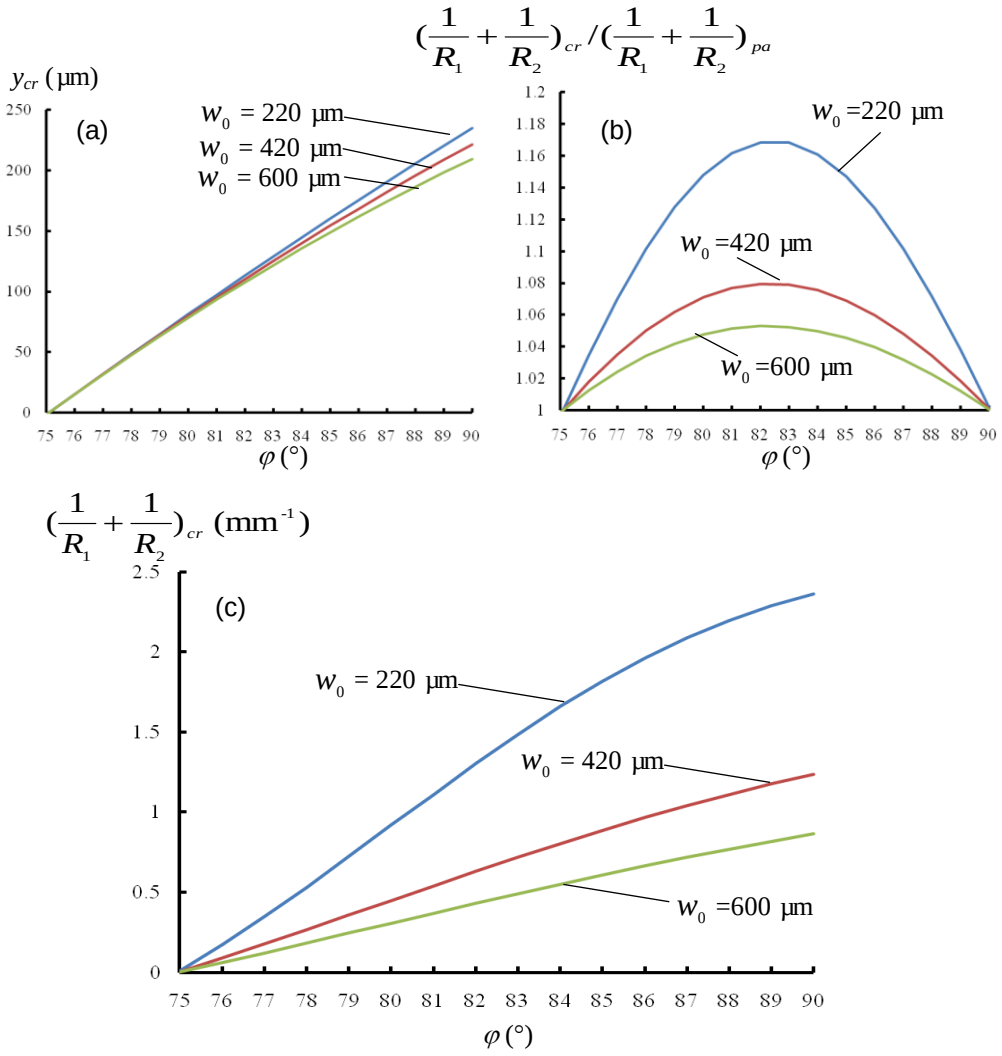

Figure 2.8: Theoretical relationships of (a) y_{cr} with φ, (b) $(\frac{1}{R_1}+\frac{1}{R_2})_{cr}/(\frac{1}{R_1}+\frac{1}{R_2})_{pa}$ with φ, and (c) $(\frac{1}{R_1}+\frac{1}{R_2})_{cr}$ with φ, when $75° < \varphi < 90°$ ($\theta_0 = 105°$) for three arrays of PDMS microlines whose widths are given in the figure. These microlines have the same height of 250 μm.

In addition, it is noticed that, after h_0, w_0 and θ_0 are given, the values of y_{cr}, $(\frac{1}{R_1}+\frac{1}{R_2})_{cr}/(\frac{1}{R_1}+\frac{1}{R_2})_{pa}$ and $(\frac{1}{R_1}+\frac{1}{R_2})_{cr}$ vary with φ. To have a better understanding about the corresponding changes, we apply eqs (2.14)-(2.16) to three arrays of PDMS microlines, whose values of w_0 are the same as those of 220-, 420- and 600-μm lines, respectively (Fig. 2.8). The arrays of microlines are set to have the same height of 250 μm. Figure 2.8(a) gives three relationships of y_{cr} with φ for the three arrays of PDMS icrolines, respectively, when φ ranges from 75º to 90º. As observed from Fig. 2.8(a), in addition to increasing with the decrease in w_0, y_{cr} also increases with the increase in φ on these three arrays of PDMS microlines. This observation implies that the interface *abc* can be stationary deep inside a gap if w_0 is small and φ approaches 90º, i.e., if the gap is narrow and the inclined angle of the microline sidewall is close to 90º Figure 2.8(b) shows the changes of $(\frac{1}{R_1}+\frac{1}{R_2})_{cr}/(\frac{1}{R_1}+\frac{1}{R_2})_{pa}$ with φ. Two points are observed from this figure. First, the ratios increase with the decrease in w_0 for the three arrays of microlines. Second, the ratios increase from the minimum value of 1 to the maximum values of 1.17, 1.08 and 1.05, respectively, for the three arrays of microlines, when φ increases from 75º to 82º, and decrease from these maximum values to 1 when φ increases from 82º to 90º. According to the second point, on any of the three arrays of microlines, when φ is 82º, a relatively large change is needed in $(\frac{1}{R_1}+\frac{1}{R_2})$ to make the transition occur after *a* crosses the low edge of a top corner. However, when φ is close to 90º, only a slight change in $(\frac{1}{R_1}+\frac{1}{R_2})$ is needed to make the transition happen. Figure 2.8(c) gives the changes of

$(\frac{1}{R_1}+\frac{1}{R_2})_{cr}$ with φ. On any of the three arrays of PDMS microlines, the values of $(\frac{1}{R_1}+\frac{1}{R_2})_{cr}$ increase with φ, making the transition more difficult to occur if φ is close to 90º.

2.2.3.3. Critical values of droplet sizes and Laplace pressure in case $90^0 \le \varphi < 180^0$

For the case that $90^0 \le \varphi < 180^0$, as seen from eq (2.11), *w* is equal to or larger than w_0. Also, due to the continuous evaporation of the water droplet, when *a* is inside the gap, the value of $(\frac{1}{R_1}+\frac{1}{R_2})$ is larger than that of $(\frac{1}{R_1}+\frac{1}{R_2})_{cr}$. Accordingly, eq (2.12) does not hold, and $\theta_1 < 270^0 - \varphi - \theta_0$. Hence, *a* is not stationary on the sidewall. Once it crosses the low edge of the top corner, it keeps moving down until the water fills the gap, which interprets the second phenomenon described in Sub-section 2.3.1. Accordingly, in case $90^0 \le \varphi < 180^0$, the particular value given in eq (2.8) is also the critical value of $(\frac{1}{R_1}+\frac{1}{R_2})$ for a water droplet to have the transition from Cassie-Baxter to Wenzel States. That is,

$$(\frac{1}{R_1}+\frac{1}{R_2})_{cr} = \frac{2\cos(270^0 - \varphi - \theta_0)}{w_0}. \qquad (2.18)$$

This equation indicates that the critical droplet size for the transition to occur decreases with the decrease in w_0. For fixed θ_0 and w_0, the value of $(\frac{1}{R_1}+\frac{1}{R_2})_{cr}$ varies with φ. For PDMS microlines of a fixed w_0, the largest value of $(\frac{1}{R_1}+\frac{1}{R_2})_{cr}$ is $\frac{2}{w_0}$, which corresponds

to that $\varphi = 165^0$. With the help of eqs (2.2) and (2.3), it follows from eq (2.18) that the critical value of $(p_w - p_a)$ is

$$(p_w - p_a)_{cr} = \frac{2\gamma \cos(270^0 - \varphi - \theta_0)}{w_0} . \quad (2.19)$$

This relationship shows that the critical Laplace pressure for the transition to occur increases with the decrease in w_0. For PDMS microlines of a fixed width, the largest value of critical Laplace pressure is $\frac{2\gamma}{w_0}$, which also corresponds to that $\varphi = 165^0$.

Eqs (2.18) and (2.19) are good to predict $(\frac{1}{R_1} + \frac{1}{R_2})_{cr}$ and $(p_w - p_a)_{cr}$, separately, for the case that $90^0 \le \varphi < 180^0$, and they are also equivalent. It is difficult to directly measure $(p_w - p_a)$ but relatively easier to determine $(\frac{1}{R_1} + \frac{1}{R_2})$ according to the shape of *abc* or the cross-sectional profiles of a water droplet at its apex. In this work, the critical values predicted by eq (2.17) were compared with the corresponding values experimentally determined on the first set of PDMS microlines. By eq (2.18), the values of $(\frac{1}{R_1} + \frac{1}{R_2})_{cr}$ predicted on 220-, 420- and 600-μm lines are 2.4 mm^{-1}, 1.6 mm^{-1}, and 1.2 mm^{-1}, respectively. On each array of the microlines, based on eq (2.3), the corresponding value of $(\frac{1}{R_1} + \frac{1}{R_2})_{cr}$ was experimentally determined at *abc* since the profile of *abc* could be directly observed using the optical microscope (see, for example, Fig. 2.3). The values of $(\frac{1}{R_1} + \frac{1}{R_2})_{cr}$ found on the 220-, 420- and 600-μm lines are 2.8 mm^{-1}, 1.5 mm^{-1} and 1.2 mm^{-1}**,** respectively. The comparison of the theoretical and experimental results indicates

that they match well. Consequently, eq (2.18) can be potentially applied to give good prediction of $(\frac{1}{R_1}+\frac{1}{R_2})_{cr}$ when a water droplet evaporates on microlines.

2.2.3.4. Design criteria of microlines

The microlines should have liquid-repellent surfaces such that a liquid droplet is easy to roll off from these microlines. This implies that $\theta_0 > 90^0$. According to eqs (2.9), (2.15) and (2.18), which give the expressions of h_{cr} , $(\frac{1}{R_1}+\frac{1}{R_2})_{cr}$ in the case of $180^0-\theta_0 < \varphi < 90^0$, and $(\frac{1}{R_1}+\frac{1}{R_2})_{cr}$ in the case of $90^0 \le \varphi < 180^0$, respectively, the following criteria are developed to design microlines for reducing the critical size of a liquid droplet that triggers the transition from Cassie-Baxter to Wenzel states.

(i) If $90^0 \le \varphi < 180^0$, then by eq (2.18) one should set $\varphi = 270^0 - \theta_0$ and w_0 should be as small as possible. Consequently, the value of $(\frac{1}{R_1}+\frac{1}{R_2})_{cr}$ is large, and the critical size of a liquid droplet for the occurrence of transition is small. After w_0 and φ are chosen, h_0 should be larger than h_{cr} , which is given in eq (2.9).

(ii) If $180^0-\theta_0 < \varphi < 90^0$, then by eq (2.16) w_0 should also be as small as possible. φ can be any allowable value. When y_{cr} is large enough (i.e., if h_0 is selected to be large enough as observed from eq (2.14)), for any chosen φ , the value of $(\frac{1}{R_1}+\frac{1}{R_2})_{cr}$ is still large. Consequently, the critical droplet size for the occurrence of transition is small. In case the largest value of h_0 is fixed by, for example, the limitation of fabrication, this largest value should be chosen for h_0. Naturally, h_0

should also be larger than h_{cr} . Subsequently, by eq (2.16) one can find the optimal value of φ that results in the maximum value of $(\frac{1}{R_1}+\frac{1}{R_2})_{cr}$. Furthermore, in comparison of this maximum value of $(\frac{1}{R_1}+\frac{1}{R_2})_{cr}$ with that given in Case (i), the one can further decide which criteria (i.e., the criteria in either Case (i) or (ii)) should be adopted to determine the values of φ , w_0 and h_0 .

The above design criteria are obtained from the standpoint of reducing the critical droplet size. They may not be compatible with other requirements. For example, w_0 needs to be large in case the apparent contact angle of a droplet on the microlines is expected to be large. However, according to the above design criteria, w_0 should be small. If this is the case, an appropriate value should be chosen for w_0 such that the requirements of critical droplet sizes and apparent contact angles could be both met to a certain degree.

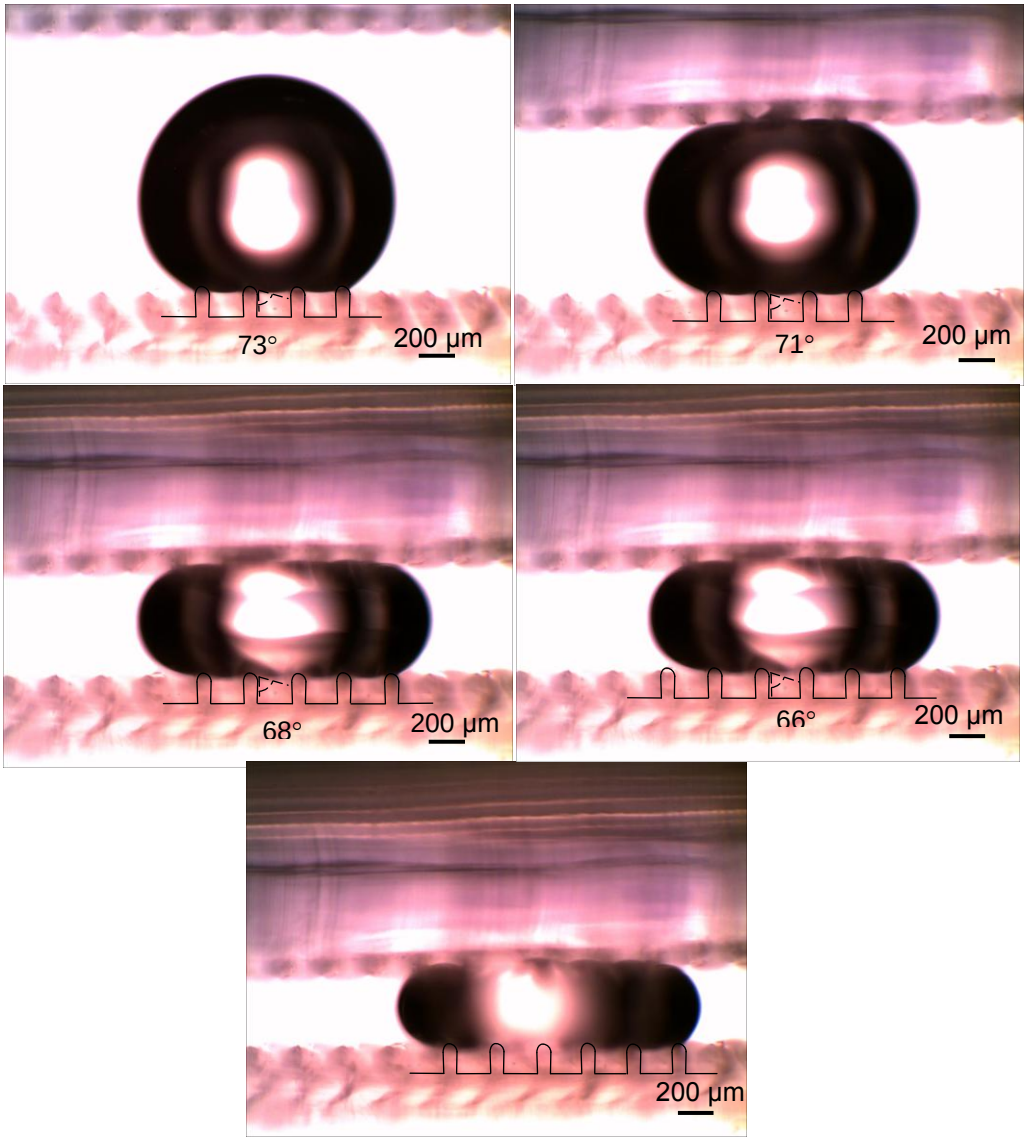

Figure 2.9: Change of an air/water interface on 220-µm lines when a water droplet of volume 5 µl was slowly pressed by a glass slide (see the interface marked with an angle for example): (a) stayed at the top corners of two PDMS microlines at the initial state of pressing, (b) crossed the low edges of the top corner, (c) moved down along the gap sidewalls, (d) continued to move down along the gap sidewalls, and (e) had contact with the bottom of the gap and collapsed. The same transition phenomena were also observed on 420- and 600-µm lines. For simplicity, the correponding images are not presented here (optical pictures and cross-sectional views).

2.3 Pressing of Water Droplets

In Section 2.2.1, the occurrence of transition is essentially due to the increase of p_w, which is induced by the evaporation of the corresponding water droplet. In addition to evaporation, p_w may also be gradually increased by slowly pressing a water droplet using a rigid plate, causing the occurrence of transition, as previously investigated in [29]. We also examine in this pressing case the relationships given in eqs (2.4), (2.6) and (2.18). Using the setup shown in Fig. 2.1(b), that is similar to the one used in [29], a water droplet was slowly pressed by a glass slide when a micrometer above the glass slide was screwed down. As in the case of evaporation, the changes of *abc* on microlines during a pressing process were also captured with the aid of the optical microscope (see, for instance, Fig. 2.9). Four phenomena were also observed during the pressing process. They are similar to those observed in the case of evaporation except for the third phenomenon. When a droplet was deeply pressed, the number of microlines on which the droplet sat did not decrease but might increase due to the spreading of this droplet along the horizontal directions (Fig. 2.9).

The corresponding values of θ_1, h and $\frac{1}{R}$ were determined in view of the observed profiles of *abc*. Figures 2.5 and 2.6 give the comparison of the experimental and theoretical results. The experimentally measured relationships of θ_1 and h with $(\frac{1}{R_1}+\frac{1}{R_2})$ have a good agreement with the corresponding relationships predicted by eq (2.4). By eq (2.6), the minimum values of θ_1 on 220-, 420- and 600-μm lines are 74º, 70º and 69º, respectively. They are close to experimentally measured results (see, for example, Fig. 2.9b), which are 71º, 68º and 66º separately. The values of $(\frac{1}{R_1}+\frac{1}{R_2})_{cr}$

measured on the 220-, 420- and 600-μm lines are 2.9 mm^{-1}, 1.5 mm^{-1}, and 1.2 mm^{-1}, respectively, which also have a good match with the corresponding values predicted by eq (2.18), which are 2.4 mm^{-1}, 1.6 mm^{-1}, and 1.2 mm^{-1}, separately. Consequently, eq (2.18) may also be applied to give good prediction of $(\frac{1}{R_1}+\frac{1}{R_2})_{cr}$ when a water droplet is pressed on microlines. Accordingly, the set of criteria developed in the evaporation case for designing microlines may apply as well to this pressing case.

2.4 Summary and Conclusions

In this chapter, we directly observed the evolution of air/water interfaces suspended between PDMS microlines when water droplets reduced their sizes due to evaporation or pressing. The inclined angles of the microline sidewalls were slightly larger than 90^0. Four important phenomena were observed regarding the transition from Cassie-Baxter to Wenzel States. Based on these two phenomena, the equilibrium of a triple line and the uniformity of pressure inside a small water droplet, critical values of the droplet sizes and Laplace pressure were derived to predict when the transition would occur on microlines. The predicted values of droplet sizes for the case that the inclined angles of these sidewalls are larger than 90^0 were validated by experimental results on three arrays of PDMS microlines in both cases of evaporation and pressing. The derived theoretical relationships indicate that air/water interfaces may be stationary on top corners and sidewalls of microlines if the inclined angles of the microline sidewalls are less than 90^0. Otherwise, the interfaces can only be stationary at the top corners of the microlines. In addition to the cases of evaporation and pressing, the theoretical relationships derived in this work may also apply to other cases, in which Laplace pressure is gradually increased inside a liquid droplet and half sizes of the droplet are

less than the capillary length of the liquid. Finally, based on developed transition criteria, a group of criteria were also proposed to design microlines for reducing the critical droplet size that triggers the transitions from Cassie-Baxter to Wenzel States.

Chapter 3

A Stable Intermediate Wetting State after a Water Drop Contacts the Bottom of a Microchannel or Is Placed on a Single Corner

In this chapter, we show that this transition criterion does not always hold true in the case of microchannels. We first theoretically prove that, when an angle criterion is satisfied, there may exist an intermediate wetting state inside a microchannel after a water drop contacts the bottom of the microchannel. In this wetting state, water does not completely fill the microchannel, and air pockets still exist in its bottom corners. Also, the wetting state is stable in the sense that its energy state is lower than that of the Wenzel model. According to the angle criterion, such intermediate states may exist, for example, in microchannels with vertical sidewalls when contact angles on the inner surfaces of these microchannels are larger than 135^0. In addition to microchannels, the aforementioned intermediate state may also exist on a single corner (which is formed by a horizontal plate and an inclined plate), when the angle criterion is met. After theoretical modeling, we then conduct four types of tests on single corners and microchannels to validate the angle criterion. In these tests, once the angle criterion is met, stable intermediate states are observed on the corresponding samples. In addition, it is found from the two types of tests conducted on microchannels that, once Laplace pressure inside a water drop is gradually reduced, such an intermediate wetting state may be transited back to the original Cassie-Baxter state. On the other hand, Wenzel state may not have such a reversal transition unless an additional force is applied to overcome energy barrier between Wenzel and Cassie-Baxter states.

3.1 Theoretical Analysis

3.1.1 Creation of an Equilibrium State inside a Microchannel

Micropillars and microchannels are often applied as structures to enhance surface hydrophobicity. [23, 24, 26, 29, 30, 37, 38, 45-50, 62, 65] As a water drop is placed on microchannels, air/water interfaces suspended on the microchannels have approximately cylindrical shapes. This makes it simple to mathematically model these air/water interfaces. The interfaces between neighboring micropillars have more complicated shapes. For easily characterizing the air/water interfaces, microchannels are chosen in this work as the surface structures.

As illustrated in Fig. 3.1(a), let *abc* denote the cross-sectional profile of the air/water interface suspended on the top edges of a microchannel when a water drop is placed on a microchannel-formed surface. Set φ to be the angle formed by the sidewall and bottom of the channel. We have $0 < \varphi < 180^0$. Let *h* denote the deflection of *abc* at its middle point *b*. It is also the maximum deflection of *abc*. Use *ed* to represent the bottom of the channel. When *abc* moves inside the microchannel after depinning from the top corners due to the evaporation of the water drop or the pressing of this water drop, [37] the middle point of *abc* first contacts the center of *ed*. This contact may also occur if *h* is larger than the depth of the microchannel. After the contact, water spreads on *ed* from the center towards the bottom corners of the channel, resulting in two air/water interfaces inside this channel. Denote the cross-sectional profiles of these two interfaces by ab_1 and b_2c, respectively (Fig. 3.1a). Due to geometric symmetry, let's only consider ab_1, and the same analysis also applies to b_2c. The length of ab_1 gradually decreases when water spreads on *ed*.

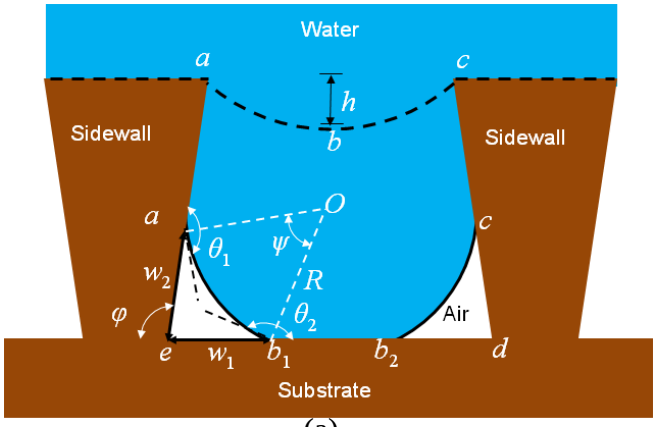

(a)

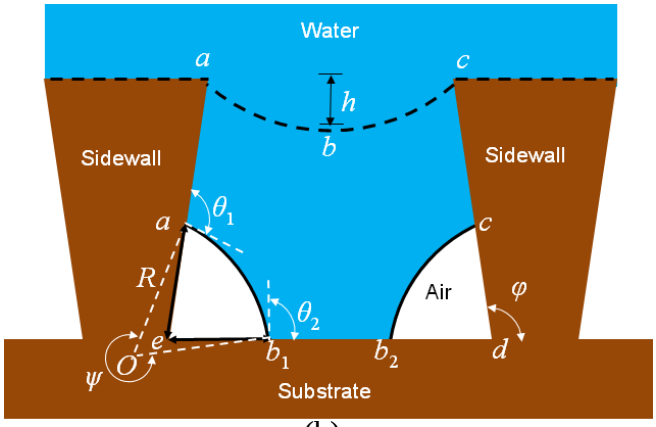

(b)

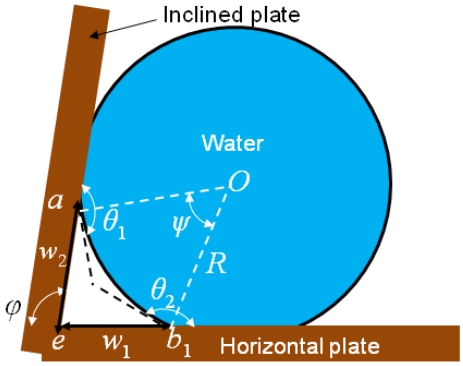

(c)

Figure 3.1:Schematics of the cross-sectional profiles: (a) an equilibrium state after water/air interface *abc* contacts the bottom of a microchannel, (b) a possible equilibrium state that is not stable, and (c) an equilibrium state in a single corner that is formed by a horizontal plate and an inclined plate after a water drop is placed on this single corner.

Static contact angles on the two sidewalls of a microchannel are considered to p_0 be the same, while they may be different from the one on the bottom of the microchannel. Set θ_1 and θ_2, respectively, to be static contact angles on the sidewalls γ and bottom of a microchannel. Both θ_1 and θ_2 are assumed to be greater than 90^0. That is, the inner surfaces of the microchannel are hydrophobic. If the sidewalls and bottom of the microchannel are smooth, then θ_1 and θ_2 are intrinsic contact angles. Otherwise, they are apparent contact angles. According to well-known Young-Dupré equation, [60] we have

$$\gamma_{SA1} = \gamma_{SL1} + \gamma\cos\theta_1,\ \gamma_{SA2} = \gamma_{SL2} + \gamma\cos\theta_2, \tag{3.1}$$

where represents surface tension of water, γ_{SL1} is surface tension of the interface between water and channel bottom, γ_{SA1} denotes surface tension of the interface between air and channel bottom, γ_{SL2} is surface tension of the interface between water and channel sidewall, and γ_{SA2} denotes surface tension of the interface between air and channel sidewall.

Next, let's consider the shape of ab_1 if it is stationary. Let p_{wa}, p_{wb_1}, and denote water pressures at *a*, b_1, and the apex of the water drop, separately. Set p_a, h_0, and h_a to be, respectively, atmospheric pressure, height of the water drop, and vertical distance between *a* and b_1. Assume that half size of the water drop is less than the capillary length of water (i.e., 2.7 mm). This assumption holds in our case. Small water drops are used in this work, and their volumes range from 3 μl to 6 μl. Subsequently, after a drop is placed on the substrate, the water surface around the apex of the drop is considered to be spherical. [29, 45] Let R_0 denote the corresponding radius, which is smaller than 2.7 mm accordingly. It was indicated in reference 67 that, gravity effect may not be neglected if a

water drop has a microliter volume (particularly for the super-hydrophobic case in which gravity has a strong effect, for example, on the measurement of contact angles) since gravity distorts the bottom shape of a water drop, and that this effect is negligible when the volume of a water drop is in the order of picoliters or smaller. Accordingly, since our water drops have microliter volumes, gravity effect is not neglected in this work in considering water pressure. On the other hand, we assume that water pressure on ab_1 is uniform. This assumption is justified below in two cases.

In the first case, a water drop is just placed on a substrate and does not suffer any external forces except gravity, as what was done in references [23, 24, 26, 29, 30, 37, 38, 45-50, 62, 65]. This is also the case in our tests on single corners (will be detailed in Section 3.3). By Young-Laplace equation, [60] we have $p_0 = \frac{2\gamma}{R_0} + p_a$. Subsequently, we get

$$p_{wa} = \frac{2\gamma}{R_0} + \rho_w g h_0 - \rho_w g h_a + p_a, \quad p_{wb} = \frac{2\gamma}{R_0} + \rho_w g h_0 + p_a, \tag{3.2}$$

where ρ_w denotes water density and g is gravitational acceleration. Microstructures that are employed to enhance hydrophobicity normally have heights lower than 200 μm (the microstructures used in this work have the maximum height of 93 μm, as will be shown in Sub-section 3.2.2). [23, 24, 26, 29, 30, 37, 38, 45-50, 62, 65] Set h_0 to be the maximum possible value of 200 μm. Also, let R_0 have the maximum allowable value of 2.7 mm. We find that, although $\rho_w g h_a$ and $\frac{2\gamma}{R_0}$ are set to have the maximum and minimum values, respectively, $\rho_w g h_a$ is still only 3.6% of $\frac{2\gamma}{R_0}$ ($\gamma = 72.7$ mN/m, g=9.8 N/kg and $\rho_w = 10^3$ kg/m^3 are used in the calculation). This comparison means that $\rho_w g h_a$ has a negligible

effect on p_{wa}. Consequently, it follows from Eq. (3.2) that p_{wa} approximately equals p_{wb_1}. Furthermore, since water pressure at any point of ab_1 is between p_{wa} and p_{wb_1}, water pressure on ab_1 can be considered uniform and has a constant value of p_{wb_1}.

In the second case, a pressing force is applied on the top of a water drop. This is actually the case in our pressing tests on microstructure-formed surfaces (will also be detailed in Section 3.3). Due to the application of the pressing force on the drop, the corresponding p_0 is larger than $(\frac{2\gamma}{R_0} + p_a)$. Subsequently, following the same line of reasoning as above, water pressure on ab_1 can still be considered to be uniform and equal to p_{wb_1} in this type of tests.

The two principal curvatures at a point of ab_1 are, respectively, 0 and $\frac{1}{R}$, where R denotes the radius of curvature. According to Young-Laplace equation, [60] $R = \frac{\gamma}{p_w - p_a}$, where p_w represents water pressure at this point of ab_1 and $(p_w - p_a)$ is so-called Laplace pressure. Since p_w is uniform on ab_1 and equals p_{wb_1}, by this relation R should be constant along ab_1 accordingly. Thus, ab_1 is a circular arc of radius *R*. Let *O* denote the center of ab_1. In practice, after a small water drop is placed or pressed on a hydrophobic surface, its top portion bends outwards. This implies that *R* is positive, which geometrically means that ab_1 bends downwards.

In summary, in order for ab_1 to be stationary, the following two geometric conditions have to be satisfied: (i) the contact angles of ab_1 at b_1 and *a* should be θ_1 and θ_2, respectively, and (ii) ab_1 should bend downwards with a circular shape. As observed from Fig. 3.1(a), in order to make the second condition met, we should have

$$0 < \psi < 180^0 . \tag{3.3}$$

Otherwise, as illustrated in Fig. 3.1(b), the point *O* would be located outside the left bottom corner, and consequently the interface ab_1 might bend upwards, which violates the second required condition. Since

$$\psi = \theta_1 + \theta_2 + \varphi - 360^0 , \tag{3.4}$$

the two inequalities in (3.3) imply that

$$360^0 < (\theta_1 + \theta_2 + \varphi) . \tag{3.5}$$

Furthermore, according to simple geometric analysis, we have

$$w_1 = \frac{2R\sin\frac{\psi}{2}\sin(\theta_2 - \frac{\psi}{2})}{\sin\varphi} , \; w_2 = \frac{2R\sin\frac{\psi}{2}\sin(\theta_1 - \frac{\psi}{2})}{\sin\varphi} . \tag{3.6}$$

It can be observed from these two relationships that both w_1 and w_2 decrease with the decrease in *R*.

3.1.2 Stability of the Constructed Wetting State

In order to make the constructed equilibrium state locally stable, its energy state should be lower than that of completely filled case. Otherwise, water continues to spread on the bottom of the microchannel until the bottom corners are completely filled. Subsequently, the wetting state is changed to that of Wenzel, which is discussed in chapter 2. Assume: (i) water spreads on both channel sidewalls and bottom in a quasi-steady manner (such that the kinetic energy of the water drop can be neglected), and (ii) the top portion of the water drop has negligible change in the shape when water spreads at the channel bottom (such that the surface energy change in the drop cap could be neglected). The second assumption is essentially equivalent to the one made in reference 50 during its consideration of the energy barrier between Cassie-Baxter and

Wenzel states. Based on these two assumptions, to make the two channel corners completely filled from the constructed equilibrium state, external work that needs to be done is

$$W = 2L\gamma_{SL1}w_1 + 2L\gamma_{SL2}w_2 - [2\gamma R\psi L + 2L(\gamma_{SA1}w_1 + \gamma_{SA2}w_2)], \tag{3.7}$$

where *W* represents the work and *L* denotes the length of the water drop along the channel direction. The summation of the first two term on the right-hand side of eq. (3.7) denotes the total surface energy that is gained after the two corners are completely filled, while the terms inside square brackets represent surface energies of ab_1, cb_2, *aeb* and cdb_2 (corresponding to the equilibrium state) that are lost after the complete filling. With the aid of eq. (3.1), it follows from eq. (3.7) that

$$W = -2\gamma R\psi L - 2\gamma L(w_1\cos\theta_1 + w_2\cos\theta_2). \tag{3.8}$$

In case *W* is positive, the energy state of the completely filled case is higher than that of the equilibrium case. Accordingly, there is an energy barrier that prevents the complete filling of the corners. Consequently, the constructed equilibrium state is locally stable, making it possible to observe this wetting state after water contacts the base of the microchannel. With the aid of eq. (3.6), it follows from eq. (3.8) that *W* is positive if

$$\psi\sin\varphi + 2\sin\frac{\psi}{2}[\cos\theta_1\sin(\theta_2 - \frac{\psi}{2}) + \cos\theta_2\sin(\theta_1 - \frac{\psi}{2})] < 0\,. \tag{3.9}$$

Ineqs. (3.5) and (3.9) are two conditions that θ_1, θ_2 and φ should meet for the existence of a stable wetting state after the water drop has contact with the bottom surface of a microchannel.

In addition, following a line of reasoning similar to that used to derive ineqs. (3.5) and (3.9), we find that these two inequalities also apply to the case when a water drop is placed on a single corner that is formed by a horizontal plate and an inclined plate (Fig. 3.1c). That is, to have a stable wetting state on this single corner, the two inequalities

also have to be met. Ineqs. (3.5) and (3.9) were solved using Matlab. As observed from the results plotted in θ_1 - θ_2 - φ rectangular coordinates (Figs. 3.2a-3.2c), the set of points (θ_1, θ_2, φ), which meet ineq. (3.5), is actually a sub-set of the one that satisfies ineq. (3.9). Accordingly, only ineq. (3.5) is needed to judge the existence of a stable wetting state. Consequently, we have arrived at an angle criterion: once θ_1, θ_2 and φ of a microchannel or a single corner satisfy ineq. (3.5), there exists a stable intermediate wetting state after a small water drop contacts the bottom of the microchannel or single corner in a quasi-steady manner.

Next, we consider a special case, in which $\theta_1 = \theta_2 = \theta_0$. Let

$$\theta_{0ct} = 360^0 - \varphi. \tag{3.10}$$

Then, by ineq. (3.5), for a given φ, θ_{0ct} is in fact the critical value for θ_0 to satisfy the angle criterion. It is also observed from Eq. (3.10) that, as φ ranges between 0^0 and 180^0, θ_{0ct} decreases with the increase in the value of φ. When φ is 90^0, θ_{0ct} is 135^0. That is, a stable intermediate state may exist inside a microchannel or on a single corner only if θ_0 >135^0. Due to the ease of fabrication, microchannels that are used to enhance hydrophobicity of a surface normally have approximately vertical sidewalls (i.e., φ is around 90^0) and their sidewalls and bottoms are also smooth. On a smooth surface, θ_0 is normally less than 120^0 even if this surface is coated with highly water-repellant materials, [29] such as Teflon. [68] This may interpret why stable wetting states were not observed when water contacted the bottoms of this type of microchannels as discussed in chapter 2.

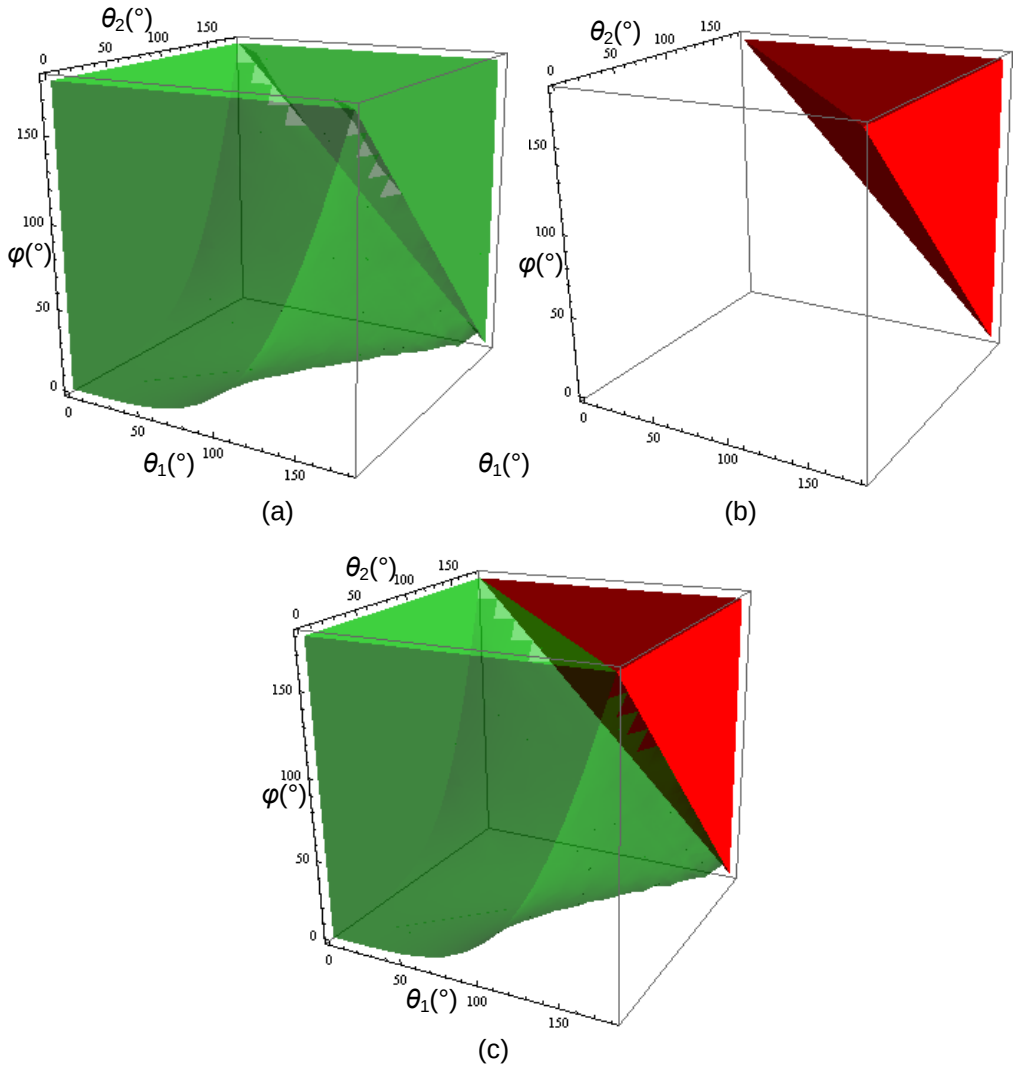

Figure 3.2: (a) volume formed by the points that meet ineq. (3.9). (b) volume formed by the points that satisfy ineq. (3.5). (c) volume shown in (b) is a subset of the one given in (a).

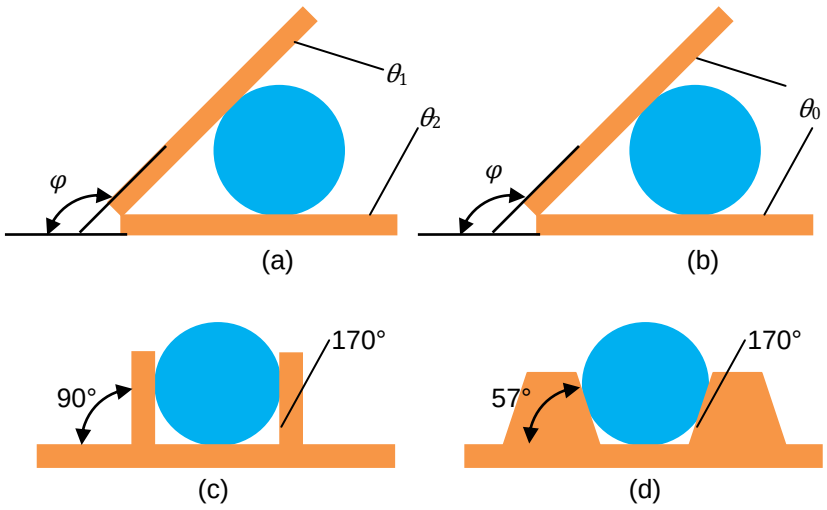

Figure 3.3: List of tests: (a) first type of tests, in which θ_1 and θ_2 are 115° and 160° respectively; (b) second type of tests, in which θ_0 is either 115° or 160°; (c) third type of tests, in which φ is 90° and θ_0 is 170°; and (d) fourth type of tests, in which φ and θ_0 are 57° and 170°, respectively. In the first two types of tests, the values of φ are increased from 10° up to 150°, and the bottom widths of the channels shown in (c) and (d) are both 600 µm.

3.2 Experimental Design

3.2.1. Design of Tests, and Experimental Setup for Observing Wetting States

Four types of tests were conducted to validate the angle criterion (Fig. 3.3). The first two types of tests were performed to observe wetting states on single corners (Figs. 3.3a and 3.3b), while another two types were done to examine wetting situations inside microchannels (Figs. 3.3c and 3.3d). These tests, together with their results, will be detailed in Section 3.3.

Figure 3.4(a) gives experimental setup used to observe the wetting state on a single corner after a water drop was placed on this corner. An optical microscope (model: mm0013000m of Metallurgical Microscopes Company) was employed for this purpose. The microscope was rotated by 90^0 with its sample stage oriented vertically. A triangular aluminum block was glued on the sample stage and served as a new sample stage. A

glass slide was glued on this new stage, and had a horizontal orientation. The single corner was formed by putting two plates on the glass slide and triangular block, respectively. A water drop was placed inside this corner using a syringe. The viewing direction of the optical microscope was along the intersecting line of the two plates that formed the single corner.

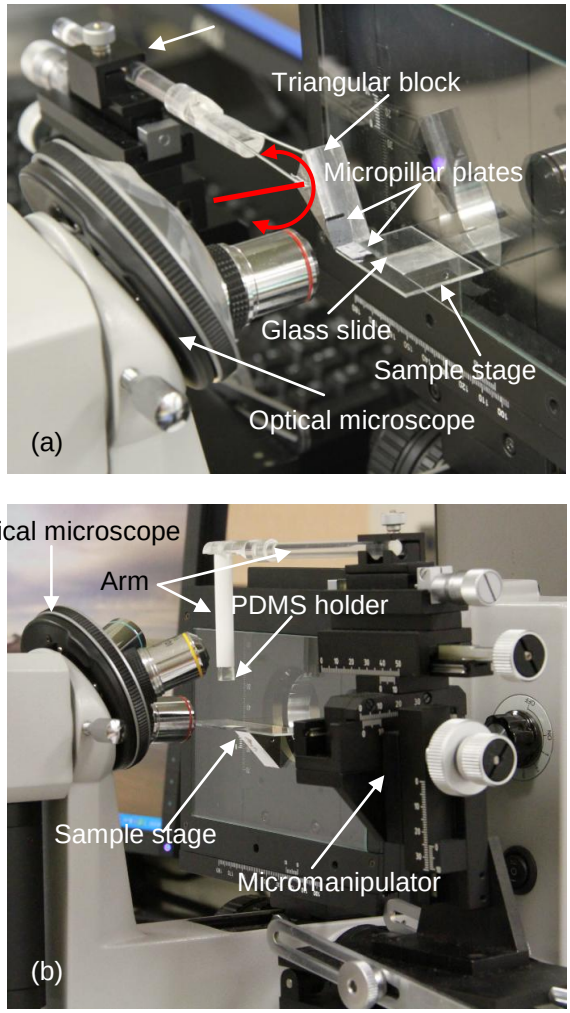

Figure 3.4: (a) Setup for observing cross-sectional profiles of a water drop on a single corner. (b) Experimental setup for observing cross-sectional profiles of a water drop on microchannels during the pressing of a water drop.

Figure 3.4(b) shows experimental setup applied to observe the wetting states inside microchannels when a water drop was slowly pressed. The optical microscope was also employed in this case to directly observe the evolution of air/water interfaces between microchannels. A microchannel-formed surface was first placed on the glass slide. A 5 mm X 5 mm X 10 mm (length X width X height) polydimethylsiloxane (PDMS) block that was connected to the arm of a micromanipulator (model: MD4R of World Precision Instruments, Sarasota, FL USA) was then employed to hold and press the water droplet. The vertical and horizontal movements of this PDMS block were controlled by the micromanipulator. A water drop was first loaded on the PDMS block using a syringe, and then moved to the top of the microchannels employing the micromanipulator. The water drop was slowly pressed against the microchannels when the PDMS block was gradually moved down.

The pictures of the air/water interfaces observed through the optical microscope were taken using Minisee software of ScopeTek Company. The contact angles of these interfaces with the inner surfaces of single corners and microchannels were determined using MB-Ruler software.

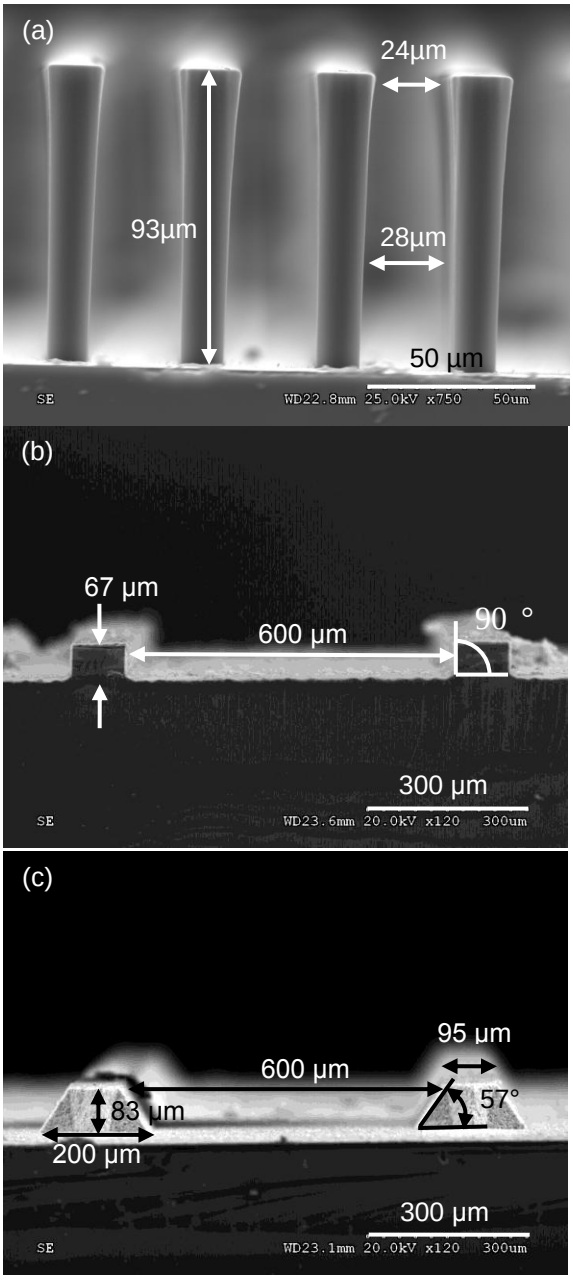

Figure 3.5: SEM pictures of microchannel-structured Si surface. (a) The second kind of sample, which has evenly distributed pillars. (b) The third kind of sample, which has vertical sidewalls. (c) The fourth kind of samples, which has sidewalls with inclined degrees of 57^0.

3.2.2. Fabrication of Samples

Four kinds of samples were used in the four types of tests (Fig. 3.5). The first kind was Teflon-coated SU-8 films. When water drops were placed on these films, the corresponding contact angles were measured to be 115°±2°, and receding and advancing angles were 89°±2° and 120°±2°, respectively. As shown in Figs. 3.5(a), the second kind was silicon wafers whose surfaces were covered with evenly distributed SU-8 pillars that were also coated with Teflon. Each pillar had dimensions of 18 X 18 X 93 μm^3 (length X width X height), and the average spacing between two neighboring pillars was 26 μm. SU-8 is a negative photoresist. SU-8 pillars were fabricated on a silicon wafer using ultra-violet (UV) lithography techniques. [46] The SU-8 pillars were also coated with Teflon to make their surfaces hydrophobic. The apparent contact angles on the micropillar-incorporated silicon wafers were measured to be 160^0 ±2° (the receding and advancing angles were 145°±2° and 167°±2°, respectively). The third kind of samples included silicon microchannels, whose bottom widths were 600 μm (Figs. 3.5(b)). These wide channels were adopted to have a clear view of air/water interfaces inside a channel. Silicon surface is hydrophilic. To make the sidewall and bottom of each channel have high contact angles, randomly distributed ZnO nanowires were grown on the inner surfaces of every channel using a hydrothermal approach (see reference 69**,** for example, for the detail of this approach). The nanowires had hexagonal cross-sections with an average length of 3.6 μm and diameter of 0.36 μm. After the incorporation of these ZnO nanowires, the sidewall and bottom of each channel had about the same apparent contact angles of 170°±2° (the receding and advancing angles were 160°±2° and 172°±2°, respectively). The sidewalls of microchannels were perpendicular to their corresponding substrates. The fourth kind of samples was the same as the third kind except that the sidewalls of the channels in the fourth kind of samples formed angles of

57°, instead of 90°, with the bottoms of the channels (Figs. 3.5(c)). The silicon microchannels in the third and fourth kinds of samples were also fabricated using UV techniques. [70, 71]

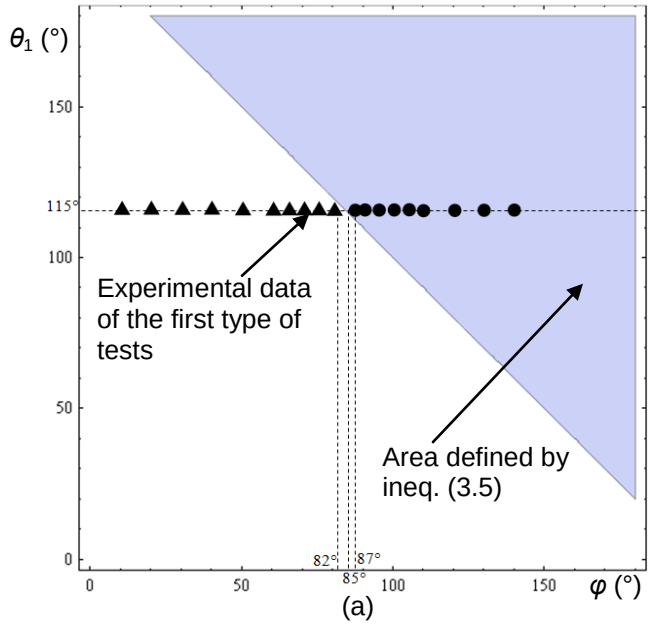

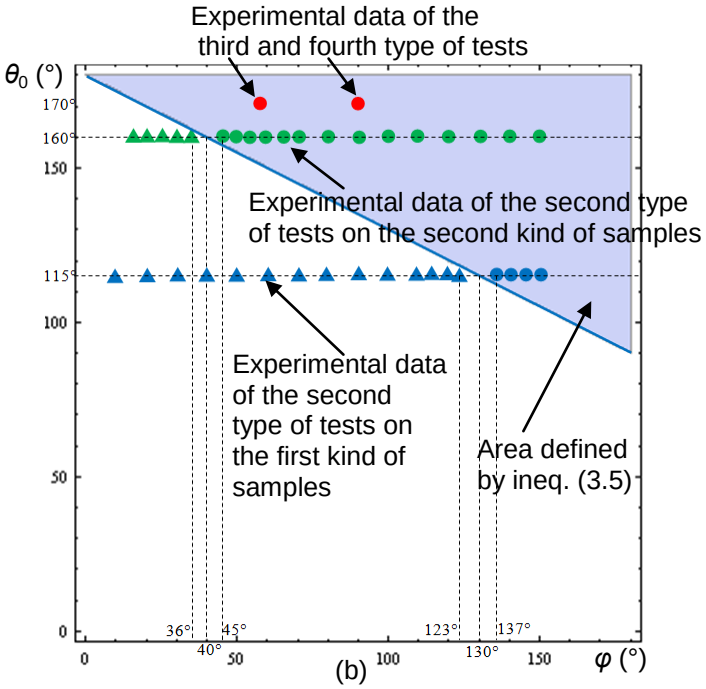

Figure 3.6: (a) Comparison of experimental data and theoretical prediction on the first type of tests, in which θ_2 =160°. (b) Comparison of experimental data and theoretical predictions on the second, third and fourth types of tests, in which $\theta_1=\theta_2=\theta_0$. Triangular dots mean that no stable intermediate states were observed, and circular dots imply that stable intermediate states were clearly observed.

3.3. Experimental Results and Discussions

As observed from Fig. 3.6, experimental data generated out of the four types of tests match well with the predications given by the angle criterion. Figures 3.7 and 3.8 give representative wetting states observed in these tests.

In the first type of tests, a set of single corners was considered (Figs. 3.3a and 3.7a). The bottom plates of these single corners were the first kind of samples, while the inclined plates were the second kind of samples. Consequently, the contact angles on the sidewall and the bottom of a single corner were 160° and 115°, respectively. In terms of ineq. (3.5), only if φ >85°, stable intermediate states exist on the first set of single corners (Fig. 3.6a). In our tests, when the values of φ were first increased from 10° up to 60° with an increment of approximately 10° and then increased to 82° with a smaller increment of about 5°, we did not observe any stable intermediate states (Fig. 3.7a). However, when φ was increased to 87° or above, stable intermediate states were clearly observed (Figs. 3.7b and 3.7c). Accordingly, the experimentally measured critical value of φ was 83.5° (the average values of 82° and 87°), which was close to the theoretically predicted value of 85°. Thus, the experimental results in this type of tests have a good match with those predicted by ineq. (3.5) (Fig. 3.6a). If advanced contact angles on the sidewall and bottom of a single corner (167° and 120°) were used in ineq. (3.5), then stable intermediate states may exist on the first set of single corners only when φ >73°. In this case, the experimentally measured critical value of φ had a difference of 10.5° from the theoretically predicted one, implying that ineq. (3.5) gives a reasonably good prediction.

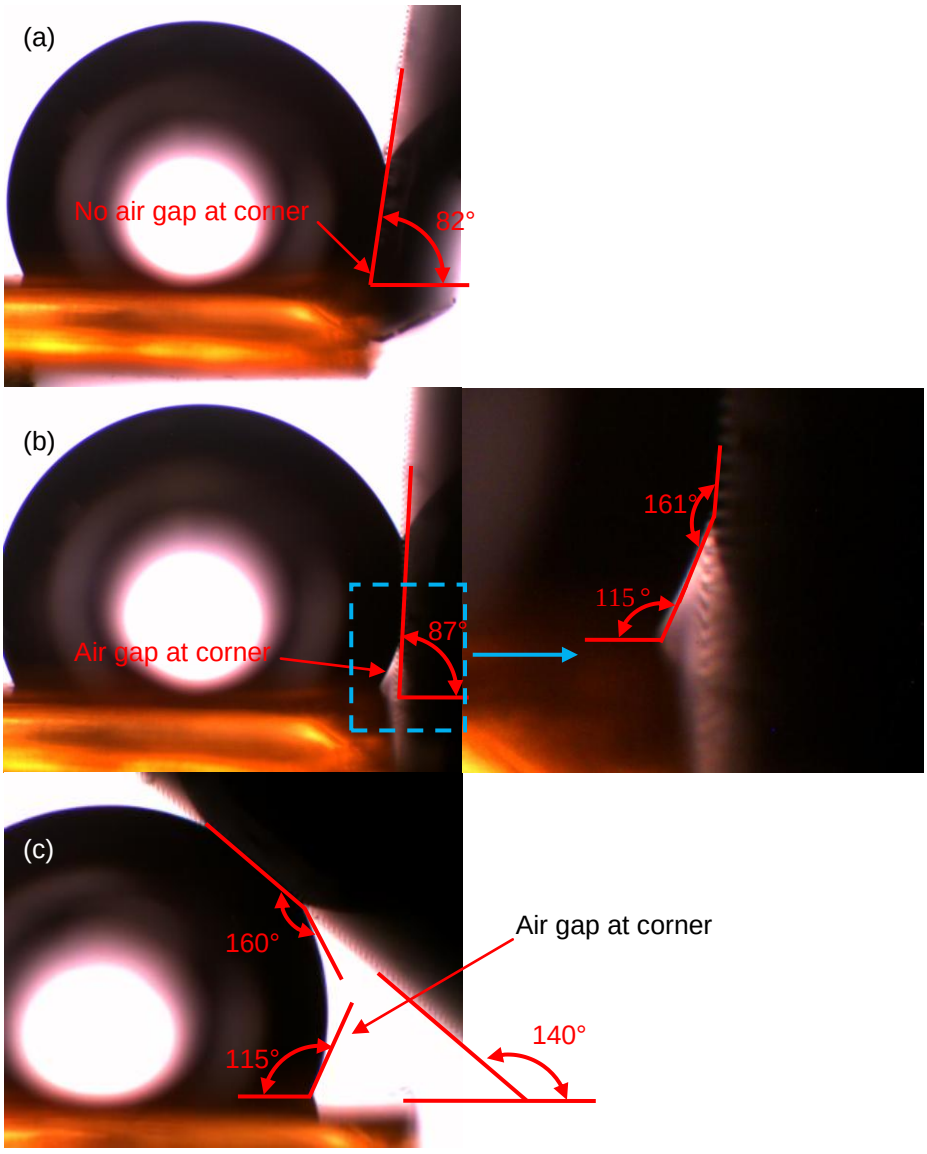

Figure 3.7: First type of tests: (a) Wenzel state at φ=82°; and stable intermediate states at (b) φ=87° and (c) φ=140°.

In the second type of tests, the contact angles on the sidewall and the bottom of a single corner were the same (Fig. 3.3b). Two sets of single corners were examined, and they were formed by the first two kinds of samples, respectively. Accordingly, the values of θ_0 were 115° and 160°, separately, on these two sets of single corners. By ineq. (3.5), when the value of θ_0 was 115°, only if $\varphi > 130°$, stable intermediate wetting states exist on the first set of single corners. In our tests, when the values of φ were increased from 10° to 123°, we did not observe any stable intermediate states. The water drops completely filled the corresponding single corners right after water drops had been placed on these single corners. However, when φ =137° or above, stable intermediate states were clearly observed. Consequently, the experimentally measured critical value of φ was 130° (the average values of 123° and 137°), which equaled the theoretically predicted value. Thus, the experimental results in this type of tests have a good match with those predicted by ineq. (3.5) (Fig. 3.6b). On the other hand, when advanced contact angles on the sidewall and bottom of a single corner (both were 120°) were used in ineq. (3.5), stable intermediate states may exist only if φ >120°. In this case, the experimentally measured critical value of φ had a difference of 10° from the theoretically predicted one, implying that ineq. (3.5) also gives a reasonably good prediction. The same testing results apply to the second set of single corners. By ineq. (3.5), when the value of θ_0 was 160°, only if $\varphi > 40°$, stable intermediate states exist on the second set of single corners. In our tests, when the values of ϕ were increased from 15° up to 36°, we did not observe any stable intermediate states. However, stable intermediate states were clearly observed when φ =45° or above. The experimental results in this type of tests agree well with the predictions given by ineq. (3.5) (Fig. 3.6b). In case advanced contact angles on

the sidewall and bottom of a single corner (both were 167°) were used in ineq. (3.5), stable intermediate states may exist only if φ >26°. In this case, the experimentally measured critical value of φ had a difference of 14° from the theoretically predicted one, implying that ineq. (3.5) gives a just fine prediction.

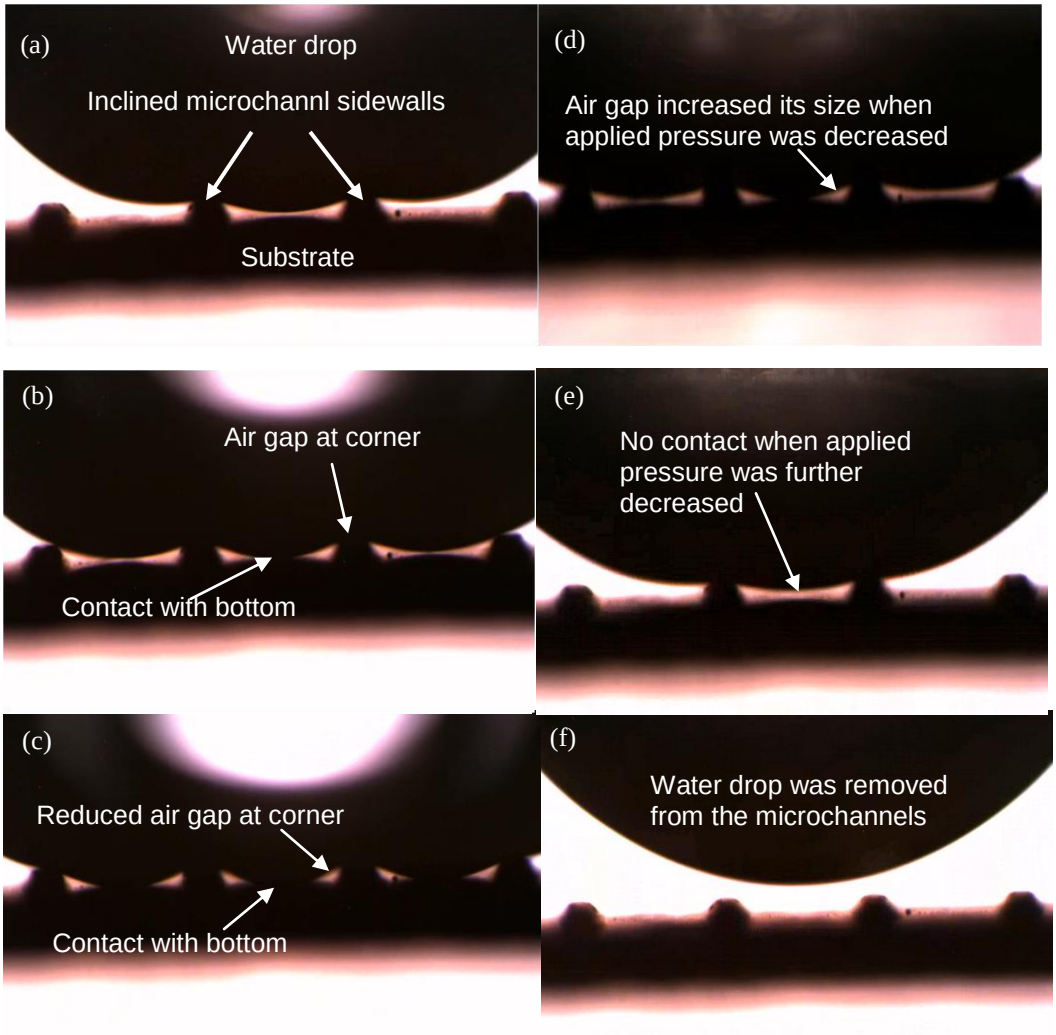

Figure 3.8: Fourth type of tests (the bottom widths of microlines are 600 μm and φ is 57°): (a) a water drop was pressed against microchannels, (b)-(c) stable intermediate states were observed after the water drop had contact with the bottoms of the microchannels, (d)-(e) intermediate states were transited back to that of Cassie-Baxter with the reduction in applied pressure, and (f) water drop was finally removed from the substrate.

In the third and fourth types of tests, the third and fourth kinds of samples were examined, respectively (Figs. 3.5c and 3.5d). By ineq. (3.5), the critical values of φ in these two types of tests were both 20° or 16° if the values of θ_0 were chosen to be 170° or 172° (advanced angle). In either case, the predicted critical value was smaller than the corresponding values of φ in the tests, which were 90° and 57°, respectively. Accordingly, stable intermediate states should be observed in these two types of tests. In both types of tests, water drops were slowly pressed on the samples to observe evolution of air/water interfaces inside microchannels using the setup shown in Fig. 3.4(b). Four points were observed from the third and fourth types of tests (Fig. 3.8). First, as predicted using the angle criterion, after a water drop had touched the bottom of a microchannel, the water drop did not collapse and a stable intermediate state was observed (Fig. 3.8b). Second, as implied by Eq. (3.6), in these two types of tests, the bottom of a water drop just spread on the bottom of a microchannel when the force applied to press the water drop was gradually increased (Figs. 3.8b and 3.8c). Third, as the applied force on the water drop (or say, Laplace pressure inside the water drop) was gradually reduced, air pockets increased their sizes, the water drop moved away from the bottom of the microchannel, and the intermediate state was finally transited back to that of Cassie-Baxter (Figs. 3.8d and 3.8e). Fourth and finally, the water drop was separated from the microchannels when the PDMS block used to press this drop was removed from the substrate (Fig. 3.8f). On the other hand, in chapter 2, since the angle criterion was violated, water drops completely filled the microchannels after they had been pressed to have contact with the bottoms of the microchannels. Furthermore, we did not observe the reversal transition from Wenzel to Cassie-Baxter states in the microchannels when applied pressures were gradually decreased. This implies that, in addition to reducing applied pressures, an

additional force, such as an electrical force, [66] is needed to overcome energy barrier between the two wetting states for making this reversal transition occur.

3.4 Summary

In this chapter, through theoretical and experimental investigations, we demonstrated that, when an angle criterion is satisfied, there may exist an intermediate wetting state inside a microchannel or on a single corner after a water drop contacts the bottom of a microchannel or is placed on the single corner. In this intermediate state, water does not completely fill the microchannels or the single corner, and air pockets still exist at the channel corners or on the single corner. Such a wetting state is also stable. The angle criterion was first theoretically derived, and then experimentally validated using four types of tests conducted on single corners or microchannels. It was also found that, when the Laplace pressure inside a water drop is reduced, an intermediate wetting state may be transited back to that of Cassie-Baxter. One of the criteria commonly used to judge the transition from Cassie-Baxter to Wenzel states is whether a water drop contacts the base of a roughness groove. The derived angle criterion may be used to modify this transition criterion for the case of microchannels.

Chapter 4

An Angle Inequality for Judging the Transition from Cassie-Baxter to Wenzel States When a Water Drop Contacts Bottoms of Grooves between Micropillars

In chapter 3, we considered the applicability of the contact criterion to the microchannels. Through theoretical and experimental investigations, we showed that this transition criterion does not always hold in the case of microchannels. When an angle inequality is violated, the contact criterion is applicable. Otherwise, the contact criterion is not applicable, and there exists a wetting state inside a microchannel after a water drop contacts the bottom of the microchannel in a quasi-static manner. This wetting state is different from that of Wenzel. As what was done in the previous chapter, it is referred to as “intermediate state” here. In an intermediate state, water does not completely fill the microchannel, and air pockets still exist in its bottom corners. Also, the wetting state is locally stable in the sense that its energy state is lower than that of the Wenzel model.

In this chapter, we further consider the application range of the contact criterion in the case of micropillars. Since the approach used in chapter 3 to consider such an application range in the case of microchannels does not apply here, a different method is adopted for the corresponding consideration. Employing this method, we also derive an angle inequality, which, to our surprise, is identical to the one derived in chapter 3 for the case of microchannels. Subsequently, we validate the angle inequality through pressing tests on micropillars.

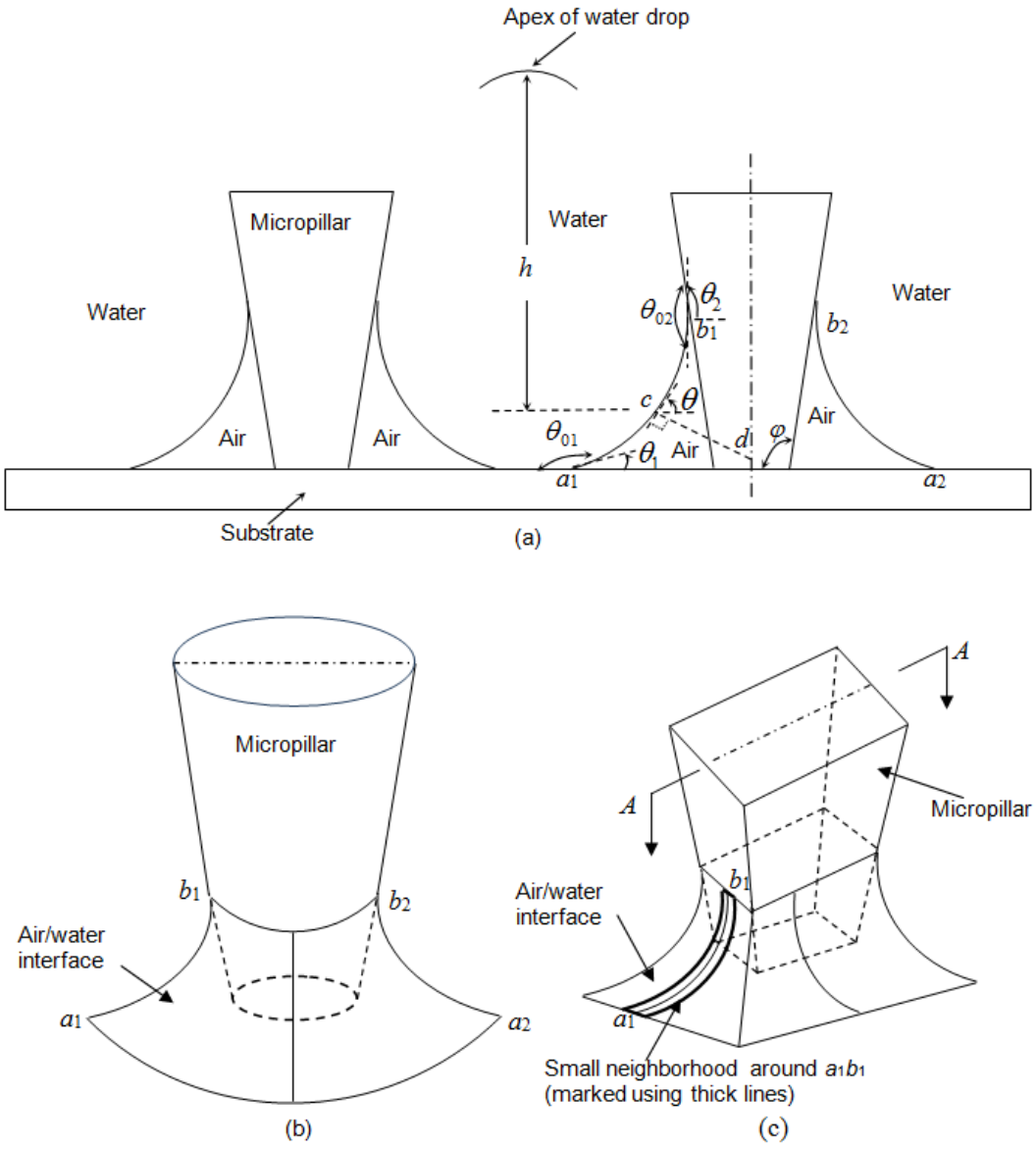

Figure 4.1: (a) Cross-sectional profile of the air/water interface around the bottom corner of a micropillar in a possible intermediate state of a water drop when the drop contacts the bottoms of the grooves between micropillars. Perspective views of the air/water interface around the bottom corner of a micropillar with (a) circular or (b) rectangular cross-sections.

4.1 Theoretical Analysis

4.1.1 Conditions to Have an Intermediate State inside Grooves

As illustrated in Figure 4.1, we consider the wetting on micropillars which have polygonal or circular cross-sections. Set θ_{01} and θ_{02}, respectively, to be static contact angles on the pillar sidewalls and groove bottoms. If the micropillar sidewalls and groove bottoms are smooth, then θ_{01} and θ_{02} are intrinsic contact angles. Otherwise, they are apparent contact angles. The values of θ_{01} and θ_{02} are affected by surface materials and structures, but not influenced by gravity. For example, if the inner surface of a groove is coated with ZnO nanowires, which is actually the case in our pressing tests as will be detailed in Section 4.2, then the two contact angles are considered to be equal. Otherwise, these angles may be different. For instance, in the case of a single corner, which is formed by a horizontal plate and an inclined plate, the values of θ_{01} and θ_{02} are different when the surface structures on the two plates are different. Let φ denote the angle formed by the sidewall and bottom of a groove (Fig. 4.1a). We have $0 < \varphi < 180^{o}$.

After a water drop is placed on the top of micropillars, it may have contact with the bottoms of grooves due to a large deflection of its bottom surface or the depinning of its bottom surface from top corners of micropillars. [37, 38, 45, 49, 50] Assume that, after the contact, there exists an intermediate state. As illustrated in Fig. 4.1(a), let a_1b_1 and a_2b_2, respectively, denote the corresponding cross-sectional profiles of a water drop around the bottom corner of a micropillar. In case the micropillar has circular cross-sections, this drop profile has an axisymmetric shape, and a_1b_1 and a_2b_2 represent two of its meridian curves (Fig. 4.1b). If the micropillar has rectangular cross-sections, then a_1b_1 and a_2b_2 denote the cross-sectional profiles that are obtained after the drop is vertically cut along a middle plane of the micropillar (such a middle plane is denoted as the *A-A*

plane in Fig. 4.1c). When the micropillar has triangular cross-sections, a_1b_1 represents the cross-sectional profile of the water drop beside a pillar sidewall. This cross-sectional profile is cut by a vertical plane, which is perpendicular to the sidewall and intersects with this sidewall at its middle line. For this triangular micropillar, a_2b_2 denotes such a cross-sectional profile beside another pillar sidewall. Without loss of generalization, only a_1b_1 is considered in the following analysis, and the same analysis also applies to a_2b_2.

Use p_0 to denote water pressure at the apex of the water drop, and let p_a be atmospheric pressure. $(p_0 - p_a)$ is so-called Laplace pressure at the apex of the drop. We assume that $(p_0 - p_a)$ is positive. This assumption is at least true in the following two cases. In the first case, a water drop with a microliter volume is just placed on a hydrophobic surface and, except gravity, does not suffer any external forces, as what was done in references [23-27, 29, 30, 37, 38, 45-50, 62, 64, 65, 67, 72]. Since the drop cap curves outwards, by Young-Laplace equation, [60] this implies that $(p_0 - p_a)$ is positive. In the second case, a pressing force is applied on the top of a water drop. This is actually the case in our pressing tests on micropillar-formed surfaces that will be detailed in Section 4.2 Due to the application of the pressing force on the drop, $(p_0 - p_a)$ is increased in compared with that in the first case and thus is also positive.

Let ρ_w and g denote water density and gravitational acceleration, respectively. Set h to be the vertical distance between the apex of the water drop and a representative point c at a_1b_1 (Fig. 4.1a). Use R_1 and R_2 to represent radii of two principal curvatures of the water surface at c. They are considered positive if their associated curves on the surface bend towards air. Otherwise, they are negative. Let γ denote surface tension of water. Accordingly, with the aid of Young-Laplace equation, [60] it is readily shown that, at c,

$$\frac{1}{R_1}+\frac{1}{R_2}=A, \tag{4.1}$$

where

$$A=(p_0+\rho gh-p_a)/\gamma, \tag{4.2}$$

and $(p_0+\rho gh)$ represents water pressure at *c*. By Eq. (4.2), *A* is positive. Let θ denote the angle formed by the horizontal direction and the tangent to a_1b_1, and set θ_1 and θ_2 to be the values of θ at a_1 and b_1, respectively (Fig. 4.1a). By simple geometric analysis, we have

$$\theta_1=180^{\circ}-\theta_{01}, \tag{4.3a}$$

$$\theta_2=\varphi+\theta_{02}-180^{\circ}. \tag{4.3b}$$

In summary, in order for ab_1 to be stationary in an intermediate state, (i) R_1 and R_2 should meet Eq. (4.1), and (ii) θ_1 and θ_2 should satisfy Eqs. (4.3a) and (4.3b), respectively.

4.1.2. Derivation of an Angle Inequality

In this sub-section, we will derive an angle inequality to modify the contact criterion for the case of micropillars which have polygonal or circular cross-sections.

We first consider the micropillars with polygonal cross-sections. Let's begin with rectangular micropillars. It is known that, when the width of a pillar sidewall is much larger than capillary length of water, the capillary profile on this sidewall is considered to have an approximately cylindrical shape with uniform cross-sections. [73, 67] However, if this width is comparable to or less than capillary length of water, such as in the case of a micropillar, then the same consideration is invalid because the two vertical edges of the sidewall affect the shape of the capillary profile. On the other hand, the edge effect on a

small neighborhood around a_1b_1 in the case of a rectangular micropillar may be negligible if the width of this neighborhood is much smaller than the height and width of a micropillar sidewall (Fig. 4.1c). Accordingly, the capillary profile in this neighborhood still has a cylindrical shape with uniform cross-sections, which are represented by a_1b_1. Thus, the curvature along the direction perpendicular to a_1b_1 is zero, and by Eq. (4.1) the curvature of a_1b_1 equals A. Subsequently, we have

$$\frac{d\theta}{ds} > 0, \tag{4.4}$$

where s represents the arc length from a_1 to c along a_1b_1, and $\frac{d\theta}{ds}$ denotes the curvature of a_1b_1 at c. Likewise, following the same line of reasoning, Ineq. (4.4) also holds when micropillars have other polygonal cross-sections (such as triangles, pentagons and hexagons).

Let us then turn attention to a micropillar with circular cross-sections. The corresponding capillary profile around this micropillar is axisymmetric. Let d denote the intersecting point between the normal to the water surface at point c and the symmetry axis of the micropillar (Fig. 4.1a). Use L to represent the length of cd. For such an axisymmetric profile, set $\frac{1}{R_1}$ to be the curvature of a_1b_1 at point c, and let $\frac{1}{R_2}$ denote the curvature associated with the curve that is located on the water surface while is perpendicular to a_1b_1 at c. [60, 67] In our case, $\frac{1}{R_2}$ is always negative since its associated curve bends towards water. [73] Then R_1 and R_2 at c satisfy the following two relations, respectively. [73, 67]:

$$\frac{1}{R_1} = \frac{d\theta}{ds}, \quad R_2 = -L\,. \tag{4.5}$$

Subsequently, it follows from Eq. (4.1) that

$$\frac{d\theta}{ds} - \frac{1}{L} = A. \tag{4.6}$$

Because both *L* and *A* are positive, this equation implies that Ineq. (4.4) holds as well when micropillars have circular cross-sections.

Ineq. (4.4) means that θ increases with increasing *s*. Accordingly, we have

$$\theta_1 < \theta_2 . \tag{4.7}$$

With the aid of Eq. (4.3), it follows from Ineq. (4.7) that

$$360^{o} < (\theta_{01} + \theta_{02} + \varphi) . \tag{4.8}$$

In chapter 3, the same inequality was also derived for the cases of microchannels and single corners based on the solution to Eqs. (4.1) and (4.3). In this work, since air/water interfaces between micropillars have more complicated shapes, we do not directly solve these two equations. Instead, as shown above, we derive Ineq. (4.8) based on a necessary condition that the solution to the two equations should satisfy. The above procedure can also be applied to derive this inequality for the cases of microchannels and single corners as well.

Ineq. (4.8) gives a necessary condition that θ_{01}, θ_{02} and φ have to meet in order for a water drop to have an intermediate state after the drop contacts the bottoms of grooves. This implies that, once θ_{01}, θ_{02} and φ satisfy Ineq. (4.8), the contact criterion may not necessarily be applicable to the corresponding micropillars. However, if this inequality is violated, then there does not exist any intermediate states. Consequently, after a water drop contacts the bottoms of grooves, it collapses and completely fills these grooves.

Due to the ease of fabrication, micropillars that are commonly adopted to enhance hydrophobicity of a surface have vertical sidewalls (i.e., φ is 90^{o}) with circular or

rectangular cross-sections. [29, 30, 37, 38, 45, 46, 47, 48, 49, 50, 62, 64, 65, 72] Their sidewalls and bottoms are smooth. On a smooth surface, both θ_{01} and θ_{02} are normally less than 120^o even if this surface is coated with highly water-repellent materials, [29] such as Teflon. [69] By Ineq. (4.8), when φ is 90^o and $(\theta_{01}+\theta_{02})$ is less than 270^o, the contact criterion is applicable. Accordingly, on the aforementioned micropillars, Cassie-Baxter state should be transitioned to that of Wenzel immediately after a water drop has contact with the bottoms of their grooves. On the other hand, if $(\theta_{01}+\theta_{02})>270^o$, then Ineq. (4.8) is met. Consequently, it is possible that Cassie-Baxter state may be transitioned to an intermediate state, instead of a Wenzel state, after a water drop has contact with the bottoms of grooves.

For the existence of a stable intermediate state, two conditions should be met. First, there exists an intermediate state after the contact. Second, there is an energy barrier between this intermediate state and that of Wenzel. The consideration of these two conditions might give precise bounds of θ_{01}, θ_{02} and φ for the existence of a stable intermediate state, which could also be used to identify the exact range that the contact criterion is applicable. Other researchers have previously considered stability of Wenzel and Cassie-Baxter states, [29, 50, 74] including that of a special Cassie-Baxter state in which water/air interfaces get deep inside roughness grooves but do not touch the base of these grooves. However, they did not consider the stability of an intermediate state. In chapter 3, we did so for the cases of microchannels and single corners, since the corresponding air/water interfaces have simple shapes. The derived angle inequality is identical to Ineq. (4.8). However, in this chapter, due to lack of analytical expression of the air/water interfaces in the case of micropillars, we do not consider the existence of a stable intermediate state, and leave the corresponding consideration to a future

investigation. Therefore, although Ineq. (4.8) of this chapter is the same as the angle inequality derived in chapter 3, different from that in the previous work for microchannels and single corners, the satisfaction of Ineq. (4.8) does not guarantee the existence of a stable intermediate state after a small water drop slowly contacts the bottoms of grooves between micropillars. On the other hand, as in the previous work, once Ineq. (4.8) is violated, such a stable intermediate state should not exist.

4.2. Experimental Results and Discussions

To validate Ineq. (4.8), we did pressing tests on six types of SU-8 micropillars, which have circular, triangular, square, hexagonal, T-shaped and star-like cross-sections, respectively (Fig. 4.2). The triangular, square and hexagonal pillars represent those micropillars that have convex polygonal cross-sections, while the T-shaped and star-like micropillars are representatives of those which have concave polygonal cross-sections. All the tested SU-8 micropillars have approximately vertical sidewalls (i.e., φ is around 90^o). Their heights are in the range of 100 to 110 μm, lateral dimensions of their cross-sections range from 50 to 150 μm, and spaces between neighboring micropillars are relatively large for clearly observing air/water interfaces located between these micropillars, which vary from 265 to 645 μm (Fig. 4.2).

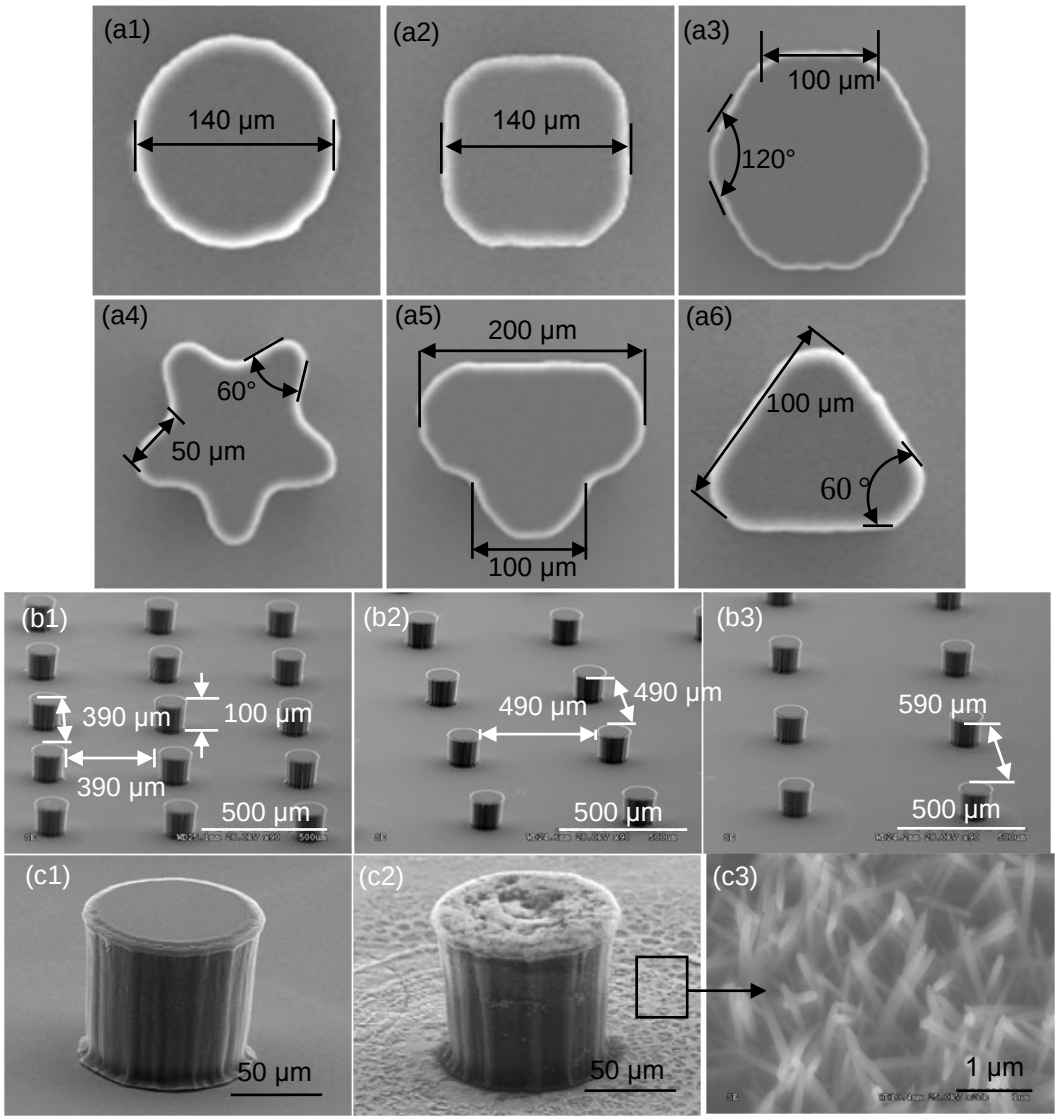

Figure 4.2: (a) Six types of micropillars, which have (a1) circular, (a2) square, (a3) hexagonal, (a4) star-like, (a5) T-shaped, and (a6) triangular cross-sections, respectively. First set of circular micropillars, which have pitches of (b1) 390, (b2) 490 and (b3) 590 µm, respectively. Representative first and second sets of circular pillars, which were covered with (c1) Teflon and (c2) ZnO nanowires. (c3) Close-up view of ZnO nanowires. All images are scanning electron microscopy (SEM) images.

Each type of micropillars includes two sets of micropillars. The first set of micropillars in every type of samples consists of three kinds of micropillars, which have identical cross-sections but differ much in the pitches between two neighboring micropillars (Fig. 4.2b). For example, in the case of circular micropilars, the pitches are 390, 490 and 590 μm, separately (Fig. 4.2b). The micropillars in the second set have the same dimensions as their counterparts in the first set. The only difference is that, to enhance hydrophobicity, the first set of micropillar is coated with Teflon while the second set is covered with ZnO nanowires (Figs. 4.2c). In other words, the sidewalls of the first set of micropillars are still smooth, but they are coated with a highly repellent material. In contrast, the second set of micropillars have rough sidewalls, since their originally smooth sidewalls are now covered by nanostructures. SU-8 is a negative photoresist. [75, 76] All the SU-8 micropillars were fabricated using ultra-violet lithography, [70, 71] Teflon was spin-coated on micropillars, and ZnO nanowires were grown on the surfaces of the corresponding micropillars using a hydrothermal approach. [70] The nanowires had hexagonal cross-sections with an average length of 3.6 μm and diameter of 0.36 μm.

In a pressing test, a plate was put on the top of a water drop to slowly press it against micropillars. The vertical movements of this plate were controlled by a micromanipulator. An optical microscope was rotated by 90o to have a side view of air/water interfaces between micropillars. Similar experimental setups have been previously used to press water drops on micropillars [29] and microchannels. [77-79] Small water drops are used in this work, and their volumes range from 3 μl to 6 μl. Such a drop has a spherical cap after it is placed on the substrate. The pictures of the air/water interfaces observed through the optical microscope were taken using Minisee software of ScopeTek Company. The contact angles of these interfaces with the inner surfaces of micropillars were determined using MB-Ruler software.

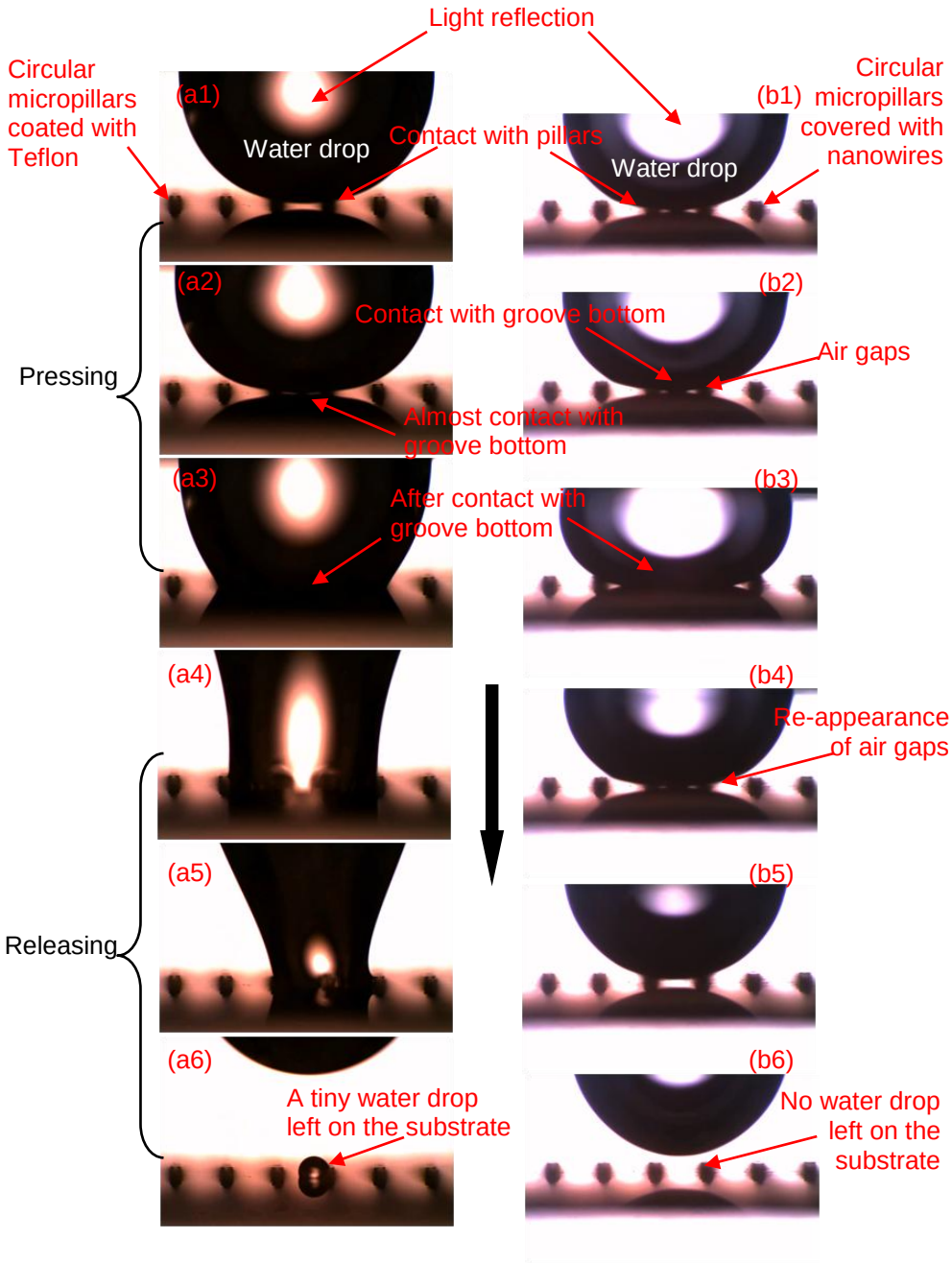

Figure 4.3: In-situ observation of the evolutions of the air/water interfaces during the pressing test on (a) a kind of the first set of circular micropillars , and (b) a kind of the second set of circular micropillars, These two kinds of micropillars have the same dimensions, which are given in Figs. 4.2(a1) and 4.2(b2).

The contact angle on an SU-8 film was measured to be about 80°. When water drops were placed on Teflon-coated SU-8 films, the corresponding contact angles were measured to be 115°±2°, and receding and advancing angles were 89°±2° and 120°±2°, respectively. The apparent contact angles on ZnO nanowire-covered SU-8 films were measured to be 160°±2° (the receding and advancing angles were 145°±2° and 167°±2°, respectively). The values of θ_{01} and θ_{02} were assumed to be equal on micropillars due to the uniform distributions of Teflon and ZnO nanowires on the substrates. The values of θ_{01} on the two sets of micropillars in each type of samples are considered to be 115^o and 160^o, respectively. Hence, the sums of θ_{01}, θ_{02} and φ for the two sets of micropillars are 320^o and 410^o, respectively. Accordingly, Ineq. (4.8) is violated for the first set of micropillars, while it still holds true for the second set. Water drops sat on the top of micropillars before they were pressed, indicating the initial wetting state was that of Cassie-Baxter. All the testing results are presented in Fig. 4.3.

Three points were observed through pressing tests on the first set of micropillars of each type of samples (Fig. 4.3a). First, as seen, for example, from Figs. 4.3(a), a water drop first contacted with the bottoms of the groove right underneath the lowest point of the drop surface. In reality, the pressure may be not ideally uniform inside the drop or the micropillars may not be exactly identical. Either cause might lead to the occurrence of this contact phenomenon. Second, as predicted using Ineq. (4.8), the water drop immediately filled grooves when it had contact with the bottoms of the grooves ((a3) in Fig. 4.3). Third, only a tiny drop of water was left on the substrate when the pressing plate was removed ((a6) in Fig. 4.3), implying that the Wenzel state was not completely transformed to that of Cassie-Baxter. In the meanwhile, when all the SU-8 micropillars are not covered by any coating, the corresponding values of θ_{01} and θ_{02} are measured to be 80°±2°. In this case,

Ineq. (4.8) is violated. Pressing and releasing phenomena of water drops on these un-treated micropillars are similar to those on the first set of micropillars (results are not shown here). A clear difference is that a relatively large portion of a water drop is left on the substrate after the removal of the pressing plate. This difference implies that the amount of water which would still stick to a substrate after a pressing test may depend on the contact angles of water on the corresponding substrate.

On the other hand, the testing results on the second set of micropillars were different from those on the first set for each type of samples (Fig. 4.3b). On the second set of micropillars in each type of samples, after water drops had contacted the bottoms of grooves, intermediate wetting states were observed inside these grooves. In such a wetting state, water did not completely fill the grooves, and air pockets existed between water drops and bottom corners of these grooves. After water had contact with the base of a few grooves, the air pockets in the middle grooves were not visible due to the block of water, while air pockets could still be seen around the outside micropillars ((b2) and (b3) in Fig. 4.3). Furthermore, the sizes of the air pockets decreased with the increase in the applied pressures, implying that there exist energy barriers between the intermediate states and that of Wenzel (i.e., the state for which the groove is completely filled by water). Consequently, these intermediate states are locally stable. Otherwise, the wetting states should be immediately transformed to that of Wenzel when the applied pressure was increased. It was also interesting to observe that, along with the reduction in the applied pressure, these air pockets gradually increased their sizes. Meanwhile, the number of grooves that had contact with the water drop was reduced, and due to this reduction the air pockets in the middle grooves re-appeared ((b3) and (b4) in Fig. 4.3). Eventually the water drop recovered its Cassie-Baxter wetting state after much reduction in the applied pressure ((b5) in Fig. 4.3). Finally, this water drop was removed from its

substrate by the pressing plate, and no water residue was observed on the substrate. These testing results on the second sets of micropillars indicate: (i) when Ineq. (4.8) is met, the contact criterion does not necessarily hold and there may exist a stable intermediate state after a water drop contacts the base of a groove, and (ii) this intermediate state may be transformed back to that of Cassie-Baxter. The observed phenomena were similar to those in the case of microchannels. When Ineq. (4.8) was met, microchannels were completely filled by water during the pressing tests. Otherwise, stable intermediate wetting states were observed.

Finally, it is worth mentioning that, in the pressing tests, we did not observe any transition from an intermediate state to that of Wenzel on the second set of micropillars. Also, water should not fill the gaps between coated ZnO nanowires during these tests, since we did not observe strong pinning effect during the reversal transition from the intermediate state to that of Cassie-Baxter. On the other hand, the intermediate state may still be transformed to that of Wenzel in special cases. For example, on the second set of micropillars, when the applied pressure is high enough to make water penetrate and fill the valleys between the coated ZnO nanowires, the corresponding value of θ_0 may be reduced, leading to the violation of Ineq. (4.8) and causing the transition from the intermediate state to that of Wenzel.

4.3 Summary and Conclusions

In this chapter, we first derive an angle inequality (i.e., Ineq. (4.8)) to examine whether the contact criterion is applicable to the case of micropillars with circular or polygonal cross-sections. The angle inequality is related to (a) contact angles on the inner surfaces of grooves between the micropillars and (b) inclined angles of the groove sidewalls. When this angle inequality is violated, the contact criterion holds for the

corresponding micropillars. Otherwise, the specific criterion may not be applicable to these micropillars. That is, after water contacts the bottoms of roughness grooves, Cassie-Baxter state may be transformed to an intermediate state instead. After theoretical modeling, we then conduct pressing tests on six types of micropillars. In these tests, once the angle inequality violated, the contact criterion holds true, and water fills the grooves immediately after it has contact with their bottoms. However, when the angle inequality is met, intermediate states are observed on the corresponding samples. Furthermore, these intermediate states (i) are stable in the sense that their energy states are lower than those of Wenzel models, and (ii) are transformed back to that of Cassie-Baxter, when applied pressures are reduced while Wenzel states do not necessarily have such a reversal transition.

Chapter 5

Existence and Stability of an Intermediate Wetting State on Circular Micropillars

In chapter 4, we considered the case of polygonal and circular pillars, and also derived an angle inequality, which is identical to the one derived in the case of microchannels. In the case of pillars, this angle inequality is a necessary condition that local contact angles and the inclined degree of the pillars should meet for the existence of an intermediate state. As in the case of microchannels, once this inequality is violated, there should not exist any intermediate state, and the contact criterion is also applicable to the case of micropillars. On the other hand, different from that in the case of microchannels, the satisfaction of this inequality does not guarantee the existence of a stable intermediate state for the case of micropillars. For the existence of a stable intermediate state, two conditions should be satisfied. First, there exists an equilibrium state after the contact. Second, there is an energy barrier between this equilibrium state and that of Wenzel. The consideration of these two conditions may give precise bounds of local contact angles and inclined degrees of pillar sidewalls for the existence of a stable intermediate state, which could also be used to identify the exact range that the contact criterion is applicable. We did so for the case of microchannels, since the corresponding air/liquid interfaces have simple shapes. However, we did not consider the two conditions in the case of micropillars due to lack of analytical expression of the related air/liquid interfaces. Accordingly, although the derived inequality is identical to the one for the case of channels, it may not give a precise range that the contact criterion is valid.

In this chapter, using a new approach, we consider the aforementioned two conditions for the case of circular pillars with vertical sidewalls. This approach does not

rely on the explicit expression of the interface profile, making it feasible to explore the applicability of the contact criterion. Subsequently, we apply the derived theoretical results to interpret some experimental results shown in both of our previous chapters and Verho et al. [52]

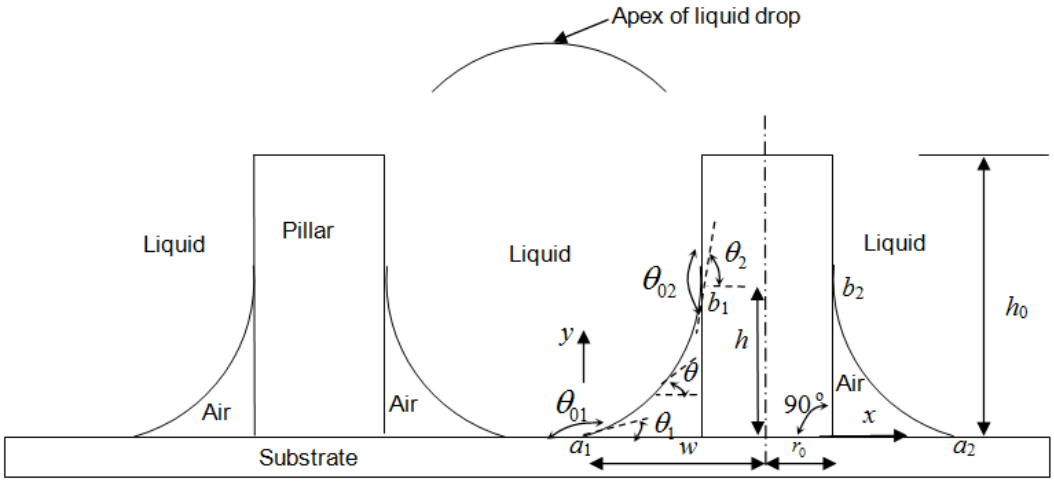

(a)

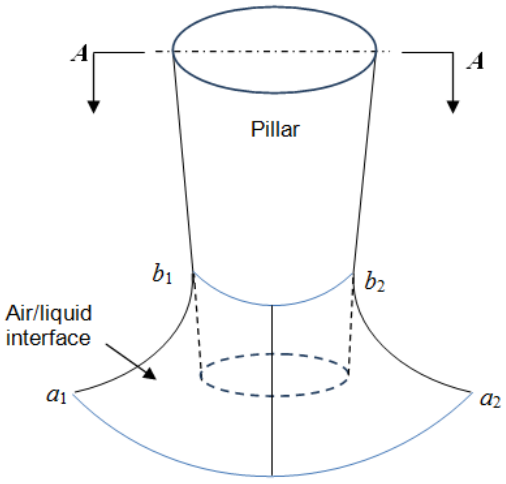

(b)

Figure 5.1: (a) Cross-sectional profile of the air/liquid interface around the bottom corner of a circular micropillar in a possible intermediate state when a liquid drop contacts the bottoms of the grooves between the micropillars, and (b) perspective view of the air/liquid interface.

5.1. Existence of an Equilibrium State inside Grooves

Assume that there exists an equilibrium state after a liquid drop slowly contacts the base of grooves, which are located between circular micropillars with vertical sidewalls (Fig. 5.1). The drop profile around the bottom corner of a circular micropillar has an axisymmetric shape. Let a_1b_1 and a_2b_2 represent two of its meridian curves (Fig. 5.1a). a_1 and a_2 are the triple-phase contact points at the base of the grooves, while b_1 and b_2 are those on the pillar sidewall. Without loss of generalization, only a_1b_1 is considered in the following analysis, and the same analysis also applies to a_2b_2. Kind r_0 to be the radius of the pillar, and let h represent the vertical distance between b_1 and the bottom of the micropillar. Furthermore, use h_0 to denote the height of the pillar. As already demonstrated before, if h_0 is less than the capillary length of liquid (it is 2.7 mm for water), which is actually the case of this work, then the gravity effect on the drop can be neglected. Accordingly, by Young-Laplace equation [60], liquid pressure inside the bottom portion of a liquid drop is uniform, and

$$p_w - p_a = 2\gamma b\,, \tag{5.1a}$$

$$p_w = p_{wt} + \rho g H, \tag{5.1b}$$

$$\frac{1}{R_1} + \frac{1}{R_2} = 2b\,, \tag{5.1c}$$

where p_w and p_a denote, respectively, liquid pressure and air pressure at a point of a_1b_1, p_{wt} represents the liquid pressure at the drop apex, H is the height of the drop, R_1 and R_2 are, respectively, radii of the maximal and minimal curvatures at this point, and b represents mean curvature at the point and is constant on the bottom surface of the drop. R_1 and R_2 are considered positive if their associated curves on the liquid surface bend

towards air. Further assume that the drop cap has a convex shape. Then, as also demonstrated before, it follows from Eq. (5.1c) that b is a positive constant.

Set up an x-y rectangular coordinate system. x- and y-axes are along horizontal and vertical directions, respectively, and the origin is located at a_1 (Fig. 5.1a). Set s to be the arc length from a_1 to a point on a_1b_1. Let θ denote the angle formed by the tangent to a_1b_1 and the horizontal direction at a point on this curve. Set θ_1 and θ_2 to be the values of θ at a_1 and b_1, respectively. Static contact angles on the sidewalls of a micropillar are considered to be the same, while they may be different from the one on the bottom of the micropillar. Let θ_{01} and θ_{02}, respectively, be static contact angles on the pillar sidewalls and groove bottoms. If the micropillar sidewalls and groove bottoms are smooth, then θ_{01} and θ_{02} are intrinsic contact angles. Otherwise, they are apparent contact angles. Furthermore, by geometric analysis, at a_1 and b_1, we have, respectively,

$$\theta_1 = 180^o - \theta_{01} \tag{5.2a}$$

$$\theta_2 = \theta_{02} - 90^o. \tag{5.2b}$$

Both θ_{01} and θ_{02} are considered to be greater than 90^o, i.e., the surfaces of the micropillars and grooves are lyophobic. Subsequently, it follows from Eqs. (5.2a) and (5.2b) that

$$0^o < \theta_1 < 90^o, \tag{5.3a}$$

$$0^o < \theta_2 < 90^o. \tag{5.3b}$$

In the case of circular micropillars, Eq. (5.1c) can be re-written in terms of θ and s as

$$\frac{d\theta}{ds} - \frac{\sin\theta}{w - x} = 2b, \tag{5.4}$$

where w denotes the distance between a_1 and the central axis of the micropillar (Fig. 5.1a). Eqs. (5.2a) and (5.2b) are also two boundary conditions for Eq. (5.4). In summary,

in order to have an equilibrium state, i.e., to make a_1 stationary, there should exist a solution to Eqs. (5.4) and (5.2) under the condition that b>0.

Equation (5.4) can be further re-written as

$$\frac{d[(w-x)\sin\theta]}{dx} = 2b(w-x), \tag{5.5}$$

where $\frac{dx}{ds} = \cos\theta$ was used in deriving this equation from Eq. (5.4). With the aid of Eq. 2(b), it follows from Eq. (5.5) that

$$\sin\theta = \frac{c}{(w-x)} - b(w-x), \tag{5.6}$$

where c is a constant and has the following expression:

$$c = r_0 \sin\theta_2 + b r_0^{\,2}. \tag{5.7}$$

With the assistance of Eqs. (5.2a) and (5.7), it follows from Eq. (5.6) that

$$b = \frac{r_0 \sin\theta_2 - w\sin\theta_1}{w^2 - r_0^{\,2}}. \tag{5.8}$$

By Eqs. (5.8), (5.2a) and (5.2b), the requirement that b>0 results in

$$\sin\theta_2 > \frac{w}{r_0}\sin\theta_1. \tag{5.9}$$

Given that Ineq. (5.9) is met, it follows from Eq. (5.8) that w is related to r_0, θ_1, θ_2, and b by

$$w = \frac{\sqrt{\sin^2\theta_1 + 4r_0 b\sin\theta_2 + 4r_0^{\,2}b^2} - \sin\theta_1}{2b}. \tag{5.10}$$

In addition, since

$$\frac{dy}{dx} = \tan\theta,$$

(5.11)

with the assistance of Eq. (5.6), it follows from Eq. (5.11) that

$$\frac{dy}{dx} = \frac{c - b(w-x)^2}{\sqrt{(1+\frac{bc}{2})(w-x)^2 - [b^2(w-x)^4 + c^2]}}. \tag{5.12}$$

Let x_p and y_p represent x and y coordinates of a representative point p on a_1b_1, where x_p ranges from 0 to (w- r_0). In view of Eq. (5.12), y_p is given below:

$$y_p(x_p) = \int_0^{x_p} \frac{c - b(w-x)^2}{\sqrt{(1+\frac{bc}{2})(w-x)^2 - [b^2(w-x)^4 + c^2]}} dx. \tag{5.13}$$

This equation gives a solution to Eqs. (5.4) and (5.2). Its right-hand side is an elliptical integral, which can be numerically integrated. Once θ_1, θ_2, w and r_0 are given, Eq. (5.8) gives a unique value to b. Subsequently, a unique value of y_p can be obtained from Eq. (5.13). Thus, Eq. (5.13) is also a unique solution to Eqs. (5.4) and (5.2). The value of h can also be determined by solving Eq. (5.13). It equals the value of y_p when $x_p = w - r_0$, and is considered to be less than h_0.

According to the above consideration, for given θ_1, θ_2, w and r_0, Ineq. (5.9) is both sufficient and necessary conditions for having a solution to Eqs (5.4) and (5.2). Next, as done in chapter 3 and chapter 4, we also derive another necessary condition that only involves θ_1 and θ_2.

Substitution of Eq. (5.6) into Eq. (5.4) leads to

$$\frac{d\theta}{ds} = b + \frac{c}{(w-x)^2}. \tag{5.14}$$

Since both c and b are positive, by Eq. (5.14) we have

$$\frac{d\theta}{ds} > 0. \tag{5.15}$$

This inequality implies that θ increases with increasing s. Hence, we have

$$\theta_2 > \theta_1, \tag{5.16}$$

which is a necessary condition for the existence of a solution to Eqs. (5.4) and (5.2), and which is also identical to the one derived in chapter 4 for the case of polygonal and circular pillars.

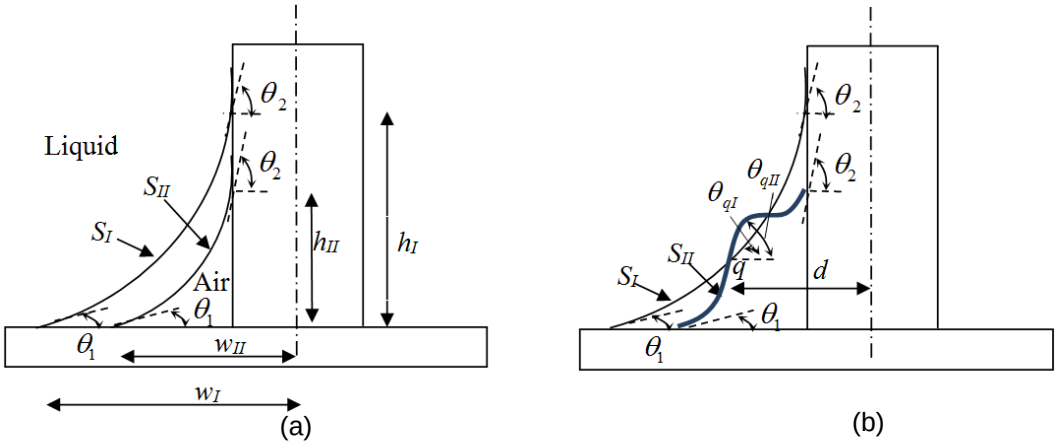

Figure 5.2: Schematics of (a) reduction of air gap around the bottom corner of a pillar with the increase in liquid pressure and (b) a possible configuration that S_I intersects with S_{II}.

5.2 Local Stability of the Intermediate State

In order to make the constructed equilibrium state locally stable, its energy state should be lower than that of completely filled case. Otherwise, liquid continues to spread on the groove base until the bottom corners of micropillars are completely filled. Subsequently, the wetting state is changed to that of Wenzel, which is the case of our previous work in chapter 2.

Next, we consider the local stability of the constructed equilibrium state. Differentiation of Eq. (5.10) with respect to *b* leads to

$$\frac{dw}{db} = \frac{\sin\theta_1}{2b^2}\left(1 - \frac{\sin\theta_1 + \frac{2r_0 b\sin\theta_2}{\sin\theta_1}}{\sqrt{\sin^2\theta_1 + 4r_0 b\sin\theta_2 + 4r_0^2 b^2}}\right). \quad (5.17)$$

It can be readily shown that, if Ineq. (5.16) holds true, then

$$\frac{dw}{db} < 0, \quad (5.18)$$

and vice versa. This inequality indicates that *w* decreases with the increasing *b*. Furthermore, based on Leibniz rule [81], it follows from Eq. (5.13) that $\frac{dh}{dw} > 0$. This implies that *h* also decreases with the increasing *b*. As demonstrated below, in addition to the two end points, other points on a_1b_1 should also move towards the bottom corner of the pillar with the increase in *b* (Fig. 5.2a). Let w_I and w_{II} denote the corresponding values of *w* when *b* is increased from b_I to b_{II}. Accordingly, we have $w_I > w_{II}$. Use s_I and s_{II} to represent a_1b_1 in these two cases respectively. Set h_I and h_{II} to be the heights of s_I and s_{II}, separately. Suppose s_I and s_{II} have some intersecting points. According to geometric analysis, under the conditions that $w_I > w_{II}$ and $h_I > h_{II}$, s_I and s_{II} should intersect at least at two points (Fig. 5.2b). Let *q* represent one of these intersecting points. Use *d* to denote the distance between *q* and the central axis of the pillar. Let θ_{qI} stand for the angle formed by the tangent to s_I and the horizontal direction at *q*. Set θ_{qII} to be the one subtended by the tangent to s_{II} and the horizontal direction at the same point. Subsequently, according to geometric analysis, we have $\theta_{qI} < \theta_{qII}$ (Fig. 5.2b). On the other hand, by Eq. (5.6), we have $\sin\theta_{qI} = \frac{r_0\sin\theta_2 + b_I(r_0^2 - d^2)}{d}$ and $\sin\theta_{qII} = \frac{r_0\sin\theta_2 + b_{II}(r_0^2 - d^2)}{d}$. Since b_I < b_{II} and *d*> r_0, we get $\sin\theta_{qI} > \sin\theta_{qII}$.

Accordingly, $\theta_{qI} > \theta_{qII}$, which contradicts with the previous result that $\theta_{qI} < \theta_{qII}$. Therefore, there is no intersecting points between s_I and s_{II}. These results imply: (i) the air gap around the bottom corner of a micropillar decreases with the increase in liquid pressure, and (ii) an additional force is needed to increase liquid pressure for reducing this air gap. Thus, if Ineq. (5.16) is met, then the intermediate state has a lower energy state than the Wenzel model, and vice versa. In this sense, Ineq. (5.16) is both sufficient and necessary conditions to make the intermediate state locally stable.

5.3 An Inequality to Meet

According to the consideration in the previous two sections, for the existence of a locally stable intermediate state, Ineqs. (5.9) and (5.16) should both be met. With the aid of Ineqs. (5.3a) and (5.3b), it is readily shown that, once Ineq. (5.9) is satisfied, Ineq. (5.16) is met. On the other hand, when Ineq. (5.16) holds true, there always exists a w_1, which satisfies the following relation:

$$\frac{\sin\theta_2}{\sin\theta_1} > \frac{w_1}{r_0} > 1. \tag{5.19}$$

This result ensures that, if w falls between r_0 and w_1, then Ineq. (5.9) is also met, implying that there always exists a region close to the bottom corner of the pillar, in which there exists a locally stable intermediate state.

The air gap around the bottom of a pillar may still be connected to the outside environment, for instance, through the gaps between nanosturctures that may be coated on the micropillars. In such a case, the pressure inside air gap still equals the atmospheric pressure. In case the air gap around the bottom of a pillar is completely isolated from the outside, the pressure in the air gap may increase when the air gap around a pillar is compressed by the liquid drop, while the air pressure on the drop top

remains the same. By eq. (5.1a), this means that actually a higher liquid pressure is needed to further compress the air gap. This also implies that air pressures around the liquid drop may be different. Subsequently, for a small drop, whose half size is less than the capillary length of the liquid and thus whose gravity effect is neglected, by Eq. (5.1a) again, the mean curvature around this drop may vary, since the liquid pressure inside the drop is uniform. Therefore, for a liquid drop to be stationary (i.e. at equilibrium), instead of examining the mean curvature, our concern is whether the liquid pressure is balanced inside this drop.

Two related points can be obtained based on the stability consideration in the previous section. First, for a given *w* in this region, the corresponding value of *b* is determined using Eq. (5.8). When p_w, calculated using Eq. (5.1a) and this value of *b*, is larger than the one calculated employing Eq. (5.1b), which is the liquid pressure at the bottom portion of the drop, to maintain the pressure balance inside the drop, a_1 moves back towards the center of the groove or the liquid drop loses contact with the bottom of the groove. Second, if the former value of p_w is less than the latter one, then a_1 continues to move towards the corner of the pillar until the two values of p_w are equal. In summary, the satisfaction of Ineq. (5.16) guarantees the existence of a locally stable intermediate state after a liquid drop contacts the base of grooves.

With the aid of Eqs. 5.2(a) and 5.2(b), Ineq. (5.16) can be re-written in terms of θ_{01} and θ_{02} as

$$(\theta_{01} + \theta_{02}) > 270^0. \tag{5.20}$$

This inequality is identical to the one derived in our previous work for the case that circular pillars have vertical sidewalls. Ineq. (5.20) was derived in the previous work as a necessary condition for the existence of an intermediate state, while it is also a sufficient

condition as shown in this work. Consequently, we have arrived at an angle criterion: once θ_{01} and θ_{02} of circular micropillars with vertical sidewalls satisfy Ineq. (5.20), there exists a locally stable intermediate wetting state after a liquid drop contacts the base of grooves in a quasi-static manner. This angle criterion is similar to the one that we have previously derived for the case of microchannels. [82]

A set of values of θ_{01} and θ_{02} may be experimentally measured, depending on the volume of a liquid drop [73, 83]. These sets of values vary between receding and advancing angles. Accordingly, the minimum requirement in designing circular pillars for having a locally stable intermediate state is that the advancing angles on the pillar sidewalls and groove bottom should meet Ineq. (5.20). For the sake of security, it is better to have the receding angles, which are the minimum possible values of θ_{01} and θ_{02} that satisfy this inequality.

5.4. Experimental Validation

5.4.1. Existing Results

In chapter 4, we did the pressing tests on six kinds of SU-8 circular micropillars, which all have approximately vertical sidewalls while vary in the pitches or in the local contact angles. On three kinds of these micropillars, groove surfaces were smooth. On a smooth surface, contact angle is normally less than 120^0 even if this surface is coated with highly water-repellant materials [29], such as Teflon. Hence, Ineq. (5.20) was violated, and water drops collapsed after their contact with the grooves. However, on another three kinds of micropillars, Ineq. (5.20) was met, since the surfaces of the grooves located between the micropillars were covered with ZnO nanowires, which made both θ_{01} and θ_{02} above 135^o. Consequently, intermediate states were found.

In Verho et al [52], two kinds of Si circular micropillars with identical dimensions (diameter 10 μm, height 5 or 10 μm, and pitch 20 μm) were examined. The first kind was coated with a hydrophobic fluoroalkylsilane monolayer, which had advancing and receding angles of 118°±2° and 102°±2°, respectively, on flat surfaces [52]. The second kind of micropillars were coated with silicone nanofilaments, which made advancing and receding angles become 170°±2° and 145°±2°, separately, on flat surfaces. Accordingly, Ineq. (5.20) was violated on the first kind of micropillars, while it was met on the second kind. Hence, intermediate states existed on the second kind of micropillars, while only Wenzel states existed on the first kind when water contacted the base of grooves, which were actually the experimental results reported in Verho et al. [52]

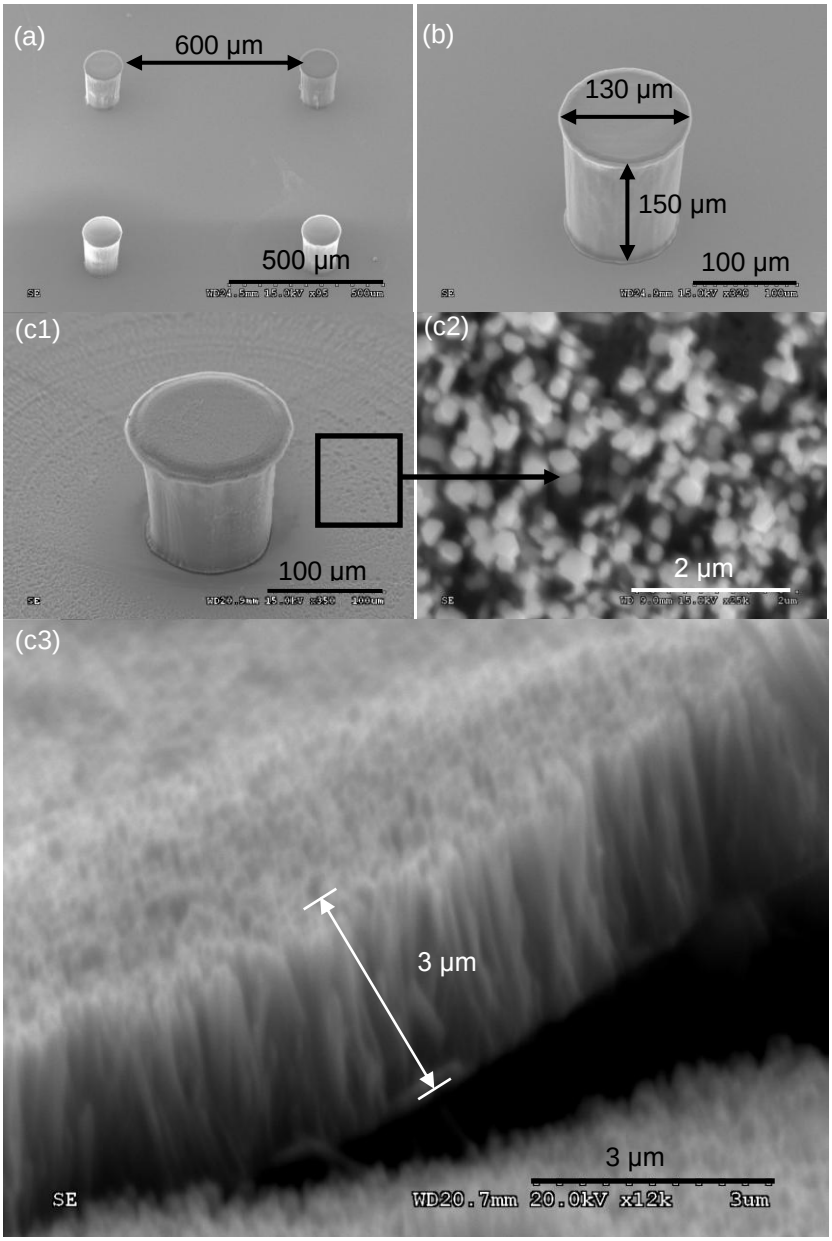

Figure 5.3: (a) Perspective views of SU-8 micropillars. Representative first and second kinds of circular pillars, which were covered with (b) Teflon and (c1) ZnO nanowires, respectively. (c2) Close-up and (c3) side views of ZnO nanowires. All are scanning electron microscopy (SEM) images.

5.4.2. New Tests

Experiments are also done in this work to have in-situ observation of how a_1 moves on the bottom of a groove when water pressure is increased or decreased. In other words, we desire to examine whether, as predicted in Section 5.3, a_1 moves towards or away from the bottom corner of a pillar with the increase or decrease in the water pressure when Ineq. (5.20) is met. For this purpose, two of the six kinds of SU-8 circular micropillars, which have been previously examined in chapter 4, are adopted in this work (Fig. 5.3). These two kinds have the largest pitch of 600 μm, which makes it relatively easy to observe the movement of a_1 on the bottom of the gap. They also have the same radii of 130 μm. On the other hand, to enhance hydrophobicity, the first kind of micropillar is coated with Teflon (Fig. 5.3b), while the second kind is covered with ZnO nanowires, which have hexagonal cross-sections with an average length of 2.8 μm and diameters of 0.15 to 0.36 μm (Fig. 5.3c). The advancing angles are adopted as the values of θ_{01} and θ_{02}. In the case of the first kind of micropillars, the values of θ_{01} and θ_{02} are 119°±2° and 119°±2°, respectively, while they are 169°±2° and 169°±2°, separately. Accordingly, the values of θ_{01} and θ_{02} for the first kind of micropillars meet Ineq. (5.20), while those for the second kind do not satisfy this inequality.

Through only side views, due to block of water, it was not clear whether water completely filled the middle grooves after the drops had contacted the bottoms of these grooves. To solve this problem, similar to what was done in Verho et al, [52] we also take top views of the pressed water drops in this work. Thus, two types of pressing tests are conducted on each kind of SU-8 micropillars. In the first type (Fig. 5.4a), an optical microscope (mm001300m of Metallurgical microscope Company) is rotated by 90^o to have a side view of air/water interfaces between micropillars, and a polydimethylsiloxane (PDMS) plate (5×5×10 mm^3) is put on the top of a water drop to slowly press it against

micropillars. The vertical movements of this plate are controlled by a micromanipulator (M3301R of World Precision Instruments) with a precision of 100 µm. In the second type of pressing tests (Fig. 5.4b), a Teflon-coated glass slide (25×25×1 mm^3) is placed on a water drop, and the optical microscope is used to observe the air/water interface from the top. Thinner glass slides (25×25×0.2 mm^3) are stacked together to serve as the supporters of the Teflon-coated glass slide. This glass slide can be lowered down or lifted up with a precision of 200 µm (which is the thickness of a thinner glass slide) to increase or decrease the applied pressure on the water drop by removing or adding thinner glass slides in the supporters. Small water drops are used in the pressing tests, and their volumes range from 6 to 9 µl. Such a drop has a spherical cap after it is placed on the substrate.

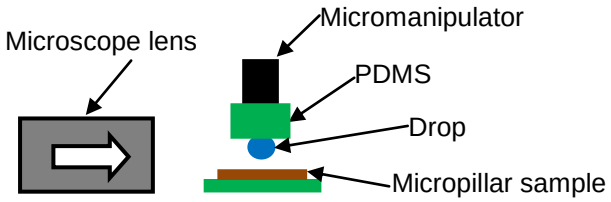

(a)

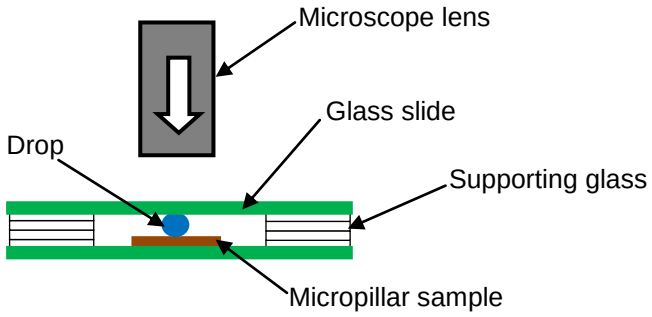

(b)

Figure 5.4: Setups for (a) first and (b) second types of pressing tests to obtain side and top views of pressing results, respectively.

An important point was observed through pressing tests on the first kind of micropillars (Fig. 5.5). After water drop had contacted the bottom of a groove, it collapsed, and water completely covered the bottom corners of the outside pillars underneath this water drop. Also, the increase or decrease in the applied pressure caused the increase or decrease in the number of the pillars covered by the water drop. The air gaps surrounding middle pillars could be clearly identified through top views according to the light reflection (see, for example, Figs. 5.5(b1) and 5.6(b)). The bottom corners of the outside pillars underneath the drop were completely covered by water according to the side view (Fig. 5.5(a2)), while the bottom corners of the middle pillars were completely covered by water based on the top view (Fig. 5.5(b2)). In addition, part of the water drop was left on the substrate when the pressing plate was removed (Figs. 5.5(a3) and 5.5(b3)), implying that Wenzel state was not completely transited back to that of Cassie-Baxter.

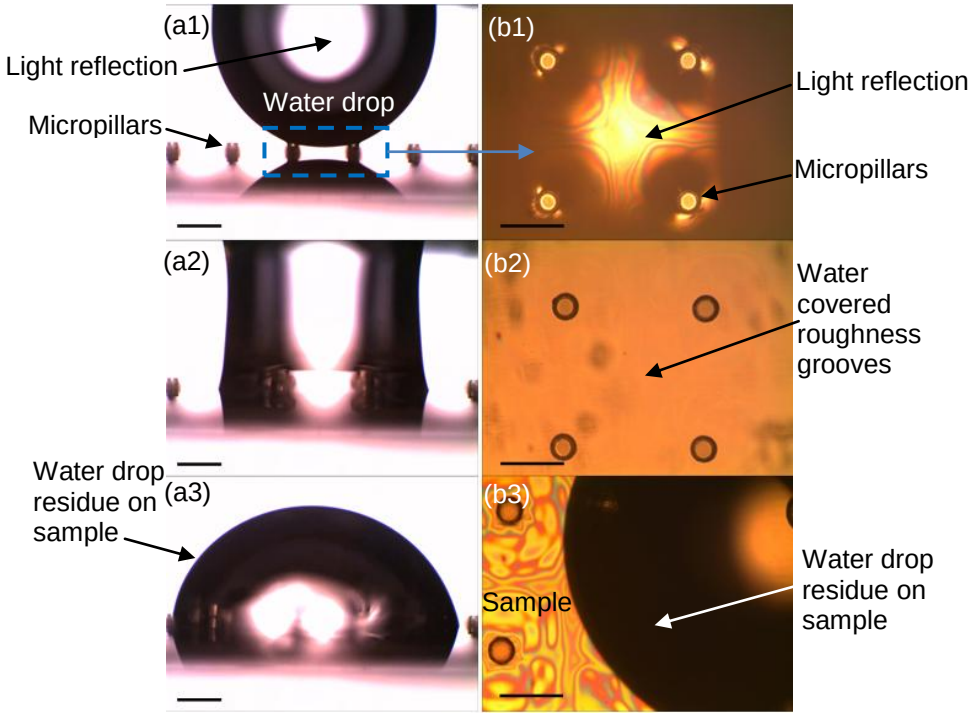

Figure 5.5: Pressing test results on the first kind of micropillars. In order to get a better understanding of these results, (a) side and (b) top views are placed together, while they were taken in the first and second pressing tests, respectively. The corresponding area of top views is boxed in (a1). (a1) and (b1) Before and (a2) and (b2) after the contact of water with the base of grooves. (a3) and (b3) Water residue on the sample after the pressing slide has been removed. The scale bars represent 420 µm.

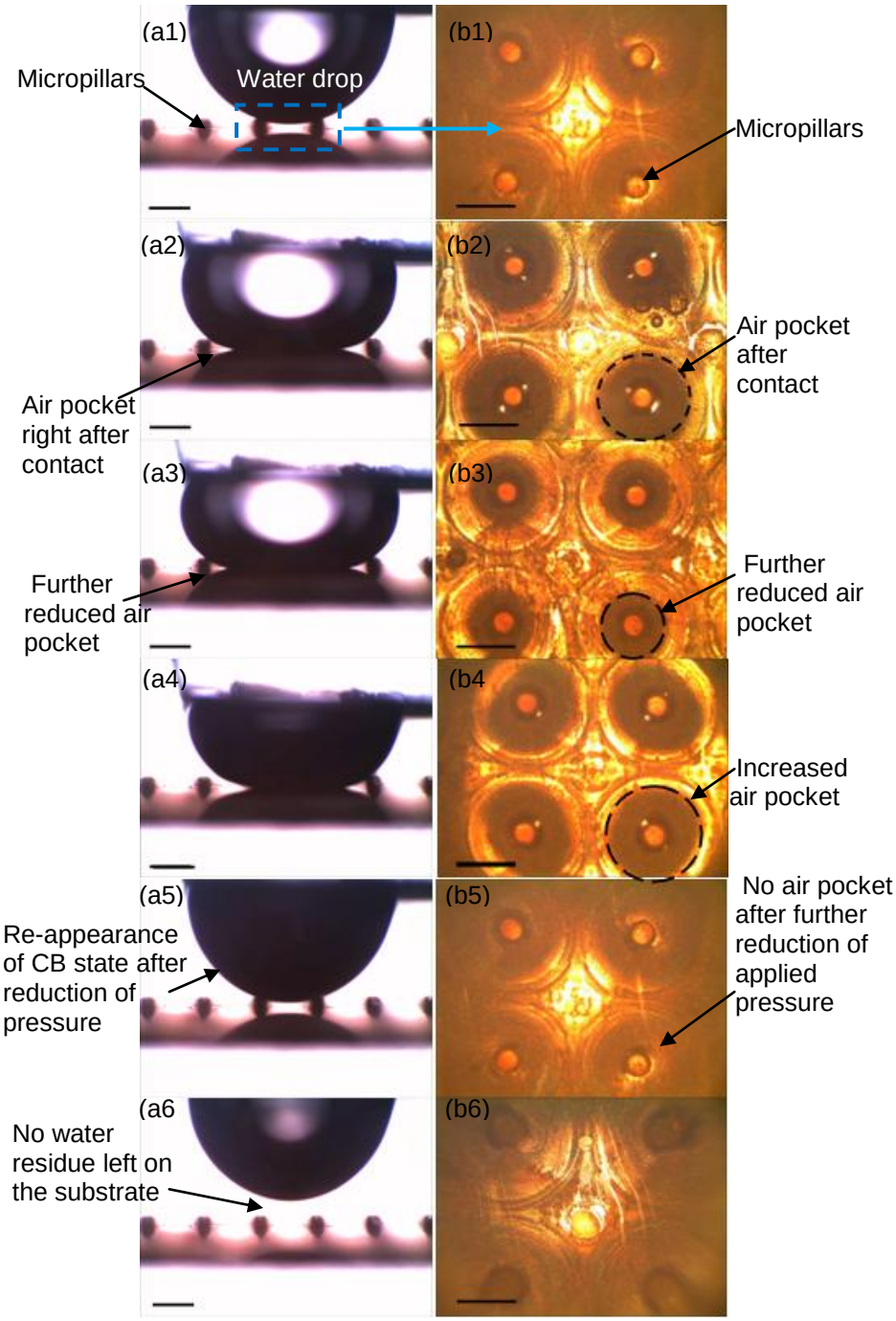

Figure 5.6: (a) and (b) side and top views of pressing test results on the second kind of micropillars. The corresponding area of top views is boxed in (a1). (a1)-(a4) and (b1)-(b4) Increase, and (a5)-(a7) and (b5)-(b7) reduce applied pressure. The scale bars represent 420 μm.

On the other hand, different results were observed on the second kind of micropillars (Fig. 5.6). After water had contact with the base of a few grooves, the air pockets could be observed around the outside micropillars through side views (Figs. 5.6(a2)-5.6(a4)). Furthermore, through top views, we could clearly see that air pockets around the middle pillars increased or decreased the sizes with the decrease or increase in water pressure (Figs. 5.6(b2)-5.6(b4)), which were invisible in the side views due to the block of water. Eventually, the water drop recovered its Cassie-Baxter wetting state after much reduction in the applied pressure (Figs. 5.6(a5) and 5.6(b5)). Finally, this water drop was removed from its substrate by the pressing plate or slide, and no water residue was observed on the substrate (Figs. 5.6(a6) and 5.6(b6)). In addition, as marked in Fig. 5.6b, during the processes of increasing and reducing the applied pressure, the air pocket had an approximately circular contact area with the base of grooves, partially supporting our previous assumption that the liquid/air profile has an axisymmetric shape.

Two points can be summarized from the pressing results on the two kinds of micropillars. First, as predicted using Ineq. (5.20), intermediate states exist on the second kind of micropillars, but not on the first kind. Second, the experimental results on the second kind of micropillars clearly demonstrate that, as predicted in Section 5.3, a_1 moves towards or away from the bottom corner of a pillar with the increase or decrease in the water pressure when Ineq. (5.20) is met.

Due to lack of simple expression of the air/liquid interface, we don not estimate the energy barrier that separates the intermediate state and the Wenzel model. On the other hand, as commented in chapter 4, when the applied pressure is high enough to make water penetrate and fill the valleys between the coated ZnO wires on the second kind of micropillars, the corresponding values of θ_{01} and θ_{02} may be reduced, leading to

the violation of Ineq (5.20) and causing the transition from the intermediate state to that of Wenzel.

5.5 Summary and Conclusions

In this chapter, we derive an angle inequality, which is Ineq. (5.20), to examine whether the contact criterion is applicable to the case of circular micropillars, and also to understand why the coverage of nanostructures on the corresponding groove surfaces may result in an intermediate wetting state after a liquid drop contacts the groove bottom. We directly observed the evolution of air/water interfaces around micropillars through the front and top views when applying pressure on the water drop. By considering the existence and stability of an equilibrium state, we demonstrate: (i) when this angle inequality is met due to the increase of local contact angles by, for example, nanostructures, there exists a locally stable intermediate state after a water drop slowly contacts the base of grooves and the contact criterion does not hold for the corresponding micropillars, and (ii) if the inequality is violated, then such an intermediate state does not exist and the contact criterion holds true.

Chapter 6

Wetting States on Circular Micropillars with Convex Sidewalls after Liquids Contact Groove Base

In this chapter we consider the applicability of the contact criterion to circular micropillars with convex sidewalls, and derive an angle inequality for judging transition from Cassie−Baxter to Wenzel States. We also consider the transition on spherical microparticles, as well as that on circular micropillars with straight sidewalls. Finally, we validate the angle inequality through pressing tests on three lotus varieties and spherical microballs.

6.1 Introduction

Depending on the dimensions of roughness structures and Young contact angle, the Cassie-Baxter state may have a higher or lower energy level than the Wenzel model. [29, 50, 74] Obviously, there is an energy barrier to surpass for the Cassie-Baxter state to change to that of Wenzel, when the former state has a lower energy level. Moreover, even if the Cassie-Baxter state has a higher energy level, an energy barrier may still exist. [50, 74] The energy barrier may be increased, for example, by creating smaller structures on the sidewalls of roughness structures to make the Cassie-Baxter state more difficult to be transitioned to that of Wenzel. [84] Once such transition happens, it is irreversible due to the existence of a much higher energy barrier, [74] unless the energy barrier can be overcome by an additional force, such as an electrical force. [66]

In addition, although this work is mainly related to Cassie-Baxter and Wenzel states, it is worth pointing out that, in addition to these two states, another wetting state is also reported: [85, 86] Cassie impregnating state. This wetting state is similar to that of

Wenzel, while it includes a thin liquid film which fills the roughness structures around the liquid drop. In special cases, its energy level may be even lower than those of both Cassie-Baxter and Wenzel models. [85, 86]

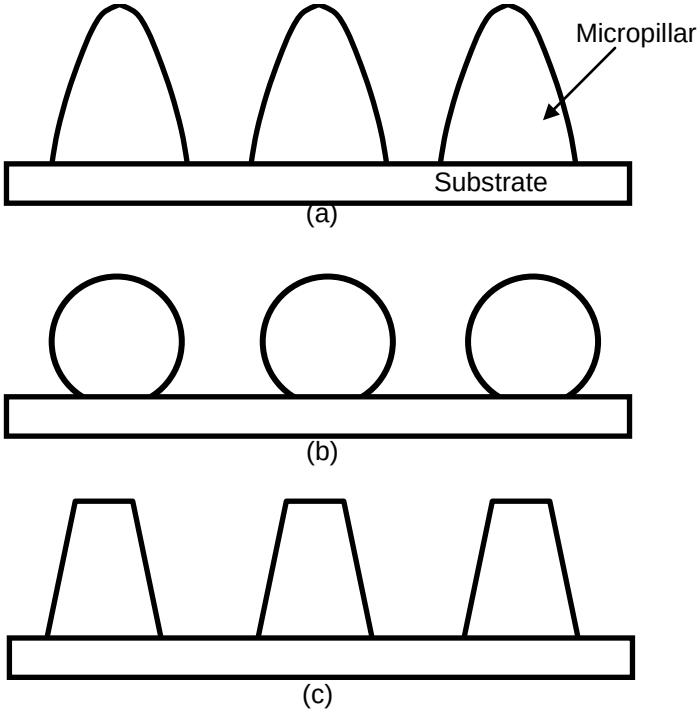

Figure 6.1: Cross-sectional profiles of (a) lotus micropillars in the form of paraboloids with revolution, (b) spherical microparticles, and (c) circular micropillars with straight sidewalls.

The lotus surface may be structured by micropillars, which are covered with nanopillars. [27] The lotus micropillars were measured [27] and modeled [54] approximately as paraboloids of revolution (Fig. 6.1a), which means that these micropillars can be considered as circular pillars whose sidewalls have convex shapes in the vertical planes. In addition, microparticles are also employed to modify surface

wetting. [55-58] It is also interesting to know whether the contact criterion applies to the case of microparticles. The microparticles may have spherical shapes, which can also be considered as circular pillars with convex sidewalls (Fig. 6.1b). Thus, in this chapter, we would like to explore the applicability of the contact criterion to circular pillars with convex sidewalls. Furthermore, when the slopes of the convex sidewalls are constant, the circular micropillars with convex sidewalls are reduced to those with straight sidewalls (Fig. 6.1c). Accordingly, the circular micropillars with either vertically or obliquely straight walls may be considered as a special type of those with convex sidewalls. Thus, in this chapter, we also explore the applicability of the contact criterion to the case that micropillars have straight sidewalls.

Let φ_0 denote the maximum angle that is formed by the tangent to the micropillar sidewall with the horizontal plane (Fig. 6.2). Based on the value of φ_0, there exist two situations, in which $0^o < \varphi_0 \leq 90^o$ and $90^o < \varphi_0 < 180^o$, respectively. In this chapter, for the micropillars with convex sidewalls, the first situation is explored with no need seeking analytical expressions of air/liquid interfaces, while the second one is considered based on approximate expressions of such interfaces.

6.2 Theoretical Modeling in the Situation $\varphi_0 \le 90^o$

In this section, we first explore in Sub-sections 6.2.1 to 6.2.3 the case of micropillars with convex sidewalls, and then consider in Sub-section 6.2.4 the case of micropillars with straight sidewalls.

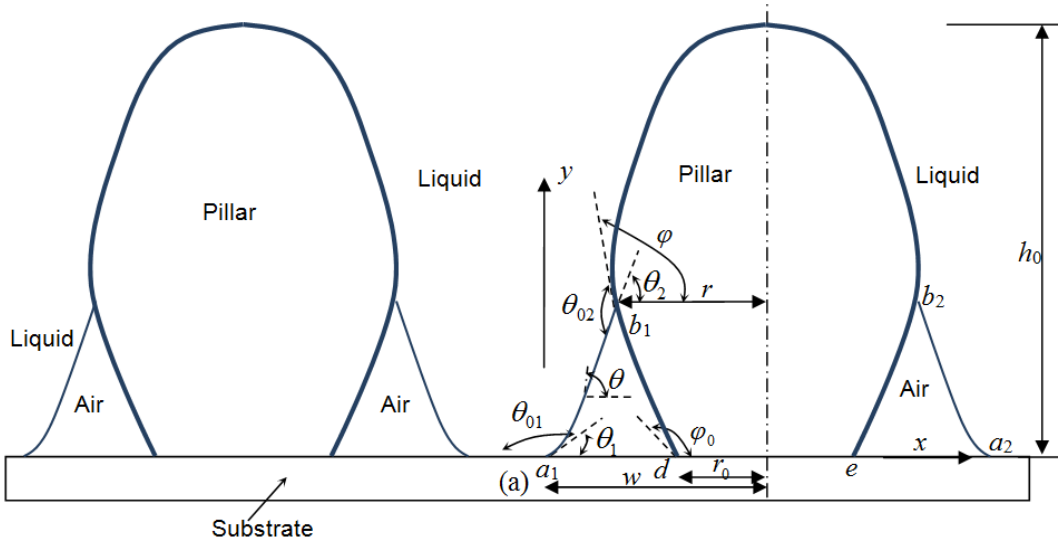

Figure 6.2: Cross-sectional profile of the air/liquid interfaces around the bottom corners of circular micropillars with convex sidewalls, when a liquid drop contacts the bottoms of the grooves between the micropillars and forms an intermediate wetting state.

6.2.1. Existence of an Intermediate State for Micropillars with Convex Sidewalls

We assume that there exists an intermediate wetting state after a liquid drop contacts the base of grooves, which are located between circular micropillars with convex sidewalls, in a quasi-static manner (Fig. 6.2). The sidewalls are considered to bend towards air and have a general convex shape. The drop profile around the bottom corner of a circular micropillar has an axisymmetric shape. Let a_1b_1 and a_2b_2 represent two of its meridian curves (Fig. 6.2). a_1 and a_2 are the triple-phase contact points at the base of the grooves, while b_1 and b_2 are those on the pillar sidewall. Without loss of generalization, only a_1b_1 is considered in the following analysis, and the same analysis also applies to

a_2b_2. Let *de* denotes the bottom of the pillar. Let φ denote the angle formed at b_1 by the tangent to the sidewall with the horizontal plane. φ gradually increases when b_1 moves down on the sidewall, and we have $0^o < \varphi \le \varphi_0 < 180^o$. Use *r* to denote the lateral distance between b_1 and the central axis of the pillar, let r_0 represent the lateral distance between *d* and the central axis of the pillar, and set h_0 to denote the height of the pillar. As already demonstrated before, if h_0 is less than the capillary length of the liquid (2.7 mm for water), which is actually the case of this work, then the gravity effect on the bottom portion of a liquid drop can be neglected. Accordingly, by Young-Laplace equation, [60] liquid pressure inside the bottom portion of a liquid drop is uniform, and

$$p_w - p_a = 2\gamma b\,, \tag{6.1a}$$

$$p_w = p_{wt} + \rho g h\,, \tag{6.1b}$$

$$\frac{1}{R_1} + \frac{1}{R_2} = 2b\,, \tag{6.1c}$$

where p_w and p_a denote, respectively, liquid pressure and air pressure at a point of a_1b_1, p_{wt} represents the liquid pressure at the drop apex, *h* is the height of the drop, R_1 and R_2 are, respectively, radii of the maximal and minimal curvatures at this point, and *b* represents mean curvature at the point and is constant on the bottom surface of the drop. R_1 and R_2 are considered positive if their associated curves on the liquid surface bend towards air. Further assume that the drop cap has a convex shape. Then, as also demonstrated before, it follows from Eq. (6.1c) that *b* is a positive constant.

Set up an *x*-*y* rectangular coordinate system. *x*- and *y*-axes are along horizontal and vertical directions, respectively, and the origin is located at a_1 (Fig. 6.2). Set *s* to be the arc length from a_1 to a point on a_1b_1. Let θ denote the angle formed by the tangent to a_1b_1 and the horizontal direction at a point on this curve. Set θ_1 and θ_2 to be the values

of θ at a_1 and b_1, respectively. Equilibrium contact angles [87] on the sidewalls of a micropillar are considered to be the same, while they may be different from the one on the bottom of the micropillar. Let θ_{01} and θ_{02}, respectively, be equilibrium contact angles on the pillar sidewalls and groove bottoms. If the micropillar sidewalls and groove bottoms are smooth, then θ_{01} and θ_{02} are Young contact angles. Otherwise, they are apparent contact angles. By geometric analysis, at a_1 and b_1, we have, respectively,

$$\theta_1 = 180^{\circ} - \theta_{01}, \tag{6.2a}$$

$$\theta_2 = \varphi + \theta_{02} - 180^{\circ}. \tag{6.2b}$$

It follows from Eqs. (6.2a) and (6.2b) that

$$0^{\circ} < \theta_1 < 180^{\circ}, \tag{6.3a}$$

$$-90^{\circ} < \theta_2 < 180^{\circ}. \tag{6.3b}$$

In the case of circular micropillars with either straight or convex sidewalls, Eq. (6.1c) can be re-written in terms of θ and s as

$$\frac{d\theta}{ds} - \frac{\sin\theta}{w - x} = 2b, \tag{6.4}$$

where w denotes the distance between a_1 and the central axis of the micropillar (Fig. 6.2). Eqs. (6.2a) and (6.2b) are also two boundary conditions for Eq. (6.4). In summary, in order to have an equilibrium state, i.e., to make a_1 stationary, there should exist a solution to Eqs. (6.4) and (6.2) under the condition that $b>0$.

Equation (6.4) can be further re-written as

$$b = \frac{r\sin\theta_2 - w\sin\theta_1}{w^2 - r^2}. \tag{6.5}$$

Once θ_{01}, θ_{02}, r, and the equation of the sidewall profile are given, there exists a unique solution to Eqs. (6.4) and (6.2).

By Eq. (6.5), the requirement that $b>0$ results in two possible sufficient conditions for having the solution to Eqs. (6.4) and (6.2). First, if $w>r$, then

$$\sin\theta_2 > \frac{w}{r}\sin\theta_1. \tag{6.6}$$

Second, if $w<r$, then

$$\sin\theta_2 < \frac{w}{r}\sin\theta_1. \tag{6.7}$$

In addition, according to the result of chapter 4, the following inequality is also a necessary condition to have a solution to Eqs. (6.4) and (6.2):

$$\theta_2 > \theta_1. \tag{6.8}$$

6.2.2. Local Stability of the Intermediate State for Micropillars with Convex Sidewalls

In order to make the constructed intermediate state locally stable, there should exist an energy barrier between this wetting state and that of Wenzel. [50, 74] Otherwise, liquid continues to spread on the groove base until the bottom corners of micropillars are completely filled. Subsequently, the wetting state is changed to that of Wenzel. In the case of microchannels, a simple analytical expression was obtained for the corresponding air/liquid interface in the intermediate state. Based on this analytical expression, we directly compared the energy level of the intermediate state with that of the Wenzel state to judge the existence of the energy barrier. [79] However, we are not using this approach here for the case of micropillars, due to lack of a simple analytical expression of the air/liquid interface in the intermediate state. Instead, as detailed below, we adopt another method to consider local stability of the constructed intermediate state, and this method does not necessarily reply on the explicit expression of the air/liquid interface.

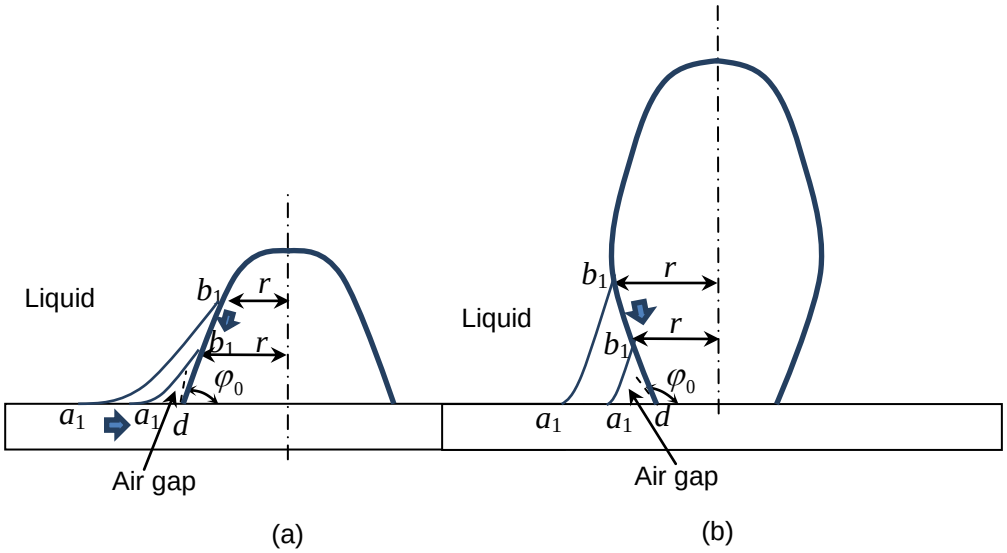

Figure 6.3: Consideration of local stability when both a_1 and b_1 move towards the bottom corner of the micropillar with convex sidewalls, if (a) $\varphi_0 \leq 90°$ or (b) $\varphi_0 > 90°$. Arrows denote the moving directions of a_1 or b_1.

If the air gap reduces its size only when liquid pressure is increased, then it implies that an additional force is needed to increase liquid pressure for changing the constructed intermediate state to that of Wenzel. Accordingly, the two wetting states are separated by an energy barrier, indicating that the constructed intermediate state is locally stable. It is observed from Eqs. (6.5) and (6.2b) that b is related to w, r and φ. Accordingly, the differential of b can be expressed in terms of dw, dr and $d\varphi$ as

$$db = \frac{\partial b}{\partial w} dw + \frac{\partial b}{\partial r} dr + \frac{\partial b}{\partial \varphi} d\varphi. \tag{6.9}$$

When $\varphi_0 \leq 90^o$, as the air gap reduces its size, both a_1 and b_1 should move towards d. Accordingly, we have (Fig. 6.3a): $dw<0$, $dr>0$ and $d\varphi > 0$. By Eq. (6.5), if

$$\sin\theta_2 > \sin\theta_1, \tag{6.10}$$

then $\frac{\partial b}{\partial w} < 0$, $\frac{\partial b}{\partial r} > 0$, and $\frac{\partial b}{\partial \varphi} > 0$. Subsequently, it follows from Eq. (6.9) that *db*>0, implying that the corresponding air gap only reduces its size with the increase in liquid pressure. Hence, under the situation that $\varphi_0 \le 90^o$, if Ineq. (6.10) is met, then the constructed intermediate state is locally stable. Accordingly, this inequality provides a sufficient condition to judge the local stability of the constructed intermediate state. Furthermore, if Ineq. (6.10) is met, it is readily shown that Ineq. (6.7) cannot hold true.

Under the situation that $\varphi_0 > 90^o$, when both a_1 and b_1 move towards *d*, we have (Fig. 6.3b): *dw*<0, *dr*<0 and $d\varphi > 0$. Furthermore, by Eq. (6.5), if Ineq. (6.10) is satisfied, then $\frac{\partial b}{\partial w} < 0$, $\frac{\partial b}{\partial r} < 0$, and $\frac{\partial b}{\partial \varphi} < 0$. Substitution of these inequalities into Ineq. (6.9) does not arrive at the conclusion that *db*>0. As will be detailed in Section 6.3, an alternative approach to determine whether we have *db*>0 is to directly differentiate an explicit expression of *b*.

6.2.3 An Inequality to Meet

According to the consideration in the previous two sub-sections, there should exist a locally stable intermediate state, if Ineqs. (6.6) and (6.10) are all met and

$$\varphi_0 \le 90^o. \tag{6.11}$$

In addition, we should also have *w* > *r*, which, as observed from Fig. 6.3(a), actually holds true when Ineq. (6.11) is met. When Ineq. (6.10) holds true, there always exist a w_1 and a r_1, which satisfy the following two relations:

$$w_1 > r_0 > r_1 > 0, \tag{6.12a}$$

$$\frac{\sin\theta_2}{\sin\theta_1} > \frac{w_1}{r_1} > 1. \tag{6.12b}$$

Ineq. (6.12b) ensures that, if w falls between r_0 and w_1, together with that r falls between r_1 and r_0, then Ineq. (6.6) is also met, implying that there always exists a region around the bottom corner of the pillar, in which there exists a locally stable intermediate state. Two related points can be further obtained based on the stability consideration in the previous sub-section. First, for given w and r in this region, the corresponding value of b is determined using Eq. (6.5). If p_w, calculated using Eq. (6.1a) and this value of b, is larger than the one calculated employing Eq. (6.1b), which is the liquid pressure at the bottom portion of the drop, then a_1 and b_1 should move away from the bottom corner of the pillar to maintain the pressure balance inside the drop. Second, when the former value of p_w is less than the latter one, a_1 and b_1 continue to move towards the corner of the pillar until the two values of p_w are equal. Accordingly, Ineq. (6.10) is a sufficient condition for having a locally stable intermediate state after a liquid drop contacts the base of grooves. Furthermore, with the aid of Ineqs. (6.11), (6.2b) and (6.3a), it is readily shown that Ineqs. (6.10) and (6.8) are equivalent, implying that Ineq. (6.10) is also a necessary condition for the existence of a locally stable intermediate state.

By Eqs. 6.2(a) and 6.2(b), Ineq. (6.8) can be re-written in terms of θ_{01}, θ_{02} and φ as

$$360^{\circ} < (\theta_{01} + \theta_{02} + \varphi) . \tag{6.13}$$

Based on the above discussions, Ineq. (6.13) is both sufficient and necessary conditions for the existence of a locally stable intermediate state after a liquid drop contacts the base of grooves in a quasi-static manner. This inequality has also been previously derived as both sufficient and necessary conditions for the case of microchannels. [79] It is also a necessary condition for the existence of a locally stable intermediate state in the case of micropillars with straight sidewalls. [82]

6.2.4 Existence and Local Stability of an Equilibrium State inside Grooves for Micropillars with Straight Sidewalls

For the case of circular pillars with straight sidewalls (Fig. 6.1a), following the line of reasoning used in Sub-sections 6.2.1-6.2.3 and noting that φ is constant now, we find: (i) $d\varphi = 0$; and (ii) once Ineq. (6.13) is met, together with that $\varphi \leq 90^{o}$, there may also exist a locally stable intermediate wetting state after a liquid drop contacts the base of grooves in a quasi-static manner.

6.3 Theorectical Modeling in the Situation $\varphi_0 > 90^{o}$

The results derived in Sub-section 6.2.1 also apply to the situation that

$$\varphi_0 > 90^{o}, \tag{6.14}$$

since the derivation in that sub-section does not specify the value of φ_0. However, as indicated in Sub-section 6.2.2, the approach employed to consider the local stability for the situation that $\varphi_0 \leq 90^{o}$ does not directly apply to that $\varphi_0 > 90^{o}$. Accordingly, for the latter situation, we desire to use an alternative approach to consider the local stability. That is, find an explicit expression of *b* to determine whether *db*>0. For this purpose, we need to get the expression of the air/liquid interface, as well as that of micropillar sidewalls. Due to the lack of theoretical expression of the air/liquid interface, as what was done before in considering small axi-symmetric air/liquid profiles, [73, 83] the cross-sectional profile of the air/liquid interface is approximated as a circular arc. Based on this approximation, spherical microparticles are specifically considered, which have known sidewall profiles and which are also a type of micropillars with convex sidewalls. Micropillars with straight sidewalls are considered as well, since their sidewall profiles can be analytically defined.

6.3.1. Spherical Microparticles

For spherical microparticles, by geometric analysis, we have approximate expressions of *b* and *w*:

$$b = \frac{\sin\frac{\psi}{2}\sin(\theta_{01} - \frac{\psi}{2})}{r_1(\cos\varphi - \cos\varphi_0)}, \tag{6.15a}$$

$$w = \frac{r_1(\cos\varphi - \cos\varphi_0)}{\sin\varphi}[\cos\varphi + \frac{\sin(\theta_{02} - \frac{\psi}{2})}{\sin(\theta_{01} - \frac{\psi}{2})}] + r_1\sin\varphi, \tag{6.15b}$$

where r_1 denotes the radius of a spherical microparticle, and

$$\psi = \theta_{01} + \theta_{02} + \varphi - 360^0. \tag{6.16}$$

By Eq. (6.15a), it is readily shown that if $\psi > 0^0$, i.e., if Ineq. (6.13) is satisfied, then the requirement that *b*>0 is met. It can also be seen from Eqs. (6.15a) and (6.15b) that both *b* and *w* are functions of φ only. Accordingly, it follows from Eqs. (6.15a) and (6.15b) that, if Ineq. (6.13) holds true, then

$$\frac{db}{d\varphi} > 0, \tag{6.17a}$$

$$\frac{dw}{d\varphi} < 0. \tag{6.17b}$$

According to geometric analysis, b_1 moves towards the bottom corner of the spherical microparticle with the increase in φ. Ineq. (6.17b) indicates that a_1 also moves towards this corner with the increase in φ, and Ineq. (6.17a) implies that *b* increases with the increasing φ. Accordingly, *b* should increase when both a_1 and b_1 move towards the bottom corner of the spherical microparticle. In other words, liquid pressure needs to be increased to reduce the air gap. Thus, if Ineq. (6.13) is met, then the intermediate state is also locally stable. In summary, Ineq. (6.13) is also both sufficient and necessary

conditions for the existence of a locally stable intermediate state in the case of spherical microparticles.

6.3.2 Circular Micropillars with Straight Sidewalls

Let w_0 denote the distance between b_1 and the bottom corner of a circular micropillar with straight sidewalls. According to geometric analysis, b can be expressed as either w or w_0 as:

$$b = \frac{\sin\frac{\psi}{2}\sin(\theta_{02} - \frac{\psi}{2})}{w\sin\varphi}, \tag{6.18a}$$

$$b = \frac{\sin\frac{\psi}{2}\sin(\theta_{01} - \frac{\psi}{2})}{w_0\sin\varphi}. \tag{18b}$$

According to these two inequalities, it is readily shown that, if Ineq. (6.13) holds true, then $b>0$ and

$$\frac{db}{dw} > 0, \tag{6.19a}$$

$$\frac{db}{dw_0} < 0. \tag{6.19b}$$

Ineqs. (6.19a) and (6.19b) imply that b increases when both a_1 and b_1 move towards the bottom corner of the micropillar. As what was discussed in the previous sub-section, this result indicates that Ineq. (6.13) is both sufficient and necessary conditions as well for the possible existence of a locally stable intermediate state in the case of circular micropillars with straight sidewalls.

According to the considerations in this and previous sections, we have arrived at a criterion for the existence of an intermediate state: there exists a locally stable

intermediate wetting state after a liquid drop contacts the base of grooves in a quasi-static manner, if and only if θ_{01}, θ_{02} and φ satisfy:

(i) both Ineqs. (6.13) and (6.11) in the case of circular micropillars with convex sidewalls, or

(ii) Ineq. (6.13) in the case of spherical microparticles or circular micropillars with straight sidewalls.

Although only circular micropillars with convex sidewalls or straight sidewalls are considered, their consideration could also be extended, for example, to circular micropillars with concave sidewalls. Following the same line of reasoning as used in Sub-sections 6.2.1-6.2.3, it is readily shown that, when both Ineqs. (6.13) and (6.14) are met, there should exist locally stable intermediate states in case of circular micropillars with concave sidewalls. Furthermore, using similar reasoning as applied in Sub-sections 6.3.1 and 6.3.2, the cases of other circular pillars with specified sidewalls, such as raspberry-like microparticles, may also be examined.

A set of values of θ_{01} and θ_{02} may be experimentally measured, depending on the volume of a water drop. [83] This set of values varies between receding and advancing angles. Accordingly, the minimum requirement in designing circular pillars for having a locally stable intermediate state is that the advancing angles on the pillar sidewalls and groove bottom should meet Ineq. (6.13), which is adopted in this work to examine whether this inequality is satisfied. For the sake of security, it is better to have the receding angles, which are the minimum possible values of θ_{01} and θ_{02}, satisfy this inequality.

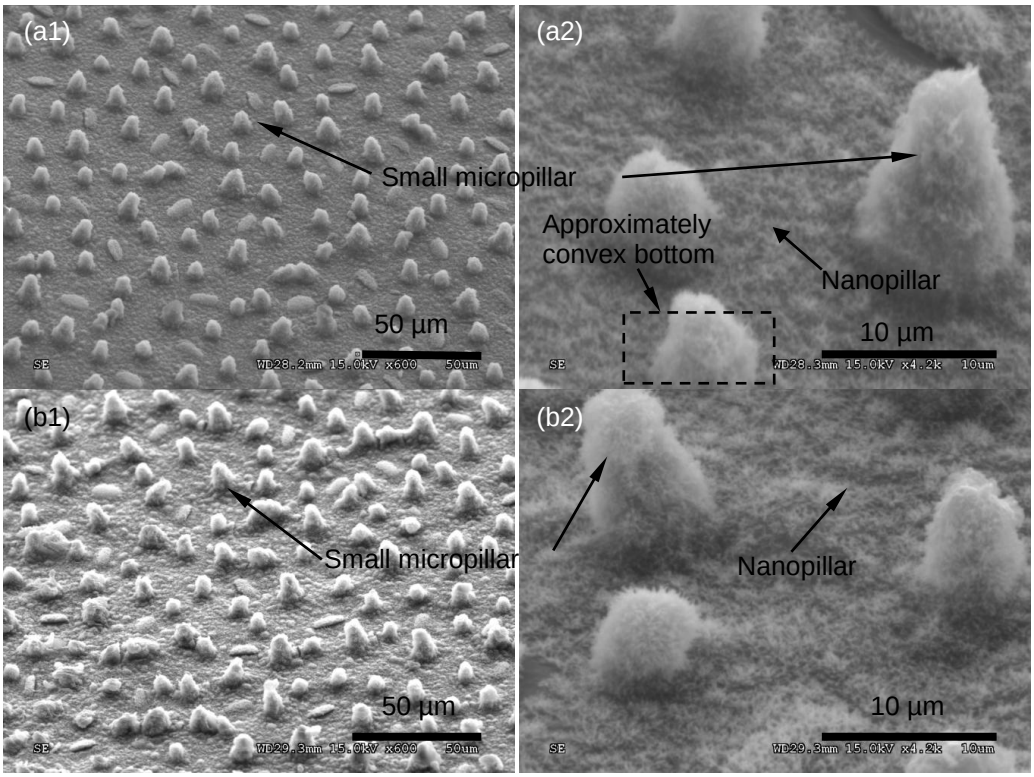

Figure 6.4: Nanopillars and small micropillars on the leaf surfaces of (a) *Chawen Basu* and (b) *Carolina Queen*, respectively. All are images of SEM.

6.4. Experimental Setup

The two points in the criterion are validated, respectively, by two types of experiments. The first type of experiments is performed on three lotus varieties: *The President*, *Carolina Queen*, and *Chawan Basu* (all were purchased from a local flower store and they are usually sold as pond plants), and the second type is on spherical microballs (Bal-tec Company, CA), which have identical diameters of 500 μm. Each type of experiments includes two tests. As will be addressed in detail later, the derived criterion is met in the first test, while it does not hold in the second test. Subsequently, the two tests in each type of experiments are conducted to examine whether the corresponding theoretical predictions are true. To be more specific, after a liquid contacts

the groove bottom, the expected equilibrium state is the intermediate state in the first test, while it is Wenzel state in the second test of each type of experiments.

Isopropyl alcohol (IPA) and water drops are, respectively, used in the first and second tests of the first type of experiments. In either test, all the three lotuses are examined. In the second type of experiments, the values of φ_0 in both tests are 150°, and only water drops are used.

Carolina Queen and *Chawan Basu* lotuses both have two-level surface structures (Fig. 6.4). Small micropillars are densely distributed on a lotus surface, and they are covered by nanopillars. The heights, base diameters, pitches, and bottom inclined degrees of the small micropillars for *Carolina Queen* are in the ranges of 9 to 15 μm, 7 to 19 μm, 7 to 58 μm and 53° to 90°, separately. They are in the ranges of 7 to 16 μm, 6 to 19 μm, 8 to 51 μm and 53° to 90°, respectively, in the case of *Chawan Basu*, similar to their counterparts of *Carolina Queen*. Accordingly, Ineq. (6.11) is met in both cases of *Carolina Queen* and *Chawan Basu*. The majority of small micropillars in either lotus can be considered to be circular micropillars with slightly convex sidewalls. As marked in Fig. 6.4(a2), some small micropillars may have bent sidewalls: the top portion of such a small micropillar bends towards one direction, while the bottom portion, which is directly related to the existence of the intermediate wetting state, can still be considered as a circular pillar with slightly convex sidewalls. Furthermore, since φ_0 for either lotus is not larger than 90°, it is good enough to use the first point in the derived criterion to judge the existence of an intermediate wetting state with no need knowing the exact sidewall profiles of the small micropillars. Thus, we did not specifically examine whether the small micropillars on the leaf surfaces of the two lotus varieties have the paraboloidic shapes of revolution, as previously reported in the case of other lotus varieties. [27]

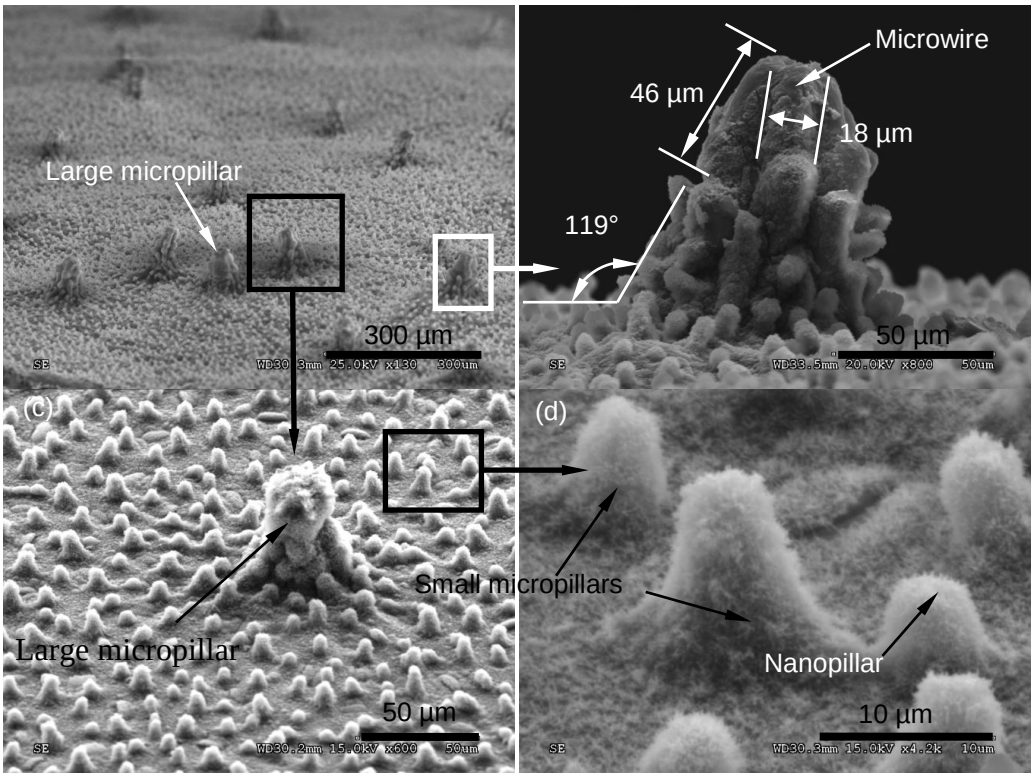

Figure 6.5: (a) Perspective, (b) front view and (c) close-up views of a large micropillar on The President. (d) Close-up view of small micropillars. All are SEM images.

We have recently reported that *The President* lotus has three-level surface structures (Fig. 6.5), and also compared its wetting properties with those of *Carolina Queen* and *Chawan Basu*. [53] In addition to small micropillars and nanopillars, it also has large micropillars (Fig. 6.5). The large micropillars are sparsely distributed throughout the whole leaf surface. Their cross-sections have approximately circular shapes, while their sidewalls are covered with six curved microwires, which extend from the middle of a sidewall to the top of each large micropillar (Figs. 6.5b and 6.5c. The bottom portion of a pillar sidewall is covered with small micropillars. Such small micropillars are also densely distributed on the valleys between large micropillars (Fig. 6.5a). Meanwhile, both large and small micropillars, as well as the valleys between the small micropillars, are also

covered by randomly oriented nanopillars (Fig. 6.5d). The heights, base diameters, pitches and bottom inclined degrees of the large micropillars are in the ranges of 42 to 89 μm, 17 to 40 μm, 204 to 928 μm and 42° to 90°, respectively. Therefore, Ineq. (6.11) is also met in the case of *The President*. The microwires on the sidewall of a large micropillar are slightly curved (Fig. 6.5b). Their straight lengths are about half of the pillar height, and both their thicknesses and widths are approximately equal to the top radius of the corresponding pillar. The shapes, dimensions, and pitches of the nanopillars and small micropillars on *The President* are about the same as their counterparts in the cases of *Carolina Queen* and *Chawan Basu*. The heights of the nanopillars on all three types of lotus vary from 500 to 1200 nm, while their diameters range from 140 to 240 nm. As in the cases of *Carolina Queen* and *Chawan Basu* for small micropillars, the large micropillars of *The President* are also considered as circular pillars with slightly curved sidewalls.

Both types of experiments are pressing tests. A needle is used in the first test of the first type of experiments to press a liquid drop, while a Polydimethylsiloxane (PDMS) block is adopted in the other tests for the pressing purpose. The vertical movements of this block are controlled by a micromanipulator (M3301R of World Precision Instruments, FL, USA). To make liquid drops contact the groove bottoms in an approximately quasi-static manner, the vertical speeds of both the needle and block are controlled to be around 10 μm/s. An optical microscope (mm0013000m of Metallurgical Microscopes Company) is rotated by 90^{o} to have a side view of air/liquid interfaces between micropillars. Similar experimental setups have been previously used to press liquid drops on micropillars [29, 82] and microchannels. [77, 79] Small water and IPA drops are used in this work, and their volumes range from 2 to 6 μl. The pictures of the air/liquid interfaces observed through the optical microscope are taken using Minisee software of

ScopeTek Company. The contact angles of these interfaces with the inner surfaces of micropillars are determined using MB-Ruler software of Dance Patterns Company.

6.5 Experimental Results and Discussions

6.5.1 The First Type of Experiments

In the first type of experiments on *Carolina Queen* and *Chawan Basu*, due to small gaps between micropillars on lotus leaves, we could not directly identify the appearance or disappearance of air gaps on the leaf surfaces through the optical microscope, while we could do so in the case of *The President* because of the existence of large micropillars. Thus, the corresponding phenomena were interpreted according to the observation on the leaf surface of *The President*.

In the first test of the first type of experiments, an IPA drop was placed against each lotus surface. Once the IPA drop contacted the lotus surface, the surface was completely wetted, and a thin IPA film was formed in this surface (Fig. 6.6). It was seen clearly in the case of *The President* that the grooves between the large micropillars were covered by the IPA (Fig. 6.6(c3)). A lotus surface is considered to be coated with wax. [27, 62] The contact, receding and advancing angles were measured to be 13°, 7° and 18°, respectively, when a drop of IPA was placed on a film of a candle wax. The angle measurement had an error of about 2º. These angles were used as the intrinsic angles of the wax on the lotus leaf with respect to IPA. According to Wenzel's equation [23] and the dimensions of micropillars, it was expected that in the first test on each lotus, the contact, receding and advancing angles were close to 0º for all the three lotuses. Thus, Ineq. (6.13) should be violated for either lotus in the first test, which may explain why Wenzel states were observed on the three lotuses during the pressing tests.

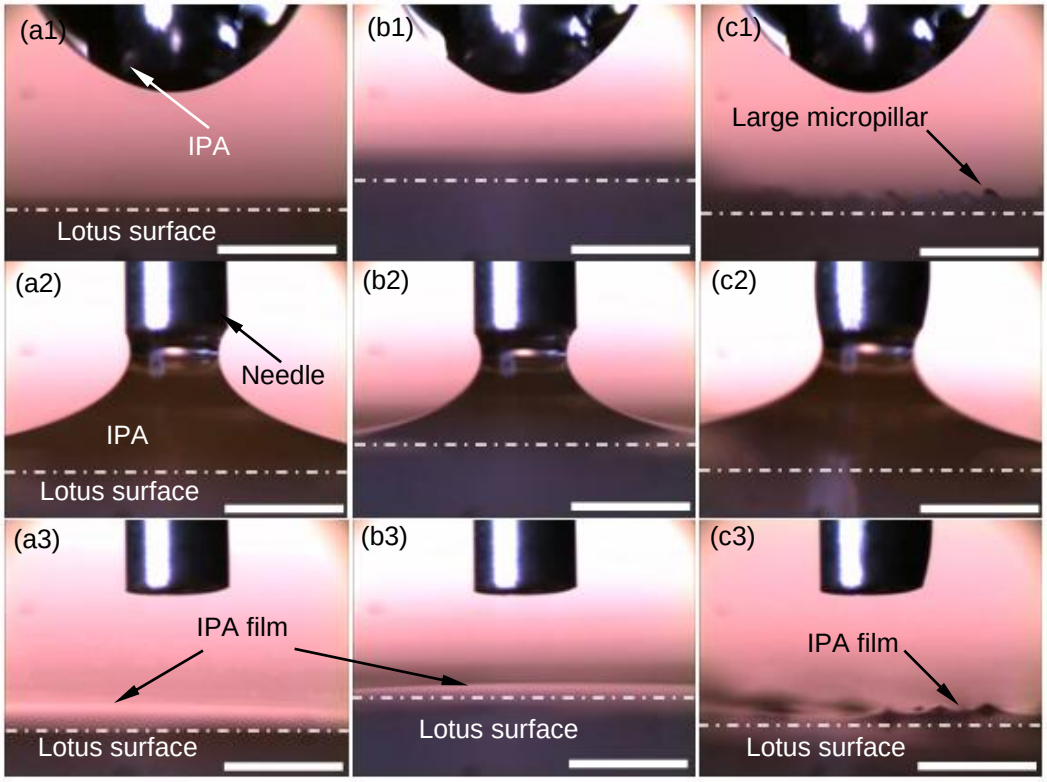

Figure 6.6: The first test of the first type of experiments: An IPA drop was placed and pressed against the leaf surfaces of (a) *Carolina Queen*, (b) *Chawan Basu* and (c) *The President*, respectively. (a1)-(c1) Placement of IPA drops. (a2)-(c2) Contact of the IPA drops with the substrates. (a3)-(c3) The complete wetting of IPA residue on the corresponding substrate after the needle has been removed from this substrate. The scale bars represent 500 µm.

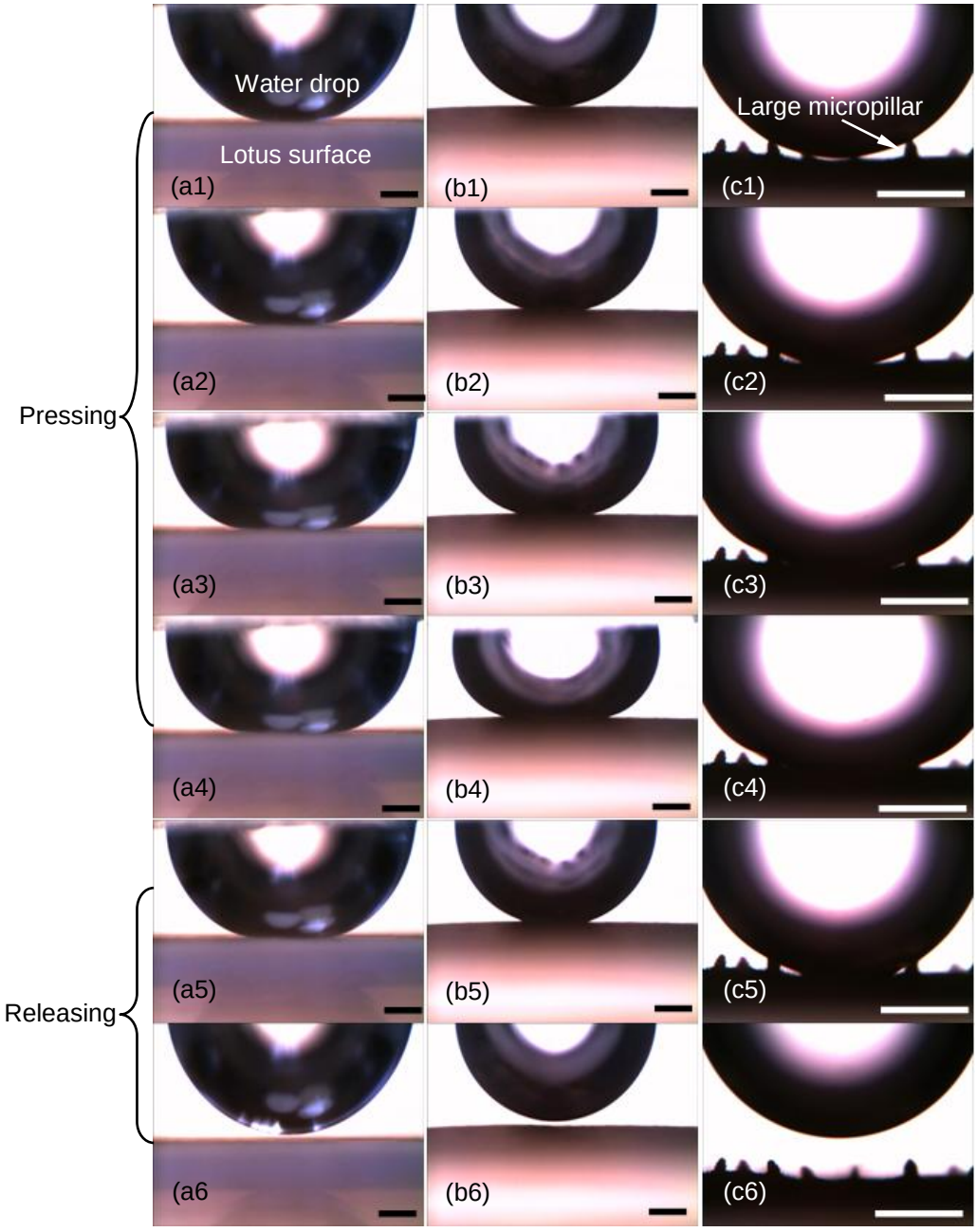

Figure 6.7: The second test of the first type of experiments: A water drop was placed and pressed against the leaf surfaces of (a) *Carolina Queen*, (b) *Chawan Basu* and (c) *The President*, respectively. The scale bars represent 450 µm.

Water drops were used in the second test. The contact, receding and advancing angles on the surface of *Carolina Queen* were 168º, 159º and 169º, respectively. They were 168º, 160º and 168º, separately, in the case of *Chawan Basu*, and were 171º, 164º and 171º, respectively, on the surface of *The President*. As shown in Fig. 6.7, two phenomena observed in this test were different from those in the first test. First, no liquid residue was observed after the pressing plate was removed, implying that liquid did not completely fill the grooves during the pressing process, resulting in the generation of intermediate states. Second, intermediate states were directly observed in the case of *The President* due to the existence of large micropillars on this lotus surface. During the test on *The President*, after water drops had contacted the bottoms of grooves, intermediate wetting states were observed inside these grooves. In such a wetting state, water did not completely fill the grooves, and air pockets existed between water drops and bottom corners of these grooves. After water had contact with the base of a few grooves, the air pockets in the middle grooves were not visible due to the block of water, while air pockets could still be seen around the outside micropillars ((c2), (c3) and (c5) in Fig. 6.7). Furthermore, the sizes of the air pockets decreased with the increase in the applied pressures, implying that there exist energy barriers between the intermediate states and that of Wenzel (i.e., the state for which the groove is completely filled by water). Consequently, these intermediate states are stable. Otherwise, the wetting states should be immediately transformed to that of Wenzel when the applied pressure was increased. It was also interesting to observe that, along with the reduction in the applied pressure, these air pockets gradually increased their sizes. Meanwhile, the number of grooves that had contact with the water drop was reduced, and due to this reduction the air pockets in the middle of grooves re-appeared ((c5) in Fig. 6.7). Eventually the water

drop recovered its Cassie-Baxter wetting state after much reduction in the applied pressure ((c6) in Fig. 6.7).

We have also previously performed experiments on artificial circular micropillars with vertical straight walls. [82] The observed experimental phenomena are similar as those in the first type of experiments. They can be justified as well using the first point of the derived criterion.

6.5.2 The Second Type of Experiments

A microball and an SU-8 substrate were adopted in the first test of the second type of experiments. The contact, receding and advancing angles on the surface of the microball were measured to be 86º, 59º and 96º, respectively, and they were 69º, 16º and 75º on the SU-8 substrate. When either receding or advancing angles of the microball and SU-8 substrate are used in Ineq. (6.13), this inequality is violated. Accordingly, there should not exist any intermediate states after water contacts the SU-8 substrate. This point was validated in the corresponding pressing tests. As shown in Fig. 6.8(a), the water drop immediately covered the bottom portion of the microball when it had contact with the SU-8 substrate ((a4) in Fig. 6.8). Furthermore, as in the first test of the first type of experiments, a portion of the water drop was left on the SU-8 substrate when the pressing plate was removed ((a6) in Fig. 6.8), implying that the wetting state did not transition back to the Cassie state. Due to the blocking of water, it was not clear whether the bottom corner of the microball was completely filled by water after the occurrence of the contact (Fig. 6.8(a3)). To solve this problem, a water drop was placed beside the microball instead. As observed from Fig. 6.9(a), after the contact with the substrate, water immediately filled the bottom corner of the microball, which provides a clear evidence that the wetting state was that of Wenzel.

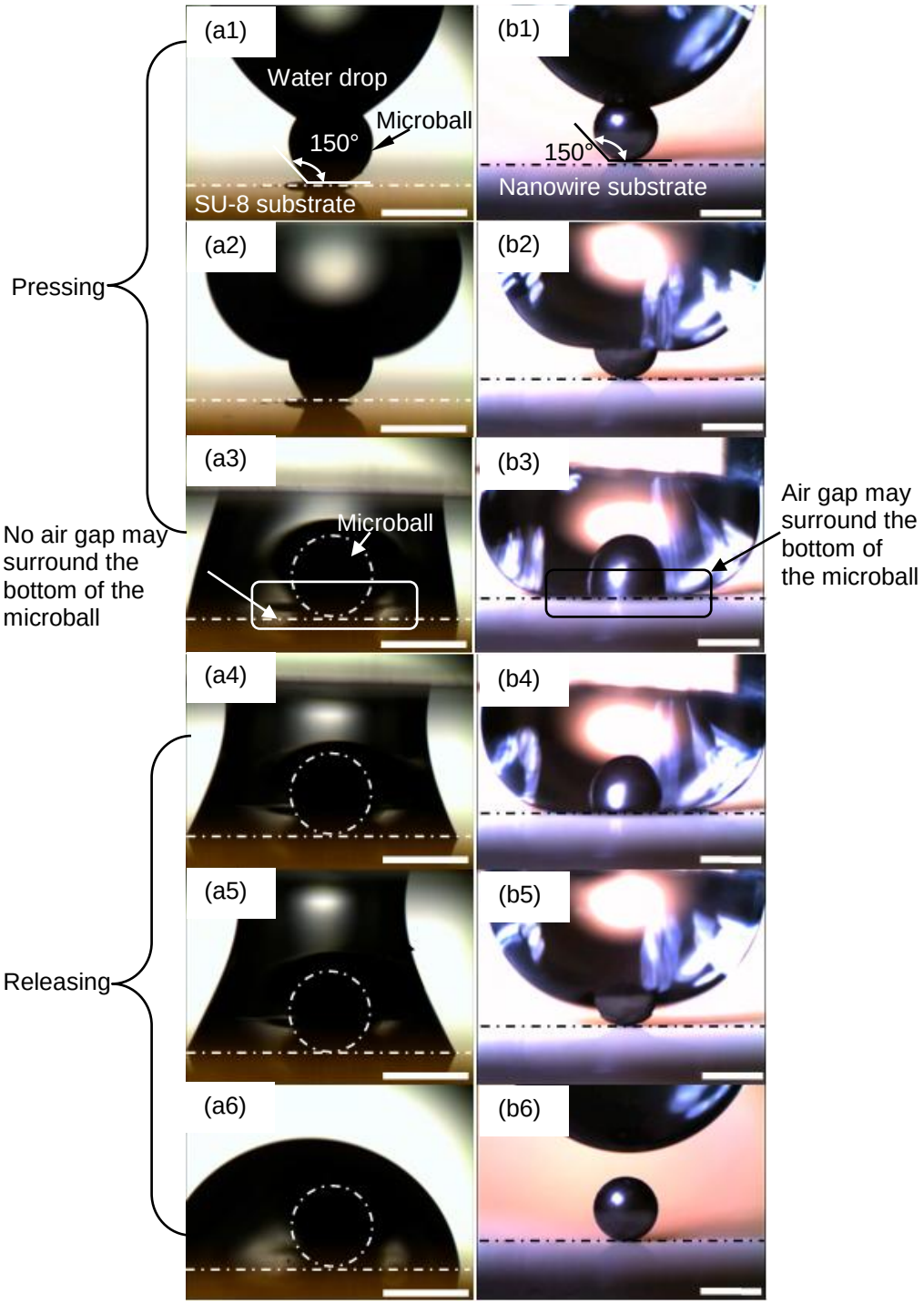

Figure 6.8: The first (a) and the second (b) tests of the second type of experiments: (a) microball and SU-8 substrate, and (b) Teflon-coated microball and nanowire-coated silicon substrate. The scale bars represent 500 μm.

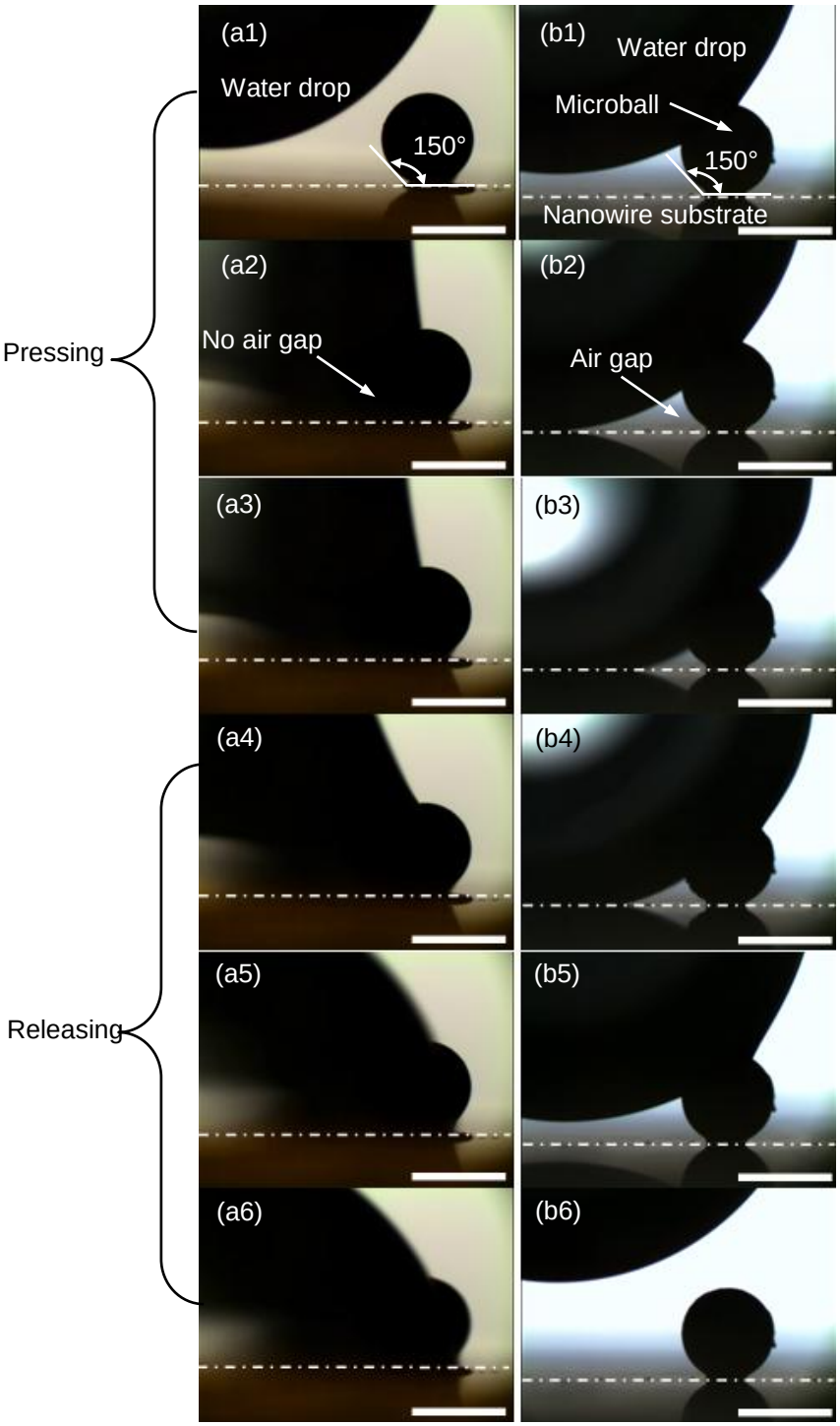

Figure 6.9: Pressing of a droplet on the side of the microball. (a) SU-8 substrate and microball. (b) Nanowire-coated substrate and Teflon- coated microball. The scale bars represent 500 µm.

In the second test of the second type of experiments, the microball and the SU-8 substrate were coated with Teflon and ZnO nanowires, respectively, to change the values of θ_{01} and θ_{02}. The contact, receding and advancing angles were, respectively, 115º, 94º and 121º on the Teflon-coated microball, while they were 170º, 160º and 172º on the nanowire-coated SU-8 substrate. When either receding or advancing angles of the microball and nanowire-covered substrate were used in Ineq. (6.13), this inequality was met. Thus, according to the second point in the derived criterion, there should exist an intermediate state after water contacts the nanowire-coated substrate. This point was also validated in the corresponding pressing test (Fig. 6.8b). The observed phenomena were similar to what was observed on *The President* in the second test of the first type of experiments. On the other hand, due to the blocking of water, it was also not clear whether there existed air gaps around the bottom corner of the microball. Accordingly, a water drop was placed beside the microball as well. As shown in Fig. 6.9(b), air gaps did exist around the bottom corner of this microball, resulting in an intermediate wetting state after the contact had occurred.

6.6 Summary and Conclusions

In this chapter, we consider the conditions for the existence of a locally stable intermediate wetting state after a liquid drop contacts the base of grooves located between circular micropillars with convex or straight sidewalls in a quasi-static manner. Through theoretical derivation, we show that there may exist a locally stable intermediate wetting state after a liquid drop contacts the base of grooves in a quasi-static manner, (i) if and only if θ_{01}, θ_{02} and φ satisfy Ineqs. (6.13) and (6.11) in the case of circular micropillars with convex sidewalls, or (ii) if and only if these angles meet Ineq. (6.13) in the cases of spherical microparticles and circular micropillars with straight sidewalls. These theoretical results are validated through pressing tests on three lotus varieties and spherical microballs.

Chapter 7

Summary and Conclusions

In summary, this dissertation aims to explore the application range of the contact criterion in different cases.

First, in chapter 2, we directly observed the evolution of air/water interfaces suspended between PDMS microlines when water droplets reduced their sizes due to evaporation. According to experimental results, two important phenomena were observed regarding the transition from Cassie-Baxter to Wenzel States. Based on this observation, we derived critical values of droplet sizes and Laplace pressure to predict when the transition would occur on microlines, and compared the predicted values of the droplet sizes with experimental results on three arrays of PDMS microlines. We also conducted in-situ observation of the evolution of air/water interfaces when water droplets were slowly pressed using a glass slide on the three arrays of PDMS microlines. The critical values of the droplet sizes derived in the case of evaporation also applied to this pressing case.

Second, in chapter 3, through theoretical and experimental investigations of the contact criterion, we found that, when an angle criterion is met, an intermediate wetting state may be formed after a water drop contacts the bottom of a microchannel or after it is placed on a single corner. In this wetting state, the microchannel or single corner is not completely filled by water, and air pocket still exists at the bottom of the structure. Since such a wetting model appears only in the transition process between Cassie-Baxter and Wenzel states, it is called an intermediate state here. This intermediate state is also stable in the sense that its energy state is lower than that of the Wenzel model.

Third, in chapter 4, we further considered the case of polygonal and circular pillars, and also derived an angle inequality, which is identical to the one derived in the

case of microchannels that discussed in chapter 3. In the case of pillars, this angle inequality is a necessary condition that local contact angles and the inclined degree of the pillars should meet for the existence of an intermediate state. As in the case of microchannels, once this inequality is violated, there should not exist any intermediate state, and the contact criterion is also applicable to the case of micropillars. On the other hand, different from that in the case of microchannels, the satisfaction of this inequality does not guarantee the existence of a stable intermediate state for the case of micropillars. For the existence of a stable intermediate state, two conditions should be satisfied. First, there exists an equilibrium state after the contact. Second, there is an energy barrier between this equilibrium state and that of Wenzel. The consideration of these two conditions may give precise bounds of local contact angles and inclined degrees of pillar sidewalls for the existence of a stable intermediate state, which could also be used to identify the exact range that the contact criterion is applicable. We did so for the case of microchannels in chapter 3, since the corresponding air/liquid interfaces have simple shapes. However, we did not consider the two conditions in the case of micropillars that discussed in chapter 4 due to lack of analytical expression of the related air/liquid interfaces. Accordingly, although the derived inequality is identical to the one for the case of channels, it may not give a precise range that the contact criterion is valid.

Fifth, in chapter 5, using a new approach, we consider the aforementioned two conditions for existing an intermediate state in the case of circular pillars with vertical sidewalls. This approach does not rely on the explicit expression of the interface profile, making it feasible to explore the applicability of the contact criterion. we demonstrate: (i) when this angle inequality is met due to the increase of local contact angles by, for example, nanostructures, there exists a locally stable intermediate state after a water drop slowly contacts the base of grooves and the contact criterion does not hold for the

corresponding micropillars, and (ii) if the inequality is violated, then such an intermediate state does not exist and the contact criterion holds true.

Sixth and finally, according to our pressing tests on three different lotus varieties, we also found that the transition did not occur when the contact happened. The lotus micropillars were approximately as paraboloids of revolution, which means that these micropillars can be considered as circular pillars whose sidewalls have convex shapes in the vertical planes. Thus, we also explored the applicability of the contact criterion to circular pillars with convex sidewalls. Through theoretical derivation and experimental validation, we show that there may exist a locally stable intermediate wetting state after a liquid drop contacts the base of grooves in a quasi-static manner, (i) if and only if θ_{01}, θ_{02} and φ satisfy Ineqs. (6.13) and (6.11) in the case of circular micropillars with convex sidewalls, or (ii) if and only if these angles meet Ineq. (6.13) in the cases of spherical microparticles and circular micropillars with straight sidewalls.

References

[1]. Blossey, R. Self-cleaning surfaces—virtual realities. *Nature materials* **2003**, *2(5)*, 301-306.

[2]. Fürstner, R.; et al. Wetting and self-cleaning properties of artificial superhydrophobic surfaces. *Langmuir* **2005**, *21(3)*, 956-961.

[3]. Choi, C.-H.; Kim, C.-J. Large Slip of Aqueous Liquid Flow over a Nanoengineered Superhydrophobic Surface. *Phys. Rev. Lett.* **2006**, *96*, 066001.

[4]. Choi, C.-H.; Ulmanella, U.; Kim, J.; Ho, C.-M.; Kim, C.-J. Effective Slip and Friction Reduction in Nanograted Superhydrophobic Microchannels. *Phys. Fluids* **2006**, *18*, 087105.

[5]. Aljallis, E.; Sarshar, M. A.; Datla, R.; Sikka, V.; Jones, A.; Choi, C.-H. Experimental Study of Skin Friction Drag Reduction on Superhydrophobic Flat Plates in High Reynolds Number Boundary Layer Flow. *Phys. Fluids* **2013**, *25*, 025103.

[6]. Kripa, K. V.; Tao, D.; Smith, J. D.; Ming, H.; Nitin, B. Frost Formation and Ice Adhesion on Superhydrophobic Surfaces. *Appl. Phys. Lett*. **2010**, *97*, 234102.

[7]. Mishchenko, L.; Hatton, B.; Bahadur, V.; Taylor, J. A.; Krupenkin, T.; Aizenberg, J. Design of Ice-Free Nanostructured Surfaces Based on Repulsion of Impacting Water Droplets. *ACS Nano* **2010**, *4*, 7699–7707.

[8]. Sarshar, M. A.; Swarctz, C.; Hunter, S.; Simpson, J.; Choi, C. H. Effects of Contact Angle Hysteresis on Ice Adhesion and Growth on Superhydrophobic Surfaces under Dynamic Flow Conditions. *Colloid Polym. Sci.* **2013**, *291*, 427–435.

[9]. Liu, K.; Zhang, M.; Zhai, J.; Wang, J.; Jiang, L. Bioinspired Construction of Mg-Li Alloys Surfaces with Stable Superhydrophobicity and Improved Corrosion Resistance. *Appl. Phys. Lett.* **2008**, *92*, 183103.

[10]. Zhang, F.; Zhao, L.; Chen, H.; Xu, S.; Evans, D. G.; Duan, X. Corrosion Resistance of Superhydrophobic Layered Double Hydroxide Films on Aluminum Angew. *Chem., Int. Ed.* **2008**, *47*, 2466–2469.

[11]. Ishizaki, T.; Masuda, Y.; Sakamoto, M. Corrosion Resistance and Durability of Superhydrophobic Surface Formed on Magnesium Alloy Coated with Nanostructured Cerium Oxide Film and Fluoroalkylsilane Molecules in Corrosive NaCl Aqueous Solution. *Langmuir* **2011**, *27*, 4780–4788.

[12]. Genzer, J.; Efimenko, K. Recent Developments in Superhydrophobic Surfaces and Their Relevance to Marine Fouling: A Review. *Biofouling* **2006**, *22*, 339–360.

[13]. Ressine, A.; Marko-Varga, G.; Laurell, T.; El-Gewely, M. R. Porous Silicon Protein Microarray Technology and Ultra-/Superhydrophobic States for Improved Bioanalytical Readout. *Biotechnology Annual Review* **2007**; *13*, 149–200.

[14]. Choi, C.-H.; Kim, C.-J. Droplet Evaporation of Pure Water and Protein Solution on Nanostructured Superhydrophobic Surfaces of Varying Heights. *Langmuir* **2009**, *25*, 7561–7567.

[15]. Chen, X.; Wu, J.; Ma, R.; Hua, M.; Koratkar, N.; Yao, S.; Wang, Z. Nanograssed Micropyramidal Architectures for Continuous Dropwise Condensation. *Adv. Funct. Mater.* **2011**, *21*, 4617–4623.

[16]. Xu, W.; Choi, C.-H. Effects of Surface Topography and Colloid Particles on the Evaporation Kinetics of Sessile Droplets on Superhydrophobic Surfaces. *J. Heat Transfer* **2012**, *134*, 051022–051027.

[17]. Miljkovic, N.; Enright, R.; Wang, E. N. Effect of Droplet Morphology on Growth Dynamics and Heat Transfer During Condensation on Superhydrophobic Nanostructured Surfaces. *ACS Nano* **2012**, *6*, 1776– 1785.

[18]. Liu, Y.; Choi, C.-H. Condensation-Induced Wetting State and Contact Angle Hysteresis on Superhydrophobic Lotus Leaves. *Colloid Polym. Sci.* **2013**, *291*, 437–445.

[19]. Betz, A. R.; Jenkins, J.; Kim, C. J.; Attinger, D. Boiling Heat Transfer on Superhydrophilic, Superhydrophobic, and Superbiphilic Surfaces. *Int. J. Heat Mass. Tran*. **2013**, *57*, 733–741.

[20]. Xu, W.; Leeladhar, R.; Tsai, Y.-T.; Yang, E.-H.; Choi, C.-H. Evaporative Self-Assembly of Nanowires on Superhydrophobic Surfaces of Nanotip Latching Structures. *Appl. Phys. Lett.* **2011**, *98*, 073101.

[21]. Lee, S.; Kim, W.; Yong, K. Overcoming the Water Vulnerability of Electronic Devices: A Highly Water-Resistant ZnO Nanodevice with Multifunctionality. *Adv. Mater.* **2011**, *23*, 4398–4402.

[22]. De Angelis, F.; Gentile, F.; Mecarini, F.; Das, G.; Moretti, M.; Candeloro, P.; Coluccio, M. L.; Cojoc, G.; Accardo, A.; Liberale, C. Breaking the Diffusion Limit with Super-Hydrophobic Delivery of Molecules to Plasmonic Nanofocusing SERS Structures. *Nat. Photon.* **2011**, *5*, 682– 687.

[23]. Wenzel, R. N. Resistance of solid surfaces to wetting by water. *Industrial and Engineering Chemistry* **1936**, *28*, 988.

[24]. Cassie, A. B. D.; Baxter, S. Wettability of porous surfaces. *Transactions of the Faraday Society* **1944**, *40*, 546.

[25]. McHale, G.; Shirtcliffe, N. J.; Aqil, S.; Perry, C. C.; Newton, M. I. Topography Driven Spreading. *Physics Review Letters* **2004**, *93(3)*, 036102.

[26]. Extrand, C. W.; Moon, S. I.; Hall, P.; Schmidt, D. Superwetting of Structured Surfaces. *Langmuir* **2007**, *23(17)*, 8882.

[27]. Neinhuis, C.; Barthlott, W. Characterization and distribution of water-repellent, self-cleaning plant surfaces. *Annals of Botany* **1997***, 79*, 667.

[28]. Ou, J.; Perot, B.; Rothstein, J. P. Laminar drag reduction in microchannels using ultrahydrophobic surfaces. *Physics of Fluids* **2004**, *16*, 4635.

[29]. Lafuma, A.; Quéré, D. Superhydrophobic states. *Nat. Mater*. **2003**, *2*, 457−460.

[30]. Yoshimitsu, Z.; Nakajima, A.; Watanabe, T.; Hashimoto, K. Effects of surface structure on the hydrophobicity and sliding behavior of water droplets. *Langmuir* **2002**, *18*, 5818−5822.

[31]. Liu, B.; Lange, F. F. J. Pressure induced transition between superhydrophobic states: Configuration diagrams and effect of surface feature size. *Colloid Interface Sci.* **2006**, *298*, 899−909.

[32]. Bormashenko, E.; Pogreb, R.; Whyman, G.; Mordehai, E. Cassie-Wenzel wetting transition in vibrating drops deposited on rough surfaces: is the dynamic Cassie-Wenzel wetting transition a 2D or 1D affair?. *Langmuir* **2007**, *23*, 6501.

[33]. Bahadur, V.; Garimella, S. V. Electrowetting-based control of static droplet states on rough surfaces. *Langmuir* **2007**, *23*, 4918.

[34]. Nosonovsky, M.; Bhushan, B. Biomimetic superhydrophobic surfaces: multiscale approach. *Nano Lett.* **2007**, *7*, 2633.

[35]. Deng, T.; Varanasi, K. K.; Hsu, M.; Bhate, N.; Keimel, C.; Stein, J.;Blohm, M. Nonwetting of impinging droplets on textured surfaces. *Appl. Phys. Lett.* **2009**, *94*, 133109.

[36]. Jung, Y. C.; Bhushan, B. Wetting transition of water droplets on superhydrophobic patterned surfaces. *Scr. Mater.* **2007**, *57*, 1057.

[37]. Reyssat, M.; Yeomans, J. M.; Quere, D. Impalement of fakir drops. *Europhys. Lett.* **2008**, *81*, 26006.

[38]. Kusumaatmaja, H.; Blow, M. L.; Dupuis, A.; Yeomans, J. M. The collapse transition on superhydrophobic surfaces. *Europhys. Lett.* **2008**, *81*, 36003.

[39]. Bartolo, D.; Bouamrirene, F.; Verneuil, E.; Buguin, A.; Silberzan, P.; Moulinet, S. Bouncing or sticky droplets: impalement transitions on superhydrophobic micropatterned surfaces. *Europhys. Lett*. **2006**, *74*, 299.

[40]. Jung, Y. C.; Bhushan, B. Dynamic effects induced transition of droplets on biomimetic superhydrophobic surfaces. *Langmuir* **2009**, 25, 9208.

[41]. Reyssat, M.; Pepin, A.; Marty, F.; Chen, Y.; Quere, D. Bouncing transitions on microtextured materials. *Europhys. Lett.* **2006**, *74*, 306.

[42]. Tsai, P.; Lammertink, R. G.; Wessling, M.; Lohse, D. Evaporation-triggered wetting transition for water droplets upon hydrophobic microstructures. *Phys. Rev. Lett.* **2010**, *104*, 116102.

[43]. Tuteja, A.; Choi, W.; Mabry, J. M.; McKinley, G. H.; Cohen, R. E. Robust omniphobic surfaces. *Proc. Natl. Acad. Sci.* **2008**, *105*, 18200.

[44]. Tuteja, A.; Choi, W.; McKinley, G. H.; Cohen, R. E.; Rubner, M. F. Design parameters for superhydrophobicity and superoleophobicity. *MRS bulletin*, **2008**, *33(08)*, 752-758.

[45]. Jung, Y. C.; Bhushan, B. Wetting behavior during evaporation and condensation of water microdroplets on superhydrophobic patterned surfaces. *Journal of Microscopy* **2008**, *229*, 127.

[46]. He, B.; Patankar, N. A.; Lee, J. Multiple Equilibrium Droplet Shapes and Design Criterion for Rough Hydrophobic Surfaces. *Langmuir* **2003**, *19*, 4999.

[47]. Quéré, D.; Reyssat, M. Non-adhesive lotus and other hydrophobic materials. *Philosophical Transactions of the Royal Society A* **2008**, *366*, 1539.

[48]. Liu, X.; Luo, C. Fabrication of Super-hydrophobic channels. *Journal of Micromechanics and Microengineering* **2010**, *20*, 025029.

[49]. Extrand, C. W. Criteria for ultralyophobic surfaces. *Langmuir* **2004**, *20,* 5013-5018.

[50]. Patankar, N. A. Transition between Superhydrophobic States on Rough Surfaces. *Langmuir* **2004**, *20*, 7097.

[51]. Cheng, Y-T.; Rodak, D. E.; Angelopoulos. A.; Gacek, T. Microscopic observations of condensation of water on lotus leaves. *Applied Physics Letters* **2005**, *87*, 194112.

[52]. Verho, T.; Korhonen, J. T.; Sainiemi, L.; Jokinen, V.; Bower, C.; Franze, K.; Franssila, S.; Andrew, P.; Ikkala, O.; Ras, R. H. A Reversible switching between superhydrophobic states on a hierarchically structured surface*. P Natl Acad Sci* **2012**, *109(26)*, 10210-10213.

[53]. Xiang, M., Wilhelm, A., & Luo, C. Existence and role of large micropillars on the leaf surfaces of the president lotus. *Langmuir*, **2013**, *29(25)*, 7715-7725.

[54]. Marmur, A. The Lotus Effect: Superhydrophobicity and Metastability. *Langmuir* **2004**, *20*, 3517.

[55]. Shiu, J. Y.; Kuo, C. W.; Chen, P. L.; Mou, C. Y. Fabrication of Tunable Superhydrophobic Surfaces by Nanosphere Lithography. *Chem. Mater*. **2004**, *16*, 561–564.

[56]. Ming, W.; Wu, D.; van Benthem; de With, G. Superhydrophobic films from raspberry-like particles. *Nano Letters* **2005**, *5*, 2298–2301.

[57]. Wang, T.; Hu, X.; Dong, S. A general route to transform normal hydrophilic cloths into superhydrophobic surfaces. *Chem. Commun.* **2007**, *18*, 1849–1851.

[58]. Zhu, L.; Jin, Y. A novel method to fabricate water-soluble hydrophobic agent and super-hydrophobic film on pretreated metals. *Appl. Surf. Sci.* **2007**, *253*, 3432–3439.

[59]. Govindaraju, A; Chakraborty, A; Luo, C. Reinforcement of PDMS using SU-8 truss structures. *Journal of Micromechanics and Microengineering* **2005**, *15*, 1303.

[60]. Adamson A V (1990) *Physical Chemistry of Surfaces* (New York: Wiley).

[61]. Oliver, J. F.; Oliver, F.; Huh, C.; Mason, S. G. Resistance to spreading of liquids by sharp edges. *Journal of Colloid and Interface Science* **1977***, 59*, 568.

[62]. Nosonovsky, M.; Bhushan, B. Hierarchical roughness optimization for biomimetic superhydrophobic surfaces. *Ultramicroscopy* **2007***, 107*, 969.

[63]. Luo, C.; Xiang, M. Existence and stability of an intermediate wetting state on circular micropillars. *Microfluidics and Nanofluidics*, 1-10. DOI: 10.1007/s10404-014-1337-7

[64]. Bico, J.; Tordeux, C.; Quéré, D. Rough Wetting. *Europhysics Letters* **2001**, *55*, 214.

[65]. Bico, J.; Marzolin, C.; Quéré, D. Pearl drops. *Europhysics Letters* **1999**, *47*, 220.

[66]. Krupenkin, T. N.; Taylor, J. A.; Wang, E. N.; Kolodner, P.; Hodes, M.; Salamon, T. R. Reversible wetting-dewetting transitions on electrically tunable superhydrophobic nanostructured surfaces. *Langmuir* **2007**, *23,* 9128-9133.

[67]. Extrand, C. W.; Moon, S. I. Contact Angles of Liquid Drops on Super Hydrophobic Surfaces: Understanding the Role of Flattening of Drops by Gravity. *Langmuir* **2010**, *26 (22)*, 17090.

[68]. Cheng, M. C.; Garra, J. A.; Gadre, A. P.; Nijdam, A.J.; Luo, C.; Paranjape, M.; Currie, J.F.; Schneider, T.; White, R. Dry lease of polymer structures with anti-sticking layer. *Journal of Vacuum Science and Technology A* **2004**, *22*, 837.

[69]. Wang, B. G.; Shi, E. W.; Zhong, W. Z. Understanding and controlling the morphology of ZnO crystallites under hydrothermal conditions. *Crystal Research and Technology* **1997**, *32(5)*, 659.

[70]. Wang, H.; Luo, C. Generation of Au Micropatterns on Two Sidewalls of a Si Channel through a PDMS Shadow Mask. *Journal of Micromechanics and Microengineering* **2011**, *21*, 067005.

[71]. Madou, M. *Fundamentals of Microfabrication* **1995**, CRC Press.

[72]. Qiao, L.; Xiang, M.; Luo, C. Increase buoyancy of a solid fragment using micropillars. *Sensors and Actuators A: Physical* **2012**, *182*, 136-145.

[73]. de Gennes, P.-G.; Brochard-Wyart, F.; Quéré, D. *Capillarity and Wetting Phenomena: Drops, Bubbles, Pearls, Waves*, Springer, **2004**.

[74]. Whyman, G.; Bormashenko, E. Wetting Transitions on Rough Substrates: General Considerations, *Journal of Adhesion Science and Technology* **2012**, *26*, 207-220.

[75]. Stumbo, D. P.; Wolfe, J. C. Ion exposure characterization of a chemically amplified epoxy resist. *Journal of Vacuum Science and Technology B* **1993**, *11*, 2432.

[76]. Information of SU-8 provided by its supplier: www.microchem.com/pdf/SU8_50-100.pdf).

[77]. Luo, C.; Xiang, M.; Liu, X.; Wang, H. Transition from Cassie–Baxter to Wenzel States on microline-formed PDMS surfaces induced by evaporation or pressing of water droplets. *Microfluidics and Nanofluidics* **2011**, *10(4)*, 831-842.

[78]. Xiang, M.; Wilhelm, A.; Luo, C. Transition from Cassie-Baxter to Wenzel States on Micropillar-Formed Surfaces Induced by Evaporation. *ASME 2011 International Mechanical Engineering Congress and Exposition* (pp. 1065-1066).

[79]. Luo, C.; Xiang, M.; Heng, X. A stable intermediate wetting state after a water drop contacts the bottom of a microchannel or is placed on a single corner. *Langmuir* **2012**, *28*(25), 9554-9561.

[80]. Chakraborty, A.; Xiang, M.; Luo, C. Fabrication of Super-Hydrophobic Microchannels via Strain-Recovery Deformations of Polystyrene and Oxygen Reactive Ion Etch. *Materials* **2013**, *6(8)*, 3610-3623.

[81]. Greenberg, M. D. (1998) *Advanced Engineering Mathematics*, Second edition, Prentice-Hall, Upper Saddle River, NJ.

[82]. Luo, C.; Xiang, M.; Angle inequality for judging the transition from Cassie–Baxter to Wenzel states when a water drop contacts bottoms of grooves between micropillars. *Langmuir* **2012**, *28*(38), 13636-13642.

[83]. Marmur, A. Solid-Surface Characterization by Wetting. *Annu Rev Mater Res* **2009**, *39*, 473-489.

[84]. Whyman, G.; Bormashenko, E. How to make the Cassie wetting state stable? *Langmuir* **2011**, *27*, 8171.

[85]. Bico, J.; Thiele, U.; Quéré, D. Wetting of textured surfaces. *Colloids and Surfaces A* **2002**, *206*, 41.

[86]. Bormashenko, E.; Pogreb, R.; Stein, T.; Whyman, G.; Erlich, M.; Musin, A.; Machavariani, V.; Aurbach, D. Characterization of rough surfaces with vibrated drops. *Physical Chemistry Chemical Physics* **2008**, *10*, 4056.

[87]. Marmur, A. A guide to the equilibrium contact angle maze. *Contact Angle Wettability and Adhesion* **2009**, *6*, 3.

[88]. Luo, C.; Xiang, M. Wetting states on circular micropillars with convex sidewalls after liquids contact groove base. *Langmuir* **2013**, *29(48)*, 15065-15075.

[89]. Heng, X.; Xiang, M.; Lu, Z.; Luo, C. Branched ZnO Wire Structures for Water Collection Inspired by Cacti. *ACS Appl. Mater. Interfaces* **2014**, *6(11)*, 8032–8041

[90]. Patankar, N. A. Consolidation of hydrophobic transition criteria by using an approximate energy minimization approach. *Langmuir* **2010**, *26(11)*, 8941-8945.

Biographical Information

Mingming Xiang received his Bachelor's degree in June 2007 from the Department of Mechanical Engineering and Automation at Wuhan University of Technology, China. During 2007 and 2008, he worked as a Product Development Engineer at Foxconn Research and Design Center. In August 2009, he came to USA and started to pursue his PhD degree in the Department of Mechanical and Aerospace Engineering at University of Texas at Arlington. His research interests include wetting, biomimetics and microfabrication.